UNIVERSITY OF TURIN

PhD School in Life and Health Sciences

Molecular Medicine

XXIX Cycle

Academic Years: 2014-2017

Targeting MET to Overcome Radioresistance of Cancer Stem-like Cells in Glioblastoma and Rectal Carcinoma

Tutor: Prof.ssa Carla Boccaccio

Candidato: Antonio D'Ambrosio

Coordinator: Prof. Francesco Novelli

Index

INDEX 2

ABSTRACT 5

INTRODUCTION 7

1. The cancer stem cell hypothesis and its implications 8
   - *1.1. CSCs can be isolated from tumors and grow as spheroids in vitro* 9
   - *1.2. CSCs can be prospectively isolated* 11
2. Cancer stem cells and radioresistance 14
   - *2.1. GSCs radioresistance: molecular mechanisms* 15
3. Crosstalk between the Receptor Tyrosine Kinases (RTKs) signaling and the DDR in GBM radioresistance 18
4. The role of the MET oncogene in invasive growth and radioresistance 20
   - *4.1. MET is predictive factor of poor prognosis in locally advanced rectal adenocarcinoma* 22
5. MET is a functional marker of a glioblastoma stem cell subset 23

AIM OF THE WORK 26

MATERIALS AND METHODS 28

Neurospheres derivation from human patients and culture 29

Xeno-rectospheres derivation from PDXs and culture 29

Nucleic acid extraction 30

Copy number analysis 30

Gene sequencing 30

Microarray analysis 31

Real-Time PCR 31

Immunophenotypical analysis and Fluorescence-Activated Cell Sorting 31

Lentiviral transduction of neurospheres 32

GBM and rectal cancer xenograft models 32

Immunohistochemistry analysis of GBM and rectal cancer xenografts 33

Limiting dilution sphere forming assay *in vitro* 34

Serial transplantation assay 34

Immunofluorescence analysis 34

Western blotting 35

Collection of matched primary and recurrent human GBMs 35

Immunohistochemical staining of MET on matched primary/recurrent GBMs 35

Cell viability assay 36

Radiobiological clonogenic assay 36

Neurospheres and xeno-rectospheres irradiation and treatment with inhibitors 37

Irradiation and radiosensitization of GBM xenografts and rectal cancer-PDXs 37

Limiting dilution assay *in vivo* 38

Collection of rectal cancer cases 39

Immunohistochemical staining of MET in rectal tumors and the matched PDXs 39
Tissue Microarray (TMA) construction and immunohistochemical analysis 40
Statistical analysis 41

RESULTS 42
1. Genetic, phenotypic and functional characterization of glioblastoma stem-like cells (GSCs) 43
2. The neurosphere GSC subpopulation is positively selected by ionizing radiation 48
3. MET-expressing GSCs are selected by irradiation in experimental model 52
4. MET expression is enriched in recurrent glioblastoma 54
5. MET^{high} GSCs are more radioresistant than the MET^{neg} subpopulation and efficiently activate DDR 57
6. MET inhibition radiosensitizes GSCs by impairing ATM and p21 activity 59
7. MET inhibition sensitizes GBM xenografts to radiotherapy 63
8. MET inhibition associated with radiotherapy deplets GSCs *in vivo* 66
9. MET is extensively expressed in locally advanced rectal carcinoma 69
10. Genetic, phenotypic and functional characterization of patient-derived rectal cancer stem-like cells (RCSCs) 74
11. MET inhibition radiosensitizes RCSCs *in vitro* 79
12. MET inhibition sensitizes rectal cancer PDX to radiotherapy and targets RCSCs *in vivo* 81

DISCUSSION 86

REFERENCES 94

Abstract

Radiation therapy is a widely employed and effective tumor treatment, but, in many cases, its success is limited by primary radioresistance of tumor cells. Compelling evidence indicates that Glioblastoma (GBM), one of the most intractable tumors, contains a subpopulation of stem-like cells (GSCs), which are endowed with inherent radioresistance and thus responsible for therapeutic failure and rapidly lethal tumor recurrence. GSC radioresistance is known to rely on efficient activation of the DNA damage response (DDR), but the mechanisms linking this response with the stem status are still unclear.

Works previously carried out in our laboratory showed that the MET receptor tyrosine kinase (i) confers radioresistance to tumor cells, and (ii) it is a functional marker of the GSC subpopulation. Here, we show that MET is specifically expressed in a subset of radioresistant GSCs and overexpressed in human recurrent GBM, likely due to positive selection induced by radiotherapy. We also found that MET pharmacological inhibition causes DNA damage accumulation in irradiated GSCs by impairing ATM and p21 activity. As result, MET inhibitors associated with radiotherapy promote GSCs depletion *in vitro* as well as in xenografts generated by GSC transplantation, leading to tumor regression.

We extended our investigation to radiosensitization of locally advanced rectal adenocarcinoma, where MET expression was found to be a predictive marker of poor response to chemo-radiotherapy often administered before surgical resection. Also in this model, we found that MET inhibition radiosensitizes rectal stem-like cells (RCSCs) *in vitro* and blocks the tumor growth of rectal cancer patient-derived-xenografts (PDX) by depleting the RCSC subpopulation.

Therefore, preclinical evidence is provided that MET can be exploited as a therapeutic target to radiosensitize tumors by converting CSCs positive selection, induced by radiotherapy, into CSCs eradication.

Introduction

1. The Cancer Stem Cell hypothesis and its implications

The term cancer stem cells (CSCs) originated from studies in leukemias, where rigorous examination of the properties of different cell subpopulations highlighted that only a small subset displayed the ability to self-renew and generate the diverse cells that comprise the tumor, thus forming a hierarchy mirroring that found in the corresponding normal hemopoietic tissue [1-3]. Subsequent experimental assessment showed that a similar hierarchy lead by stem-like cells could be found virtually in every tumor type, including glioblastoma, colorectal and breast cancers [4-8]. CSCs share important properties with normal tissue stem cells, in the first place self-renewal (by symmetric and asymmetric division) and long-term propagation. Moreover, they exhibit tumor-propagating activity in transplantation assay and generate heterogeneous cell populations, including (pseudo)-differentiated (non-stem) cells, which acquire a status of negligible tumorigenic potential [9, 10].

Recently developed genetic-lineage tracing strategies allowed to identify defined subpopulations retaining CSC properties in mouse endogenous tumors, and to formally demonstrate that tumor tissues are hierarchically organized [11-13].

It has progressively become clear that CSCs are not necessarily rare like normal stem cells. It has been shown that limitations inherent in the experimental models, in particular the use of standard immunocompromised mice for cell transplantation, could lead to underestimation of the actual frequency of tumorigenic cells (i.e. CSCs) in human tumors [14]. Indeed, it must be noticed that CSC rarity is not an essential prerequisite of the model: CSC frequency is expected to be very variable, as: (i) this frequency is inversely proportional to the differentiation degree of the tumor, and directly proportional to its malignancy [15]; (ii) the CSC status is 'plastic', i.e. it can be actively sustained or induced by extracellular signals such as those promoting epithelial-mesenchymal transition [16-18].

The study of cells isolated from tumors for displaying stem-like properties has highlighted important implications for cancer therapy: these cells are often endowed with inherent resistance against standard chemo-radiotherapy, owing to their tendency to be relatively quiescent, and to the constitutive activation of molecular mechanisms promoting DNA repair and survival [19, 20]. Therefore, if it is necessary to eradicate CSCs to get rid of "the roots of the tumor", capable of causing relapse after an apparent remission, it is mandatory

to hit the molecular mechanisms that operate inside CSCs and sustain their unruly phenotype.

1.1. CSCs can be isolated from tumors and grow as spheroids in vitro

Isolation of CSCs from solid tumors has been hindered by the lack of unequivocal, robust cell-surface markers such as those that characterize the hemopoietic hierarchy and allowed the so-called 'prospective' identification of leukemia stem cells [21]. As the stem-like status is a functional cell-state and not a fixed cell identity, the CSC phenotype is weakly associated with the expression of specific markers, but it is operationally defined as the ability to long-term propagate *in vitro* (clonogenicity) and to generate tumors after transplantation into immunocompromised mice (tumorigenicity) [22].

After leukemias, GBM is the first solid tumor where a cell hierarchy including tumorigenic (stem) and non-tumorigenic (non-stem) cancer cells has been identified. Critical to this early success was the application and adaptation of the principles of prospective isolation and functional analysis established for leukemia stem cells, on the one hand, and *in vitro* propagation of normal neural stem cells as 'spheroids', on the other hand [23-25]. Later, by exploiting the spheroid culture method established for GBM stem cells, putative CSCs have been isolated and expanded from other several tumor types [26, 27].

Glioma spheroids (neurospheres)

The current standard for determining the presence of stem cells in dissociated neural tissues is through the neurosphere assay [28]. This *in vitro* assay employs serum-free, growth factor-supplemented medium and non-adherent conditions to create an environment that permits stem cells to proliferate and form clonal colonies, growing in suspensions as spheroids, called neurospheres. These clonal populations remain highly enriched in stem cells, which can be serially dissociated and replated to form additional neurospheres, thus displaying self-renewal and long-term proliferative ability. In the meantime, neurosphere cells retain other distinctive stem properties, such as (i) an undifferentiated phenotype and (ii) multilineage differentiative potential, i.e. the ability to generate neurons, astrocytes and/or oligodendrocytes when transferred on adherent plates and in a medium deprived of mitogens and supplied with serum [24, 28, 29] (Figure 2). The neurosphere assay crucially contributed to demonstrate the presence of stem/progenitor cells in human adult brain

[30], and to identify specific surface markers for direct isolation of these cells [31]. The neurosphere assay was then essential to show that cells displaying remarkable functional and molecular similarities with neural stem cells are present also in brain tumors, including glioblastoma and lower grade gliomas and medulloblastomas [5, 32-35].

Ignatova and coworkers were the first to report in human cortical gliomas the presence of stem-like cells able to form clonal spheres in serum-free and non-adherent culture conditions, which exhibit a multipotent differentiation potential and a gene expression profile suggestive of deregulated cellular signaling [33]. In 2004, Galli and collaborators reported the first isolation and detailed functional analysis of CSCs from adult human glioblastomas by rigorously applying the operational criteria used to define neural stem cells [5]. They showed the ability of glioblastoma-derived neurospheres to extensively self-renew *in vitro*, and to display a partial differentiation potential toward neural or glial lineages. Importantly, they showed the ability of neurospheres to generate *in vivo* tumors that recapitulate the histological feature distinctive of human glioblastomas, including pseudo-palisading necrosis, microvascular proliferation, and invasion; finally, they also showed that from these experimental tumors neurospheres can be rederived, and sustain serial transplantation of the tumor itself [5].

Interestingly, it was found that neurospheres mirrored the genotype and phenotype of primary tumors more closely than conventional cell lines selected in serum culture, an observation that confers to the model also the technical value of being a more faithful *in vitro* representative of glioblastoma cells [34].

Colorectal cancer spheroids (colospheres)

The first evidence that colorectal cancer follows the stem cell model was published in 2007 by two independent laboratories, which followed the same methodological approaches previously used to demonstrate the presence of CSCs in leukemia and brain tumors [6, 7]. Ricci-Vitiani and colleagues showed that cells isolated from primary colorectal tumors were able to grow indefinitely as tumor spheroids in a typical stem cell medium (i.e. serum free medium supplemented with EGF and bFGF), thus displaying self-renewal potential. Moreover, these cells maintained the ability to form tumors in mice that resembled the parental tumor, even after a high number of passages *in vitro*[7]. The evidence that colospheres are cell cultures enriched with cells displaying properties of colorectal CSCs was

supported by further works [36, 37]. Indeed, it was demonstrated that colospheres derived from a single-cell cloning expressed the CSCs markers and, when transplanted in mice, maintained the ability to generate a tumor identical to the parental [37]. Moreover, it was also shown that, in standard culture conditions (i.e. in the presence of serum and adhesive dishes), colospheres could differentiate into cells that lost the tumorigenic potential and expression of CSCs markers, and upregulated typical markers of intestinal differentiation[37].

1.2. CSCs can be prospectively isolated

A further step toward the understanding of the hierarchical nature and heterogeneous tumorigenic potential of glioblastoma, colorectal cancer and other tumors, was made by prospective isolation of stem-like cells, namely by the association of the cancer stem cell phenotype with the expression of a specific cell-surface marker. In first studies, CD133 (prominine-1) was found to mark CSCs in different types of brain tumors, including glioblastoma, pediatric medulloblastoma and ependymomas [35, 38, 39]. In addition, CD133 was exploited to identify CSCs in colorectal [6, 7] and pancreatic carcinomas [40]. CD133 itself appears to be a marker of normal neural stem cells in both humans [31] and mice [41]. By analogy with leukemic stem cells, cells isolated (usually by florescence-activated cell sorting) for their expression of a given marker deserve the title of cancer stem cells only if they satisfy rigorous operational criteria, such as (i) the ability to reform a phenotypic copy of the original tumor in immunocompromised mice; (ii) a frequency of tumor-initiating cells, measured by limiting dilution assay, greater than the tumor cell subpopulation negative for expression of the same marker; (iii) the ability to regenerate a cell hierarchy in the experimental tumor, from which they can be prospectively re-isolated, and sustain tumor serial transplantation [14, 22]. By this methodology, Singh and colleagues showed that the ability to form glioblastoma in SCID mice was an exclusive property of the CD133+ cell subpopulation. Indeed, as few as 100 CD133+ cells were capable of forming tumors, while up to 10^5 CD133- cells were ineffective. Notably, they also showed that the CD133+ cell subpopulation represented a minority of the overall tumor population, mostly composed by CD133- cells [35]. These findings greatly contributed to the general concept that cancer stem cells, in either leukemia or solid tumors, are present at low frequency, and can be unequivocally identified by cell surface markers.

Although theoretically elegant, prospective isolation of CSCs by means of cell surface markers has however proven to be often unreliable, in the case of glioblastoma as well as colorectal cancer [14, 42]. The universal validity and specificity of CD133 was questioned by several reports. It was shown that 40% of freshly isolated glioblastoma specimens do not contain CD133+ cells [43] and that, although with different kinetics and aggressiveness, both the CD133+ and CD133- daughter cells can generate tumors [44]. Also in colon cancer, CD133, as well as other markers (CD24, EpCam, CD44, CD166), did not prove to be robust enough to unequivocally isolate a pure subpopulation of colon CSCs. Indeed, in some cases CD133 can be expressed also by differentiated cells both in murine and human normal intestine [45]. Moreover, in metastatic colorectal cancer, it has been shown that also CD133- are tumorigenic [45]. Thus, although it remains firmly established that selecting for CD133+ cells can provide enrichment of the CSC fraction in some tumors, this marker is often associated with the CSC phenotype in a random and unpredictable fashion. Other than CD133, a number of cell surface markers have been exploited for the isolation of cell subsets enriched in CSCs, including CD44, CD24, epithelial cell adhesion molecule (EpCAM), also known as epithelial specific antigen (ESA), ATP-binding cassette B5 (ABCB5), as well as $Hoechst_{33342}$ exclusion by the side population cells [46]. It is still unclear whether these markers represent mere identifiers or can regulate CSC function. Notably, none of these markers is exclusively expressed by solid tumor CSCs, highlighting the imperative to delineate more specific markers or to use combinatorial markers. The dispute about marker validity for CSC identification is unsettled, but there is consensus in believing that, in tumors, markers should be used to integrate CSC identification based on demonstration of distinctive functional properties *in vitro* (sphere formation and long-term propagation) and *in vivo* (serial tumor transplantation) [47]. Importantly, more reliable markers should be searched not among proteins such as CD133, whose functional role is undetermined, but among those that actively sustain the stem phenotype. Surface proteins with a key role in modulating the self-renewal and tumorigenic capabilities of CSCs are, among others, tyrosine kinase receptors.

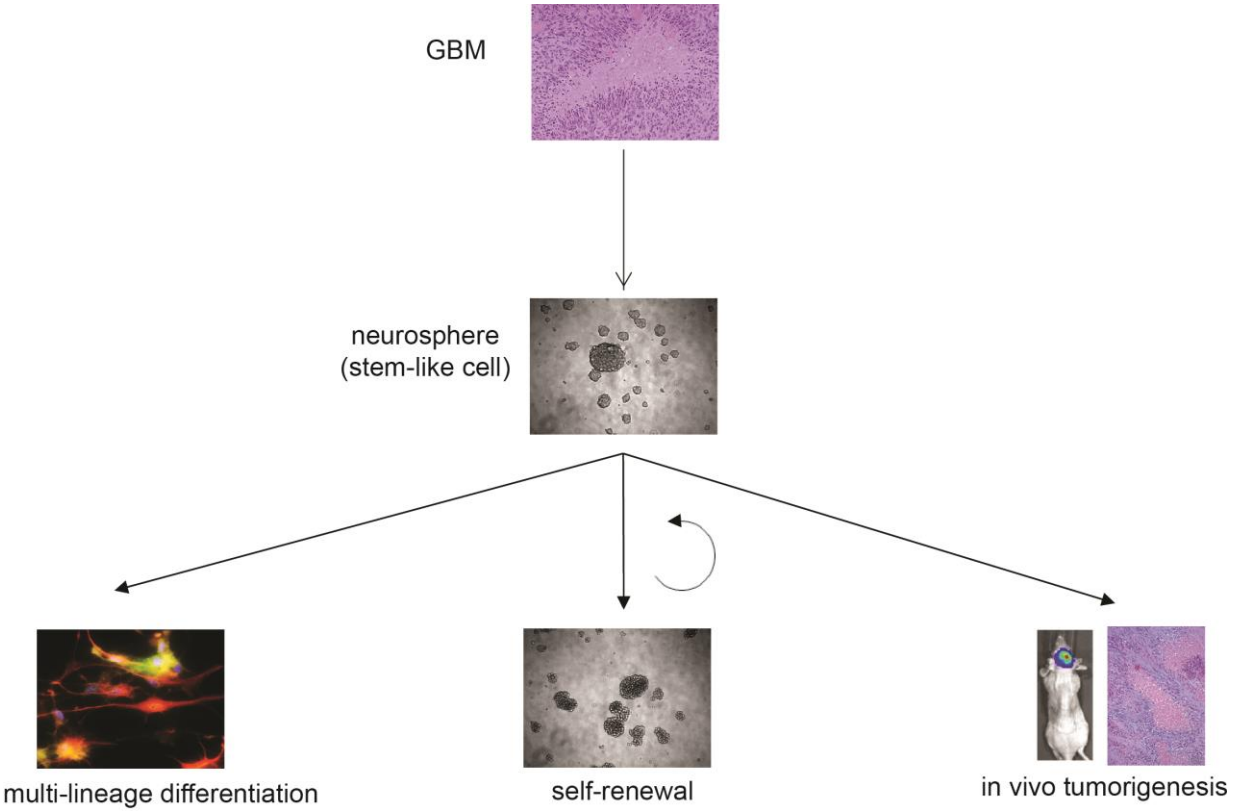

Figure 1. Isolation of glioblastoma stem-like cells in culture as neurospheres (modified from Vescovi et al., Nat Rev Cancer 2006) [24].

2. Cancer stem cells and radioresistance

Radiation therapy significantly contributed to cancer therapy. However, despite continuous improvements, as in the case of other therapeutic modalities, tumors develop adaptive responses and become more radioresistant, aggressive, and invasive [48].

A newly emerged plausible explanation for tumor radioresistance is the intrinsic refractoriness of CSCs to irradiation as well as chemotherapy [2, 49]. Taking into account that tumors can in principle arise even from a single residual CSC, the failure of radiation treatments might be attributed to the incomplete eradication of the CSC subpopulation[50]. First described for GBM and breast cancer, CSC radioresistance seems to be associated mainly with enhanced DNA-repair capacity and defense against reactive oxygen species (ROS), as compared to the non-CSC subpopulation [19, 20, 51, 52]. Ionizing radiation (IR) and radiomimetic drugs induce formation of double-strand breaks (DSBs) in DNA, eliciting in CSCs an efficient DNA-damage response (DDR) and cell survival. Conversely, in non-CSC DDR cannot efficiently repair DSBs, and persistence of DNA damage induces cell death by the so-called mitotic catastrophe [53]. Moreover, in some tumors, CSCs, like their normal counterparts, have been shown to contain more efficient antioxidant machinery and lower ROS levels compared to their non stem-like progeny [51]. As ROS are critical mediators of ionizing radiation-induced cell killing [54], CSCs develop less DNA damage and are preferentially spared after irradiation compared to non-CSC, which may contribute to tumor radioresistance.

CSCs can drive tumor recurrence not only by exploiting inherent/adaptive mechanisms of radioresistance, but also by evolving under therapeutic pressure. Tumor genetic heterogeneity implies coexistence of multiple tumor cell subclones, each fueled by a founder, genetically distinct CSC [22, 55-57]. Different genetic alterations can correlate with diverse ability to resist to radio-chemotherapy, thus conferring distinct selective advantages. Indeed, we have shown that CSCs isolated from glioblastomas recurring after chemo-radiotherapy harbor genetic alterations distinct from those found in CSC derived from primary tumors, but pre-existing in the primary tumor tissue [58].

Finally, it has been shown that radiotherapy itself can modulate the CSC phenotype, inducing the reprogramming of non-CSC into CSC, as observed in breast cancer, where radiation-induced breast CSCs displayed enhanced mammosphere formation and

tumorigenicity, and also expressed the same stemness-related genes as the breast CSCs isolated from non-irradiated samples [59]. Overall, molecular mechanisms underlying radiation resistance in tumors remain poorly understood and require more extensive characterization.

2.1. GSCs radioresistance: molecular mechanisms

GBM is one of the most lethal human malignancies (median survival 12-15 months) [60]. IR, either alone or adjuvant after surgery, is, together with temozolomide, part of standard treatment. However, prognosis of patients with glioblastoma still remains poor because of refractoriness to radio-chemotherapy [19, 61, 62].

It has been well demonstrated that IR causes single- and double-stranded DNA breaks that evoke a multifaceted DNA damage response (DDR). At the apex of the DDR lie the serine/threonine protein kinases ataxia telangiectasia mutated (ATM) and ataxia telangiectasia and Rad3-related (ATR), which safe-guard genomic integrity by activating p53, cell-cycle checkpoint kinases and the ensuing DNA-repair pathways [63, 64]. ATM is mainly activated by DNA double-strand breaks (DSBs), whereas ATR responds to single-stranded regions of DNA generated at stalled replication forks and during processing of DSBs by nucleases [65-67]. The MRN (MRE11–RAD50–NBS1) complex has key roles in sensing and processing DSBs as well as activating ATM and ATR [68]. ATR activates cell-cycle checkpoint kinase proteins, including Chk1, whereas ATM primarily activates Chk2. These downstream checkpoint kinases activate G1 and G2–M cell-cycle checkpoints, including phosphatases such as CDC25, eventually inhibiting cyclin-cyclin dependent kinases (cyclin-cdk) complexes and blocking the cell cycle [69] (Figure 2). Then enzymatic DNA repair mechanisms can operate, and, if the damage is repaired, cell cycle can resume.

In a seminal study, Bao et al. reported that CD133-positive represented the radioresistant cell subpopulation and could be the source of tumor recurrence after radiation [19]. This cell subpopulation showed to retain stem-like features and contributed to glioma radioresistance via preferential activation of the DNA damage checkpoint response and an increased DNA repair capacity: in both neurospheres and in intracranial xenografts, CD133-expressing cells survived IR relatively better compared to CD133-negative cells and activated Chk2-dependent checkpoint responses to a greater extent than CD133-negative cells [19].

In a follow-up study, it has been shown that, in GSCs, the ATM pathway is supported by L1CAM (CD171) [70]. In irradiated cells the L1CAM intracellular domain undergoes nuclear translocation and modulates c-Myc activity thereby regulating expression of NBS1, a critical component of the MRN complex that activates ATM [70].

Other groups have also shown that GSCs are more resistant to radiation compared to non-GSCs due to high expression of phosphorylated checkpoint proteins. For example, Squatrito and colleagues demonstrated that loss of ATM/Chk2/p53 pathway components accelerated tumor development and contributed to radiation resistance in gliomas. Chk2 seemed to be required for glioma response to IR *in vivo* and for DNA-damage checkpoints in neural stem cells [71]. Additionally, it was reported that the polycomb group protein BMI1 conferred radioresistance to GSCs through recruitment of the DNA damage response machinery [72].

Recently, it was also reported that inhibition of ATM kinase radiosensitizes GSCs and effectively abrogate the enhanced GSCs DSB repair proficiency [73]. In addition, inhibition of PARP, a key player in DNA single-strand break repair, has also been shown to overcome GSCs radioresistance [74].

These findings corroborate and extend the landmark study by Bao and colleagues, in which inhibition of Chk1 and Chk2 was shown to enhance the radiosensitivity of GSCs [19]. The observation that GSCs exhibit upregulated DDR signaling provides both opportunities and challenges. While targeting individual DDR components can clearly increase GSC radiosensitivity, it could be even more advantageous to broadly inhibit DDR, by interfering with upstream regulatory systems.

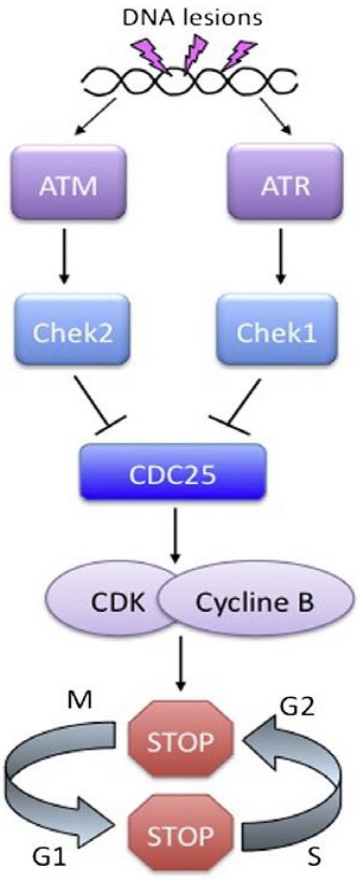

Figure 2. Upregulation of the cell cycle control mechanisms in CSCs. The family of checkpoint kinases (Chk1/2 kinases) is activated after ionizing radiation stress and arrest the cell cycle to allow DNA repair. In response to DSBs, ATM and ATR orchestrate the DNA damage repair, activating the downstream kinases Chk1 and Chk2. These kinases are expressed at higher basal and inducible levels in CSCs than in non-stem cells (from Moncharmont C. et al., Cancer letter 2012) [75].

3. Crosstalk between the Receptor Tyrosine Kinases (RTKs) signaling and the DDR in GBM radioresistance

Recently, it has been envisaged that GBM radioresistance can rely on RTK signaling. Indeed, RTK genetic alteration seems to be an essential oncogenic events in the majority of GBMs, leading to hyperactivation of PI3K/Akt/mTOR and Ras/Mitogen-Activated Protein Kinase (MAPK) downstream signaling pathways [76, 77]. Several studies have shown that the activation of these pathways in cancer cells is significantly associated with radiotherapy resistance, either through the modulation of cell survival signaling or by direct regulation of the DNA repair machinery [76].

The epidermal growth factor receptor (EGFR) is one of the most frequently altered RTK in GBM patients, being amplified in 40% of GBM overall and in 80% of GBMs of the "classical" subtype [76]. The first evidence indicating a possible role of EGFR in the regulation of DNA repair came from studies showing that EGFR directly interacts with DNA-dependent protein kinase (DNA-PK), one of the key components of the non-homologous end-joining (NHEJ) machinery [78]. This initial work, carried out in different mammalian cell lines (A431, DiFi, HER14 and MDA-MB453) was followed by reports showing that either IR or cisplatin induces the translocation of EGFR into the nucleus, where it interacts with, and promotes DNA-PK activity [79]. In another study, performed in lung and breast cancer cell lines, inhibition of EGFR nuclear translocation by pre-incubation with the EGFR antibody cetuximab, resulted in radiosensitization [80]. Similarly, cetuximab enhanced *in vitro* and, more importantly, *in vivo* radiosensitivity of head and neck squamous cell carcinoma [81, 82]. Recently, Golding and co-workers suggested that, in U87 glioma cells, EGFR signaling promotes both homologous recombination (HR) and NHEJ DNA repair mechanisms, in a EGF dose-dependent manner, an effect significantly reduced in the presence of a specific EGFR inhibitor [83].

$EGFR^{vIII}$, a deletion mutant of EGFR that lacks the extracellular ligand-binding domain, is the most common alteration leading to EGFR constitutive activation, reported in about 50% of EGFR-amplified GBMs [76]. Unlike activated EGFR, which stimulates both the Ras/Raf/MAPK and PI3K/Akt pathways, $EGFR^{vIII}$ appears to preferentially activate only the PI3K/Akt signaling cascade [83-85]. Interestingly, $EGFR^{vIII}$ and the PI3K/AKT pathway displays an increased activation in response to IR [86]. Consistently, inhibition of PI3K/Akt

signaling impaired DSB repair and enhanced radio-sensitivity of GBM harboring $EGFR^{vIII}$ [87, 88]. Moreover, Johns et al. showed that treatment with the anti-EGFR monoclonal antibody mab-806 radiosensitizes $EGFR^{vIII}$-positive U87 glioma cells [89]. Taken together, these data suggest that EGFR signaling, either directly through the interaction with the DNA repair machinery, or indirectly through the activation of PI3K/Akt and Ras/MAPK signaling pathways, modulates sensitivity to radiation, supporting the biological rationale for its targeting in association with IR, at least in the subset of glioma patients in which this signaling is hyperactivated.

Beside EGFR, several other RTK systems have been associated with cancer cells response to DDR and hence are considered as molecular targets for tumor radiosensitization.

The platelet-derived growth factor (PDGF) signaling is constitutively activated in a subset of GBMs, mostly belonging to the so-called “proneural” subtype, either as result of genetic alterations (such as PDGFRA gene amplification, intrachromosomal deletion, or activating point mutations), or by overexpression of the PDGF ligand [90]. Even though direct modulation of the DDR machinery by PDGFR has not been described to date, various reports showed that treatment with the PDGFR inhibitor imatinib increases radiation sensitivity in glioma cells *in vitro* and as well as in xenografts [91].

Although the molecular crosstalk between the RTK signaling and the DDR is beginning to be characterized in GBM, this issue has not been fully addressed in GSCs. EGFR signaling was known to sustain self-renewal and multipotency of neural stem cells [47], and was later found to support the stem and tumorigenic phenotype of GSCs propagated as neurospheres [92]. Activation of pro-survival PI3K/Akt pathway, which is downstream of EGFR and other RTKs, has been shown to be more intense in GSCs compared to non-stem glioma cells. Interestingly, Hambardzumyan et al. showed the importance of the activation of PI3K/Akt/mTOR pathway in conferring radioresistance in subpopulations of medulloblastoma cells, a highly malignant brain cancer [93]. Further characterization and, potentially, inhibition of these pathways hold promises to improve the current radiotherapy efficacy in glioma treatment by overcoming the intrinsic radioresistance of the GSC subpopulations.

Moreover, an increasing body of evidence suggested that MET signaling may also be linked with critical pathways of the DDR [94]. Interestingly, works previously carried out in our laboratory showed that the MET receptor tyrosine kinase (i) confers radioresistance to

tumor cells [95], and (ii) it is a functional marker of the GSC subpopulation [96]. In this thesis we showed that MET is specifically expressed in a subset of radioresistant GSCs and that its inhibition radiosensitize GSCs by impairing the DDR signaling.

4. The role of the MET oncogene in invasive growth and radioresistance

The MET oncogene, encoding the hepatocyte growth factor receptor, has been known for inducing invasive growth, a genetic program largely overlapping with epithelial–mesenchymal transition (EMT), and governing physiological and pathological processes such as tissue development and regeneration, as well as cancer dissemination [97]. Interestingly, it has been shown that induction of the EMT program by other factors results in concomitant acquisition of stem properties [98]. Consistently, we and others have shown that MET sustains both the stem and the invasive phenotype in glioblastoma stem cells (see below).

In human cancers, MET is affected by genetic alterations, such as mutations or amplifications, which lead to a constitutively activation of the receptor, either ligand-independent, or sensitive to otherwise subliminal HGF concentrations [99]. As result, the activated MET oncogene behaves as a cell-autonomous selectable driver of tumor growth. Consistently, MET amplification (i) sustains oncogene addiction, that is dependence for cell proliferation and survival [99], and (ii) is a selectable mechanism of resistance to therapies attacking other regulators of cell proliferation such as Epidermal Growth Factor Receptor (EGFR)[100, 101]. The role of MET in tumors is not restricted to the relatively rare genetic alterations (1–3% of tumors), but relies on the frequent overexpression of the wild-type gene [99, 102, 103]. In the latter case, activation of the tyrosine kinase requires the ligand HGF [102].

Recent studies showed that MET enables cells to overcome damages inflicted by cancer anti-proliferative targeted therapies, radiotherapy [95, 104, 105] or anti-angiogenic agents [106]. After exposure to such therapies, clones of MET-amplified cancer cells arise within the context of genetically heterogeneous tumors and drive recurrence [97]. As part of the invasive growth program, MET not only restores the proliferative signal, but it exerts an effective anti-apoptotic activity that protects from cell and DNA damaging agents. Indeed, this response arises either during targeted or conventional cancer therapies, such as

radiotherapy.

In our previous study, we showed that doses of ionizing radiation commonly used for tumor radiotherapy induce MET transcriptional upregulation in glioblastomas and other tumor types[95]. The signaling pathway leading to MET overexpression starts with ATM kinase, which orchestrate the DNA repair response, and among other effectors, ends in activating transcription nuclear factor kappa B (NF-kB), that upregulates a panel of genes responsible for adaptive response [107, 108]. These genes include MET that is overexpressed at the cell surface and thus undergoes ligand-independent activation or, at least, sensitization to otherwise subliminal HGF concentrations, which play a dual role by concomitantly promoting invasion and protecting from radiation induced apoptosis (Figure 3). Consistently, in mice xenografts treated with radiotherapy, MET inhibition results in increased cell death and tumor regression [95].

It was further shown that MET inhibition prevents formation of the RAD51-BRCA2 complex, required for DNA repair by homologous recombination [109]. Concerning the cell response to DNA damage, recent works highlight an intriguing interplay between MET and p53 [110, 111]. These studies suggest that MET effectively protects cells from death induced by DNA damage in the presence of normal p53, and can be even more active in case of p53 mutation [97].

Moreover, it was found that, as in the case of resistance to EGFR inhibitors, MET sustains primary radioresistance and can drive clonal selection under the pressure of radiotherapy. This was observed in mouse models of radiation-induced glioblastoma, where the most significant oncogenic event, possibly induced by DNA damage and then selected, was MET amplification [112].

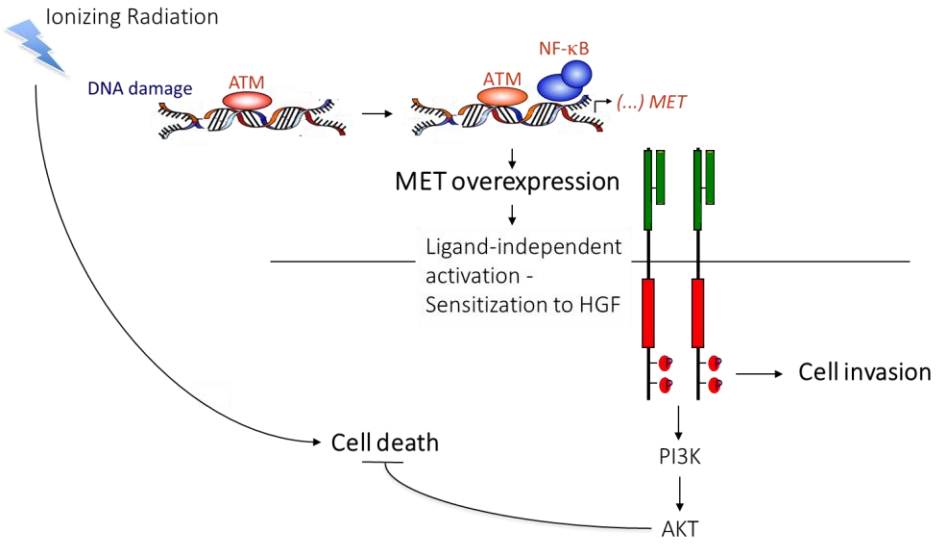

Figure 3. Effects of ionizing radiation (IR) on transcription and activation of the MET signaling pathway (modified from De Bacco et al., JNCI 2011) [95].

4.1. MET is predictive factor of poor prognosis in locally advanced rectal adenocarcinoma

Neoadjuvant chemoradiotherapy (CRT) followed by surgical resection, according to the principle of total mesorectal excision, is the standard treatment for locally advanced rectal cancer [113]. This approach, determines tumor downstaging in 28–62% [114] of the cases and improves local control [115]. However, irrespective of the tumor stage, treatment response is very heterogeneous, as complete tumor pathological regression is achieved in 10–30% of cases [114, 116] and many rectal cancer patients are resistant to preoperative CRT[117]. Moreover, tumor recurrence and metastasis, which develop after resection, are virtually inevitable and are a major cause of death. Recently, Senetta and colleagues have found that YKL-40 and MET immunohistochemical expression in pre-treatment rectal cancer biopsies reliably predicts a lack of response to neoadjuvant CRT [118]. Moreover, they demonstrated that MET and YKL-40 are independent predictors of poor response to CRT [118].

As MET is a candidate for target therapy [103] and a related marker of radioresistance [95], the efficacy of neoadjuvant CRT in these patients would benefit of therapy sensitizers, i.e. targeted MET-inhibitors to improve responsiveness.

5. Met is a functional marker of a glioblastoma stem cell subset

Biological proofs in normal tissues and preliminary results on tumors strongly support the evidence that MET is expressed by CSCs. In adult tissues MET expression is mainly localized to stem and progenitor cells compartments, as seen in the bone marrow, skeletal muscle, cardiac muscle and the epithelia of the gastrointestinal tract [102, 119]. Moreover, MET was also implied in neural stem cell self-renewal[120]. If cancer stem cells originate from the malignant transformation of normal stem cells or early progenitors, it is conceivable to assume that MET overexpression in tumors should also be a consequence of the expansion of a CSC subpopulation. This, together with the observation that MET expression can be increased in tumors by genetic lesions and by the reactive stroma, strongly suggests that MET overexpression will sensitize CSCs to HGF to switch on the invasive growth program, thus promoting invasiveness. Preliminary data regarding the expression and the function of MET in CSCs were obtained in glioblastoma [121] and colorectal cancer [122]. Interestingly, the study of Li and coworkers suggested that MET induces a network of reprogramming transcription factors (such as Sox2, c-Myc, Klf4, Oct and Nanog) that sustains the glioblastoma stem cell phenotype [121].

In our previous study, we showed the MET is preferentially expressed in a subset of neurospheres (~40%) (MET-positive-NS) derived from primary GBM, and that MET expression is almost mutually exclusive with EGFR and associate with distinct genetic alterations and transcriptional profiles: MET-positive-NS (EGFR-negative) preferentially showed to retain a wild-type EGFR gene together with mutation/deletion of PTEN tumor suppressor gene, and were classified as “mesenchymal” or “proneural” neurospheres, according to Verhaak’s signature [123]. Conversely, MET-negative-NS (EGFR-positive) showed to harbor EGFR amplification and PTEN wild type gene and mostly belonged to the so called “classical” subtype. These neurospheres displayed different biological properties *in vitro* and *in vivo*, thus suggesting that MET and EGFR identify different glioblastoma stem cell subtype. These findings seem consistent with observations in mouse model systems where brain progenitors inheriting high levels of EGFR give rise to astrocytes, whereas those inheriting low levels generate oligodendrocytes [124]. Moreover, we found that MET-positive neurospheres, although clonal, are heterogeneous and contain cells that express different levels of MET. MET-positive neurosphere cells could thus be sorted into MET^{high}

and MET^{neg} subpopulations (Figure 4), which displayed opposite properties. MET^{high} retains (i) long-term self-propagating and multi-potential ability *in vitro*; (ii) tumorigenic properties *in vivo*; (iii) ability to reconstitute a mixed MET^{high}/MET^{neg} population *in vitro* and *in vivo*. In contrast, the MET^{neg} subpopulation is devoid of any of the above properties. Thus, we concluded that, in MET positive neurospheres, MET marks a cell subset endowed with cancer stem cell properties, which generates a pseudo differentiating progeny losing stem and tumorigenic properties together with MET expression. Moreover, we showed that MET plays a functional role in glioblastoma stem cells, as the MET ligand HGF sustains their clonogenicity and long-term self-propagation, and, interestingly, also *in vitro* cell invasion, a typical property of "mesenchymal" cells [96].

Along with our study, a report by Joo and coworkers [125] showed that MET expression is heterogeneous within the same glioblastoma tissues, with dominant expression in two apparently unrelated regions: the proximities of blood vessels and the hypoxic edges. The first region may correspond to the "perivascular" niche, a microenvironment required to maintain glioblastoma stem-cell properties [126]. Hypoxic areas, which should be far from blood vessels and adjacent to necrotic areas, were previously associated with MET expression in many tumors, since a transcription factor activated by hypoxia (HIF1: Hypoxia-inducible factor 1) activates the MET gene promoter [106]. In the same study, MET was successfully used as a surface marker for prospective isolation of glioblastoma stem cells, and MET signaling was shown to actively sustain the stem phenotype [125]. In summary, MET seems a promising target to inhibit both glioblastoma growth and invasiveness, possibly by hitting CSCs. In this perspective, it would be crucial to better address the role of MET as a therapeutic target in the context of CSCs.

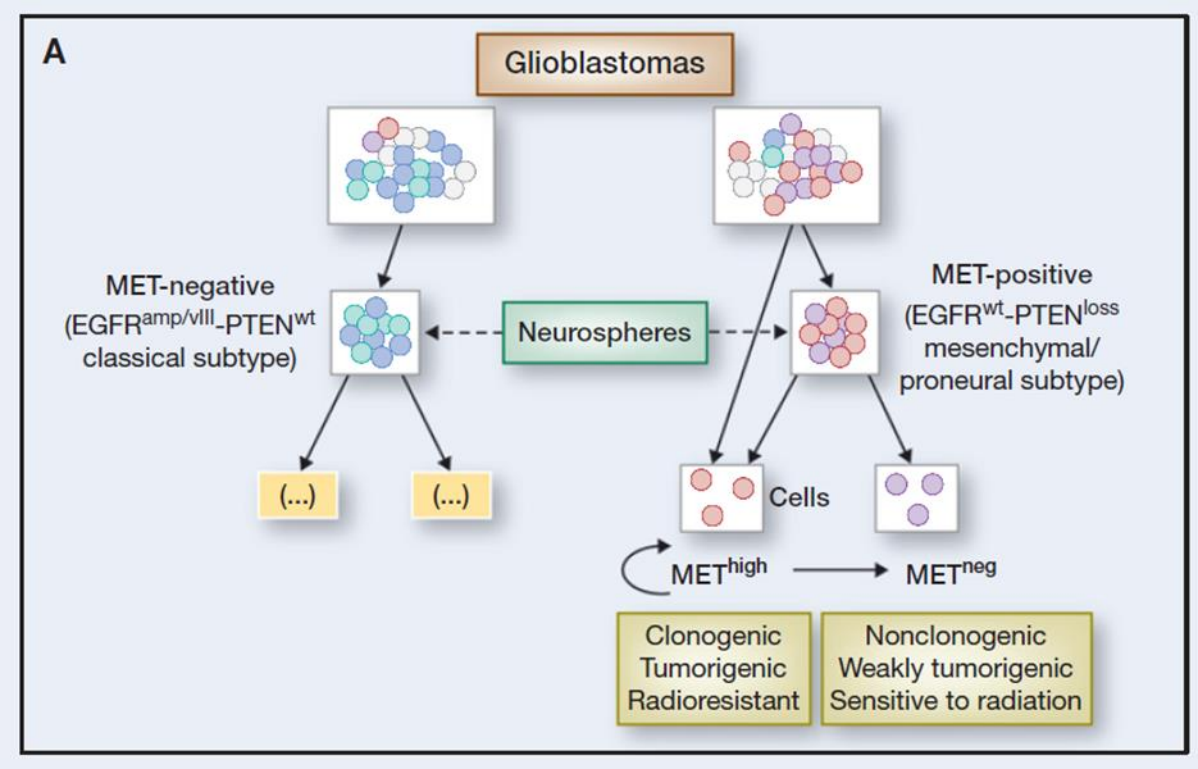

Figure 4. **MET and EGFR identify different glioblastoma stem cells** (from Boccaccio and Comoglio, Cancer Res 2013) [127].

Aim of the work

Failure of radiotherapy has been explained by the observation that a small subpopulation of cancer cells endowed with stem-like properties (cancer stem-like cells, CSCs) are inherently radioresistant, thanks to their ability to promptly activate the molecular mechanisms responsible for DNA repair. These mechanisms involve intracellular effectors whose activity is modulated by receptors that regulate cell proliferation and survival. In this line, we and others recently reported that the tyrosine kinase receptor for HGF, encoded by the MET proto-oncogene, sustains radioresistance of conventional cell lines and that MET behaves as a functional marker of a glioblastoma stem cell subset (GSCs).

Based on this evidence, the primary aim of this PhD project was to investigate whether MET could mediate GSC radioresistance and whether it could be exploited as a therapeutic target to achieve radiosensitization of glioblastoma (GBM), a lethal tumor whose genetic heterogeneity hampers targeted therapy, and whose treatment is still mainly based on radiotherapy.

In the first section of the work, our data provide evidence that MET is a marker of radioresistance in GSCs and that MET inhibition radiosensitizes a subgroup of MET-expressing GBM by targeting and depleting the GSC subpopulation.

These findings compelled us to investigate whether this experimental approach could be extended to the radiosensitization of other tumors whose radioresistance depends on MET. Such tumors can include locally advanced rectal cancer, where MET expression was recently found to be a predictive marker of poor response to the neoadjuvant radiotherapy.

As limited information is available on CSCs derived from rectal cancer, in the second part of the thesis, we isolated and characterized rectal cancer stem-like cells (RSCSs), and we investigated their radiosensitization through MET inhibition.

Materials and methods

Neurosphere derivation from human patients and culture

From 20 surgical samples of consecutive primary GBM (provided by the Fondazione IRCCS Istituto Neurologico C. Besta, according to a protocol approved by the institutional Ethical Committee), neurospheres were derived by mechanical dissociation and digestion of tumor specimens with collagenase I (Life Technologies-Invitrogen). Single cell suspensions were plated at clonal density (1-10 cells/ul) in standard stem cell medium containing: DMEM/F-12 (Life technologies-GIBCO), 2mM glutamine (Sigma), penicillin-streptomycin (1:100, EuroClone), B27 (1:50, Life Technologies-GIBCO), human recombinant fibroblast growth factor 2 (bFGF, 20 ng/ml; Peprotech) and epidermal growth factor (EGF, 20 ng/ml; Peprotech). During the first passages, medium was replaced or supplemented with fresh growth factors until cells started to grow forming floating aggregates. To expand cultures, spheres were mechanically dissociated, counted with trypan blue to evaluate the number of live cells, and then re-plated as single cells at clonal density in complete fresh medium. Cells were incubated at 37°C, 5 % CO_2, H_2O saturated atmosphere.

For *in vitro* experiments, neurospheres were kept in a modified medium with a lower concentration of EGF and bFGF (10 ng/ml), and supplemented with human recombinant HGF (10 ng/ml). Both media sustain the same NS proliferation rate (data not shown).

Xeno-rectosphere derivation from PDXs and culture

All procedures involving animal experimentation were approved by the Italian Ministry of Health and by the internal Ethical Committee for Animal Experimentation (FPRC-CESA). Xenopatients (PDXs) were obtained as described [128] and their tumors were mechanically dissociated, digested with Collagenase I (1 mg/ml, Life Technologies-Invitrogen), filtered through a 70 µm cell strainer (BD Falcon), and cleared with histopaque-1077 (Sigma), according to manufacturer instructions. Single cell suspension were plated in ultra-low attachment plastics (Sigma-Corning) at clonal density (1-10 cells/ul) in standard stem cell medium containing: DMEM/F-12 (Life technologies-GIBCO), 2mM glutamine (Sigma), penicillin-streptomycin (1:100, EuroClone), N2 supplements (Life Technologies-GIBCO), 0,4% BSA (Sigma); 4 µg/ml heparin (Sigma), CD Lipid human recombinant concentrate (1:100, Life Technologies-GIBCO), human fibroblast growth factor 2 (bFGF, 10 ng/ml; Peprotech) and epidermal growth factor (EGF, 20 ng/ml; Peprotech). To expand cultures, spheres were enzymatically dissociated using ATV (0.05% trypsin, 0.1% glucose and 0.5 nM EDTA), counted with trypan blue to evaluate the number of live cells, and then re-plated as single

cells at clonal density in complete fresh medium. Cells were incubated at 37°C, 5 % CO_2, H_2O saturated atmosphere. For *in vitro* experiments, where indicated, xeno-rectospheres were cultured supplemented with human recombinant HGF (10 ng/ul) or in basal medium completely avoid of exogenous factors.

Nucleic acid extraction

From neurospheres and xeno-rectospheres, nucleic acids were extracted as follows: genomic DNA (gDNA), using the Wizard® Genomic DNA Purification kit (Promega); total RNA, using the mRNeasy Mini kit (Qiagen), according to manufacturer's instructions. Extracted purified nucleic acids were quantified with Nanodrop ND1000 (Thermo Scientific).

Copy number analysis

EGFR, PDGFRA, MET, HGF, CDKN2A, PTEN, PIK3CA and IGF2 gene copy number was assessed on gDNA with real-time PCR using TaqMan® Copy Number Assays (Applied Biosystems). Relative gene copy number data were calculated by normalizing against endogenous controls (TERT, GREB1 and RNase P). A normal diploid human gDNA was used as calibrator to obtain ΔΔCt. The copy number of each gene was calculated with the formula 2x 2-ΔΔCt. Homozygous deletion was define by lack of PCR amplification for the target gene in the presence of PCR product for control probles; heterozygous deletion was defined by a copy number <1,5; a copy number between 1.5 and 3 was considered as normal. PDGFR and IGF2 amplification was defined by a copy number higher than 5 while to discriminate between real EGFR or MET amplification and polysomy of the chromosome harboring the two genes (Chr7), the calculated copy number was normalized against the copy number of another gene mapped on chr7, and usually not amplified (HGF). We define true amplification only a copy number difference between EGFR and HGF, or MET and HGF, greater than 5. Copy number included between 3 and amplified was considered as copy number gain.

Gene sequencing

TP53 (full coding region except exon 3), PTEN, APC (exon 15), IDH1 (exon4), KRAS (exon 2,3,4), NRAS (exon 2,3), BRAF (exon 2), PIK3CA (exon 9,20) purified gDNAs were amplified using Platinum® Taq DNA Polymerase (Invitrogen) and specific primer pairs described in [129, 130]. PCR conditions were as follow: 95°C for 3 min; 3 x [95°c for 15 sec, 64°C for

30sec, and 70°C for 1 min]; 3x [95°C for 15 sec, 61 °C for 30 sec, and 70°C for 1 min]; and 70°C for 5 min. PCR products were purified using ExoSAP-IT® (Affimetrix) according to manufacturer's instructions. Cycle sequencing was carried out using BigDye Terminator v3.1 Cycle Sequencing kit (Applied Biosystems). Sequencing products were purified using Agencourt CleanSeq (Agencourt Bioscience, Beckman Coulter) and analyzed on a 3730 DNA Analyzer ABI capillary electrophoresis system (Applied Biosystems). Sequences were then analyzed using Chromas Lite 2.01 software (http://www.technelysium.com.au/chromas_lite.html) and compared with reference sequences from the Homo sapiens assembly GRCh37 (February 2009).

All identified mutations were than compared with those reported in the Catalogue of Somatic Mutations in Cancer (COSMIC, http://www.sanger.ac.uk/genetics/CGP/cosmic/).

Microarray analysis

Gene expression profiling and neurospheres classification according to Verhaak's subtypes[123] was performed as previously described[96].

Real-Time PCR

500 ng of purified mRNA was reverse-transcribed using High Capacity Reverse Transcriptase kit (Applied Biosystem) according to manufacturer's instructions. Real-time PCR was performed using commercially available primers and probe sets for MET, RAD51, and ATM with TaqMan PCR Master Mix (Applied Biosystems), and ABI PRISM 7900HT sequence detection system. Expression levels were normalized against endogenous controls (β2 microglobulin or β actin) and non-treated cells were used as calibrator. Reported values are the mean ± SEM of at least two independent experiments in triplicate.

Immunophenotypical analysis and Fluorescence-Activated Cell Sorting

Neurospheres and xeno-rectospheres were dissociated and resuspended in PBS 3% BSA at a concentration of 2×10^5 cells/100 µl. The following antibodies were used: HGF R/c-MET-PE (clone 95106, R&D System); EGFR-PE (clone EGFR.1, Invitrogen); BMI-1-PE (clone 384515, R&D System); SOX2-APC (clone 245610, R&D System); CD44-FITC (clone MEM-263, Immunological Sciences); Notch-1-APC (clone 527425, R&D System); Nestin-APC (clone 196908, R&D System); CD133/2-PE (clone AC141, Miltenyi Biotec GmbH); CD24-FITC (clone

SN3, Invitrogen). Before analysis, DAPI (Roche) was added to exclude dead cells. Analysis was performed on a CyAn ADP (Beckman Coulter) equipped with 488 nM, 405 nM and 642 nM solid state lasers. Data were collected and processed using Summit 4.3 software (Beckman Coulter). For Fluorescence-Activated Cell Sorting, dissociated cells were stained with anti-MET-PE antibodies, and filtered with Filcons filters (50 µm, BD Biosciences) to avoid aggregates. Cell sorting was performed with a MoFlo™ XDP nine-color cell sorter (Beckman Coulter).

Lentiviral transduction of neurospheres

Neurospheres were dissociated to single-cell suspensions, and 10^5 cells were transduced in standard medium with lentiviral particles expressing a bicistronic luciferase-GFP construct (CMV-Luc-IRES-GFP [131]) at a Multiplicity Of Infection (MOI) of 5. Transduction efficiency was determined 72 h post-infection by quantifying the amount of GFP-positive cells by FACS analysis (an average of 95% and 99% was obtained).

GBM and rectal cancer xenograft models

All animal procedures were approved by the internal Ethical Committee for Animal Experimentation (FPRC-CESA) and by the Italian Ministry of Health. To generate xenograft models, neurospheres and xeno-rectospheres were dissociated into single-cell suspensions, and injected subcutaneously or orthotopically into 6-8 weeks old female NOD.CB17-Prkdcscid/J mice (Charles River Laboratories).

For subcutaneous transplantation, 10^5 cells were resuspended in 100 µl 1:1 v/v PBS/Matrigel (BD Biosciences) and injected into the right flank. Tumor diameters were measured every 3 days by caliper and tumor volume was calculated using the formula: $4/3\pi \times (d/2)2 \times (D/2)$, where d and D are the minor and the major tumor axis, respectively. Tumors were established upon reaching an average volume of 400 mm^3. For neurospheres orthotopic transplantation, 2.5×10^5 cells expressing the bicistronic luciferase-GFP construct (see above) were resuspended in 2 µl PBS, and delivered into the corpus striatum of the right hemisphere by stereotactic injection (coordinates were as follows: antero-posterior = + 0.8 mm; medio-lateral = + 2.0 mm; dorso-ventral = − 3.0 mm). Intracranial tumor growth was monitored by bioluminescence (BLI) imaging (IVIS® SpectrumCT, Caliper Life Sciences) once a week until animals reached the clinical or experimental endpoints. For BLI, luciferin

(firefly D-Luciferin potassium salt, Caliper Life Sciences) was dissolved in PBS (150 mg/kg) and administered to mice by subcutaneous injection. Mice were anesthetized with 2.5% isoflurane in 100% oxygen at a flow rate of 1 L/min.

Immunohistochemistry analysis of GBM and rectal cancer xenografts

Tumors explanted from GBM xenografts were formalin-fixed and paraffin-embedded according to standard procedures. 4-µm thick tissue sections were dried in a 37°C oven overnight. Slides were de-paraffinized in xylene and rehydrated through graded alcohol to water. Endogenous peroxidase was blocked in 3% hydrogen peroxide for 30 minutes. Microwave antigen retrieval was carried out using a microwave oven (750 W for 10 minutes) in 10 mmol/L citrate buffer, pH 6.0. Slides were incubated with individual primary antibodies overnight at 4°C inside a moist chamber. After washings in TBS, anti-rabbit secondary antibody (DakoEnvision+System-horseradish peroxidase–labeled polymer, Dako) was added. Incubations were carried out for 1 hour at room temperature. Immunoreactivities were revealed by incubation in diaminobenzidine (DAB) chromogen (DakoCytomation Liquid DAB Substrate Chromogen System, Dako) for 10 minutes. Slides were counterstained in Mayer's hematoxylin, dehydrated in graded alcohol and cleared in xylene. A negative control slide was processed with secondary antibody, omitting primary antibody incubation. The following antibodies were used: anti-human Ki67 mouse clone MIB1 1:100, Dako; anti-human EGFR mouse clone E30 1:20, Dako; anti-MET rabbit (C12) 1:50, Santa Cruz Biotecnology.

In the case of rectal cancer xenografts and the matched human tumors, 3µm thick serial paraffin sections were collected and processed by immunohistochemistry using an automated immunostainer (Ventana BenchMark AutoStainer, Ventana Medical Systems, Tucson, AZ, USA) with antibodies against anti-human cytokeratin 7 (CK7) rabbit monoclonal (SP52), Ventana (Roche®); anti-human cytokeratin 20 (CK20), mouse monoclonal (ks20.8), Dako; anti-human CDX2, mouse monoclonal (dak-cdx2), Dako. The antigen retrieval step was included in the automated programme. DAB (Ventana Medical Systems, Tucson, AZ, USA) was used as the chromogen, according to standard protocols. Images were captured with the LEICA LAS EZ software with the use of a LEICA ICC50 HD microscope.

Limiting dilution sphere forming assay *in vitro*

Limiting dilution sphere forming assay was performed to assess the frequency of GSC in (i) neurospheres established from original tumors, or (ii) in cells freshly dissociated from xenografts obtained by neurospheres transplantation, or (iii) to assess the frequency of RSC in xeno-rectospheres derived from rectal PDX. Cells were plated into 96-well plates at decreasing concentrations (ranging from 150 cells/well to 1 cell/well). The number of growing spheres was counted 14 days after seeding. Data were evaluated through the ELDA software (http://bioinf.wehi.edu.au/software/elda/) [132], and reported as percentage of stem-like cells ± CI.

Serial transplantation assay

Neurospheres were irradiated *in vitro* (p0) with a 5 Gy single dose. 24 hrs after irradiation 10^3 cells, both from irradiated and control groups, were resuspended in 100 µl v/v PBS/Matrigel, and subcutaneously injected in 4 mice (p1). Tumor formation was monitored once a week by caliper as described above. From p1 tumors, cells were dissociated as described above for human tumor specimens, and, when neurospheres formed, 10^3 cells in 100 µl v/v PBS/Matrigel were subcutaneously injected in 6 mice (p2). From p2 tumors, cell isolation and neurospheres formation was repeated as above, and cells were assessed by *in vivo* limiting dilution assay, by injecting 10, 10^2, 10^3, or 10^4 cells in 6 mice per condition (p3). Frequency of stem-like cells was calculated using ELDA software as above and reported as stem-like cells per 10,000 cells.

Immunofluorescence analysis

GBM xenograft specimens were embedded in OCT, cryo-sectioned at 10 µm, and incubated with mouse monoclonal anti-Met DO-24 (1:100 in PBS/1% BSA) [133], followed by anti-mouse Alexa-Fluor 555 (1:1000, Molecular Probes by Life Technologies) and nuclei counter-stain with DAPI, according to standard protocols. Images were acquired with Leica fluorescence microscope (LEICA DMI 3000 B) and the Relative Fluorescence Intensity was estimated with Leica LAS AF lite software, counting at least 6 HPF (63× magnification) in two sections from each tumor, for a total of 3 mice/group.

Western blotting

Protein expression and phosphorylation were analyzed in whole-cell lysates solubilized in boiling Laemmli buffer or RIPA buffer or in snap-frozen and mechanically dissociated xenograft tissues, solubilized in RIPA buffer. Equal amounts of proteins were resolved by SDS-PAGE in reducing conditions and analyzed by western blotting with the following antibodies: rabbit polyclonal anti-MET (C12; #SC-10, Santa Cruz Biotechnology), anti-AKT (#BK9272), anti-phospho-AKT (#BK4060), antiphospho-Chk2 (#BK2661), anti-RAD51 (#BK8875), anti-phospho H2AX (#BK9718), anti-cleaved caspase 3 (#BK9664), anti-cleaved PARP (#BK9546) and anti-ATM (#BK2873) (Cell Signaling Technology), and anti-phospho MET (Tyr 1349) (#04-1063, Merck Millipore), and mouse-monoclonal anti-phospho ATM (#ab1292, Abcam). For control of equal amount of sample loading, rabbit polyclonal anti-β actin (#8457), anti-GAPDH (#5174), anti-H3 (#4499) (Cell Signaling Technology), or antivinculin (#V9131, Sigma) antibodies were used. Antibodies were visualized with appropriate horseradish peroxidase-conjugated secondary antibodies (Amersham), and the enhanced chemiluminescence system (Promega). Blot images were captured using a molecular imager (GelDoc XR; Bio-Rad Laboratories) and are representative of results obtained in at least two independent experiments.

Collection of matched primary and recurrent human GBMs

Surgical samples were derived from primary and matched recurrent GBMs surgically removed at the Spedali Civili di Brescia, according to a protocol approved by the institutional Ethical Committee. All Patients signed an informed consent. Patients were treated with standard fractionated radiotherapy (60 Gy) and concomitant chemotherapy (75 mg/m2 of Temozolomide) on daily basis for 6 weeks, and then with Temozolomide alone (150-200 mg/m2) for 5 days in a 28-day for 6 cycles, and up to 12 cycles, if no treatment related adverse events were noted or there was no evidence of tumor progression based on both clinical evaluation and MRI findings. At tumor progression, second surgery was performed, and a second line treatment was offered to selected Patients (Fotemustine).

Immunohistochemical staining of MET on matched primary/recurrent GBMs.

MET immunohistochemical staining were performed on representative paraffin embedded sections (2 μm thick), incubated with rabbit polyclonal anti-Met C12 (1:50 in TBS/1% BSA,

Santa Cruz Biotechnology), after blocking of endogenous peroxidase activity with 0.3% H2O2 in methanol and antigen retrieval in 1mM Citrate buffer (pH 6.0) in a thermostatic bath. Signal was revealed using the NovoLinkTM Polymer Detection System (NovocastraTM), followed by Diaminobenzidine (DAB) as chromogen and Hematoxylin as counterstain. Images were acquired with an OlympusBx60 microscope equipped with a DP70 camera and CellF imaging software (Soft Imaging System GmbH). Expression of MET was evaluated by two pathologist and was scored semi-quantitatively as percentage of positive cells and staining intensity. For the percentage of positive immunoreactive cells, the following scores were used: 0, 0-5%; 1, 6-29%; 2, 30-69%; and 3, 70-100%. The staining intensity was evaluated as follows: 0, negative staining; 1, low intensity; 2, moderate intensity; 3, strong intensity. The cumulative score (from 0 to 6) was obtained by adding the positivity score (percentage of positive immunoreactive cells) and the intensity score (staining intensity of cells).

Cell viability assay

To assess neurospheres and xeno-rectospheres viability, ATP cell content were measured using Cell Titer Glo® according to manufacturer's instructions. Cells were plated at clonal density (10 cells/µl) in 96-well plates, and treated as described 24 h after seeding (day 0). Cell viability were measured using a GloMax 96 Microplate Luminometer (Promega). Data are reported with respect to non-treated cells (or viability at time 0) as mean ± SEM of at least two independent experiments in quadruplicate.

Radiobiological clonogenic assay

Met^{high} and Met^{neg} cell subpopulations were sorted as described above and seeded as single cell/well. 24 h after sorting, cells were irradiated in the presence or in the absence of MET inhibitors, and then cultured for 14 days. The number of growing neurospheres was counted, and the surviving fraction was calculated using the formula, modified from [134]: [(n° of NS formed after treatment) / (PE)] x 100, where PE (plating efficiency) is the percentage of NS in control conditions. The reported values are the mean ± SEM of two independent experiments.

Neurospheres and xeno-rectospheres irradiation and treatment with inhibitors

Neurospheres and xeno-rectospheres were irradiated with a 200 kV X-ray blood irradiator (Gilardoni), and a 1 Gy/min dose-rate. In some experiments, HGF (20 ng/ml) was added to standard medium 1 h before irradiation. For MET targeting, the kinase inhibitors JNJ38877605 (500 nM, Janssen Pharmaceutica) [95] was added to cells 2 h before irradiation.

Irradiation and radiosensitization of GBM xenografts and rectal cancer-PDXs

To establish treatment groups and to minimize the effect of subjective bias, mice bearing subcutaneous tumors generated by neurospheres transplantation or rectal cancer-PDX of approximately 400mm^3, or intracranial tumors with a BLI average radiance signal of 7×10^5 p/s/sr/cm2, were randomized and group allocated by LAS software [135]. During randomization and generation of the experimental arms, mice were excluded from the studies if the tumor volume was indicated as outlier by LAS software. No tumor formation, due to technical problems during neurosphere injections, was also considered as a criterion of exclusion. Xenografted mice or rectal cancer-PDX were anesthetized by i.p. injection (zoletil 40 mg/kg + xylazine 7.5 mg/kg) and placed in a plexiglass pie cage (2Biological Instruments). Two days before irradiation, high-resolution CT scans (Toshiba Aquilion LB) were acquired to delineate the Planning Target Volume (PTV). For subcutaneous xenografts or rectal cancer-PDX, lungs and gastro-intestinal tract were considered organs at risk (OARs). For intracranial xenografts, the PTV corresponded to whole mouse head (no OARs exclusion). A total dose of 6 Gy for GBM models or 5,4 Gy for rectal cancer-PDX was delivered in 3 consecutive fractions (day 0, 1, 2) with TomoTherapy HD or the equivalent Hi-Art (Accuray, Inc.). TomoDirect Intensity Modulated Radiation Therapy (IMRT) technique was applied, allowing the delivery of 95% of the prescribed dose to PTV, while sparing OARs. In order to further optimize dose delivery, a bolus layer (ELASTO-GEL) was placed upon mice's body for subcutaneous xenografts and rectal cancer-PDX, and upon mice's head for intracranial tumors. Before the delivery of each IR dose, a Megavoltage Computed Tomography was performed in order to verify the correct mouse positioning. After irradiation, mice were awakened on a heating bed and housed in their cages. For radiosensitization experiments, in the case of GBM models mice were randomized into four groups: (i) vehicle treated; (ii) treated with IR (2 Gy × 3 consecutive days); (iii) treated with

JNJ38877605 (50 mg/kg, by daily oral gavage); (iv) treated with association of JNJ38877605 and IR as above (combo). In the latter case, JNJ-38877605 was administered starting from the day before irradiation (day -1), up to 15 or 30 days after irradiation in subcutaneous or orthotopic xenografts, respectively. For radiosensitization of rectal cancer-PDX mice were randomized into four groups: (i) vehicle treated; (ii) treated with IR (1,8 Gy × 3 consecutive days); (iii) treated with JNJ38877605 (50 mg/kg, by daily oral gavage) or Crizotinib (Pfizer®-PF-02341066, 50mg/kg, by daily oral gavage); (iv) treated with association of JNJ38877605 or Crizotinib (Pfizer ®) and IR as above (comboJNJ or comboCrz). In the latter case, JNJ-38877605 was administered starting from the day before irradiation (day -1), up to 15 or 20 days after irradiation. In an independent experiment JNJ-38877605 or Crizotinib (Pfizer ®) were administered from the day before irradiation (day -1), up to 10 days. Mice were monitored daily and, in case of systemic suffering, neurological symptoms or significant loss of body weight, were sacrificed by intraperitoneal (i.p.) anesthesia (zoletil 40 mg/kg + xylazine 7.5 mg/kg) followed by CO2 inhalation. In survival experiments (subcutaneous xenografts or rectal cancer-PDX) mice were sacrificed when tumor size reached the pre-established clinical endpoint of 1600 mm^3; animals euthanized before reaching the clinical endpoint were included in survival curve as censored observations. In GBM orthotopic model, mice were euthanized at day 62 (at the onset of neurological symptoms in the control group). Explanted brains were immediately analyzed for GFP signal detection (ex 465 nm, em 520 nm; IVIS® SpectrumCT).

Limiting dilution assay *in vivo*

In vivo serial dilution tumor-propagating assay was performed to evaluate the relative frequency of GSCs in subcutaneous xenografts after radiosensitization treatment. Subcutaneous xenografts were obtained as described above. Mice were randomized into four groups: (i) vehicle treated; (ii) treated with IR (2 Gy × 3 consecutive days); (iii) treated with JNJ38877605 (50 mg/kg, by daily oral gavage); (iv) treated with association of JNJ38877605 and IR as above (combo). The inhibitor JNJ-38877605 was administered starting from the day before irradiation (day -1) and prolonged up to day 10 in which 50% of tumor volume regression was reached in the combo group, as compared to day 0. At this point, tumors from each group were explanted and dissociated to re-derive tumor cells immediately cultured in stem conditions as described above. After cell recovery (about 10

days), single-cell suspensions of viable tumor-derived cells for each group (trypan blue exclusion test) were injected in the right flank of NOD-SCID mice at the following dilution dose 10, 10^2, 10^3 or 10^4 in 100 µl v/v PBS/Matrigel (6 mice/condition). The frequency of stem-like tumor propagating cells within heterogeneous cell populations was evaluate on the efficiency of secondary xenografts formation and data were evaluated through the ELDA software as above and reported as stem-like cells per 10,000 cells.

Collection of rectal cancer cases

Twenty-eight rectal cancer surgical specimens (formalin fixed-paraffin embedded samples, FFPE) were retrieved from consecutive cohorts from the archives of Candiolo Cancer Institute FPO-IRCC (pathology division). All patients had a locally advanced rectal adenocarcinoma (TNM classification: cT3-T4 stage). Six patients (21,4%) received neoadjuvant chemo/radiotherapy (CRT) or neodjuvant radiotherapy alone (RT) according to the standard criteria.

All patients provided informed consent, and samples were procured and the study was conducted under the approval of the review boards of the institutions.

Immunohistochemical staining of MET in rectal tumors and the matched PDXs

MET immunohistochemical staining were performed on representative paraffin embedded sections (3 µm thick) incubated with rabbit monoclonal anti-Met (SP44), Ventana (Roche ®) and processed by using an automated immunostainer (Ventana BenchMark AutoStainer, Ventana Medical Systems, Tucson, AZ, USA). Images were acquired with an OlympusBx50 microscope equipped with a DP70 camera and CellF imaging software (Soft Imaging System GmbH). Expression of MET on human samples was evaluated by two pathologists and was scored semi-quantitatively as percentage of positive cells and staining intensity. For the percentage of positive immunoreactive cells, the following scores were used: negative (neg.), <5%; low, 5-35%; mid, 36-75%; and high, >75%. The staining intensity was evaluated both in the cytoplasm and in the membrane of the cells, as follows: 0, negative staining; 1+, low intensity; 2+, moderate intensity; 3+, strong intensity. Combining the percentage of positive cells and the intensity of the staining, pathologists have identified four groups: MET high (>75%; intensity: at least 2+ in the membrane and/or in the cytoplasm); MET mid (36-

75%; intensity: from low to moderate); MET low (5-35%; intensity: from low to moderate); MET neg (<5%, intensity:low).

Tissue Microarray (TMA) construction and immunohistochemical analysis

For each rectal cancer-PDX, we selected the tumor foci for the TMA construction by marking them on the more representative hematoxylin–eosin (H&E)-stained slide with a waterproof pencil. The number of selected fields varied depending on the heterogeneity of the histological pattern and were at least three for each PDX tissue in triplicate (n=9 fields/condition). Care was taken to select areas from both the leading edge and the center of the tumor. In some cases, two different slides of the same tumor (corresponding to two different tissue blocks) were marked. One area of normal tissue was selected whenever possible to build up an internal control. TMA blocks were prepared and sliced by a dedicated technician and processed for immunohistochemical staining. Using the advanced tissue arrayer (mod. ATA-100, Chemicon International, Tamecula, CA, USA), tissue cylinders with a diameter of 1 mm were punched under the stereomicroscope from the specific areas of the "donor" block and brought into the "recipient" paraffin block. The block was incubated in an oven at 45°C for 20' to allow complete embedding of the grafted tissue cylinders in the paraffin of the recipient block, and then stored at 4°C until microtome sectioning. For immunohistochemical reaction, sections of 3 µm thick were collected on Super Frost Plus slides (Menzel Glaser, Braunschweig, Germany) and processed by immunohistochemistry using an automated immunostainer (Ventana BenchMark AutoStainer, Ventana Medical Systems, Tucson, AZ, USA) with antibodies against Ki67 (Dako; mouse monoclonal, clone MIB1, 1:100) and phospho-S6 ribosomal protein (Cell Signaling Technology; rabbit polyclonal #4858, 1:100).The antigen retrieval step was included in the automated programme. Diaminobenzidine (Ventana Medical Systems, Tucson, AZ, USA) was used as the chromogen, according to standard protocols. Images were captured with the LEICA LAS EZ software with the use of a LEICA ICC50 HD microscope. Positive cells quantification was performed using NIH ImageJ software (National Institutes of Health, Bethesda, MD). Ki67 (brown nuclei) and phospho-S6 (brown cytoplasmatic area) stainings were quantified by averaging the number of immunoreactive cells in 3 high-power fields (HPF) (×10 magnification) for each PDX (n = 3 per group), excluding the necrotic area.

Statistical analysis

Values were expressed as mean ± standard error of the mean (SEM). Student *t*-test, one-way Analysis of Variance (ANOVA) or Wilcoxon test were used as indicated. Survival curves were analyzed using the Kaplan-Meier method with groups compared by respective median survival; log-rank P value was measured using the Mantel-Cox test. Chi-squared tests and confidence intervals 95% (CI 95%) for limiting dilution assays were performed by ELDA software. A p-value < 0.05 was considered to be significant for all the statistical tests used.

Results

1. Genetic, phenotypic and functional characterization of glioblastoma stem-like cells (GSCs)

In collaboration with the group of Dr. G. Finocchiaro (Istituto Neurologico C. Besta, Milan, Italy), we derived neurospheres (NS) from 20 human GBM samples removed by surgery without prior treatments.

NS were analyzed for the presence of genetic alterations known to occur at high frequency in GBM, such as: copy number alterations of EGFR, PDGFRA, MET, PTEN and CDKN2A and mutations of TP53, PTEN and IDH1. NS were then classified as proneural, classical, or mesenchymal by transcriptional profiling, according to the Verhaak's signature [123] (Table 1).

We have previously shown that the MET oncogene is preferentially expressed in a subset of NS (~40%). Interestingly, MET expression is almost mutually exclusive with EGFR and associates with distinct genetic alterations and transcriptional profiles: MET-pos-NS (EGFR-negative) preferentially retain a wild-type EGFR gene together with mutation/deletion of PTEN tumor suppressor gene, and are classified as "mesenchymal" or "proneural" NS. Conversely, MET-neg-NS (EGFR-positive) usually harbor EGFR amplification and PTEN wild type gene, and basically belong to the "classical" subtype [96]. We further demonstrated that in each MET-pos-NS MET marks and functionally sustains a GSC subpopulation retaining cancer stem-like cell properties [96].

To investigate the relationship between MET expression and GSC radioresistance, from our panel we chose a subset of MET-pos-NS (Table 2).

In order to assess the stem-like phenotype of the established MET-pos-NS, we analyzed the expression of some relevant stem markers such as BMI-1, SOX2, Nestin, CD44, Notch-1 and CD133, which have been proposed as specific of the stem-like cell subpopulation [35, 123, 136-139]. Flow cytometric analysis showed that in MET-pos-NS, BMI-1, SOX2 and Nestin are expressed at high levels by the majority of cells, while Notch-1, CD44 and CD133 are more heterogeneously expressed among and within neurospheres (Figure 1A). Moreover, this analysis showed that in MET-pos-NS, EGFR expression is barely detectable or absent [96] (Figure 1A).

All MET-pos-NS displayed the features of GSCs, namely, self-renewal, clonogenicity, and tumorigenicity, as they propagated *in vitro* at clonal density for an indefinite number of

passages, and generated tumors that phenocopy the originals after transplantation both subcutaneously and intracranially in NOD-SCID mice.

Histopathologic analysis of subcutaneous xenografts demonstrate a striking glioblastoma-like tissue pattern. This was characterized by the presence of several areas of necrosis and many mitotic figures (Figure 1B). Notably, tumors derived from conventional glioblastoma cell lines usually do not display human glioblastoma-specific features [5]. Strikingly, when transplanted orthotopically, MET-pos-NS were able to form intracranial tumors characterized by the presence of several areas of necrosis surrounded by typical pseudo-palisade structures (Figure 1C), an elevated extent of proliferation as measured by Ki67 staining (Figure 1D) and, in some cases, a migratory and infiltrative pattern distinctive of human GBM (data not shown). Interestingly, immunohistochemical analysis showed that xenografts derived from MET-pos-NS gave rise in turn to MET-positive/EGFR-negative glioblastomas, maintaining the specific pattern of mutual exclusion (Figure 1D).

Neurosphere code	EGFR^{CNA}	PDGFRA^{CNA}	MET^{CNA}	CDKN2A^{CNA}	PTEN^{CNA}	PTEN (full coding region)		TP53 (full coding region -Ex3)		IDH1 (hot spot)		GEP
						Mutation	Consequence	Mutation	Consequence	Mutation	Consequence	Subtype (a)
BT205	+ +	+ +	+	- -	wt	c.955-958delACTT	p.T319fs*1	760-762delATC	p.I254del	-	-	CL
BT287	+	wt	wt	- -	-	c.16A>G	p.K6E*	c.814G>A c.818G>A	p.V272M p.R273H	-	-	MES
BT302	+	+ +	+	- -	-	c.389G>A	p.R130Q	-	-	-	-	MES
BT308	+	+ +	+	wt	wt	c.673-674delTA	p.Y225fs*17	c.490A>C c.833C>G	p.K164Q p.P278R	-	-	PN
BT314	+	+	+	wt	wt	c.493G>A	p.G165R	c.722C>T	p.S241F	-	-	PN
BT328	+	wt	+	- -	wt	c.69_79delAGACT TGACCT	Splicing	c.524G>A c.643A>G	p.R175H p.S215G	-	-	CL
BT337	+	wt	wt	- -	-	-	-	-	-	-	-	PN
BT347	+	wt	+	- -	-	c.801+1G>C	Splicing	c.844C>T	p.R282W	-	-	MES
BT371	wt	-	wt	wt	-	-	-	c.455C>T	p.P152L	-	-	MES
BT398	+	wt	wt	- -	- -	Exon 1 deletion	p?	-	-	-	-	CL
BT437	+	wt	-	- -	- -	Exon 2 deletion	p.?	-	-	-	-	CL
BT452	+ +	+	wt	- -	wt	c.388delC	p.R130fs*4	c.734G>A	p.G245D	-	-	MES
BT463	+	+	wt	wt	wt	-	-	c.659A>C	p.Y220S	-	-	PN
BT273	+ +	+ +	+	- -	-	-	-	c.731G>A	p.G244D	-	-	CL
BT275	+ +	+ +	+	- -	-	-	-	c.745A>G	p.R249G	-	-	CL
BT334	+ +	+	+	- -	-	-	-	-	-	-	-	CL
BT358	+ +	+	wt	wt	-	-	-	-	-	-	-	MES
BT373	+ +	+	+	wt	-	-	-	-	-	-	-	CL/PN
BT421	wt	wt	-	wt	-	c.82A>G	p.? p.I28V	-	-	-	-	CL
BT443	+	+	wt	- -	wt	-	-	c.530C>G	p.P177R	-	-	CL

Table 1. Neurosphere genetic alterations. Copy number alterations are expressed as follows: --: homozygous deletion (lack of PCR amplification for the target gene in the presence of a PCR product for control probes); -: heterozygous loss (copy number <1.5); wt: copy number between 1.5 and 3; ++: amplification (PDGFR copy number >5; copy number difference between EGFR and HGF or MET and HGF greater than 5) +: copy number gain (copy number >3 in absence of amplification).PTEN, TP53 and IDH1 mutations are indicated on both coding and protein sequences. (a): gene expression profile (GEP) subtype according to the Verhaak's signature [123] ; CL:classical;MES:mesenchymal;PN:proneural.

	NS	MET mRNA[a]	MET protein (% pos cells)[b]	HGF mRNA[a]	HGF protein (a.u.)[c]
MET-pos-NS	**BT205**	5.9	5.1 ± 0.1	3.11	8.8
	BT287	12.7	64.22 ± 0.28	11.66	n.a.
	BT302	7.4	17 ± 2	4.6	2.4
	BT308	13.7	46 ± 2	3.26	5.2
	BT314	3.1	15.5 ± 0.5	11.09	3.4
	BT328	12.6	16.77 ± 4.77	3.02	n.a.
	BT337	12.5	92 ± 2	neg	0.8
	BT347	9.5	17.75 ± 1.25	6.497	n.a.
	BT371	15.4	90.5 ± 8.5	7.6	2
	BT398	11	93.04 ± 1.045	6.75	n.a.
	BT437	8.4	17.91 ± 3.03	4.21	n.a.
	BT452	13.8	95.45 ± 0.85	3.77	3.3
	BT463	10.6	70 ± 0	2.97	5.2
MET-neg-NS	**BT273**	2.6	neg	neg	neg
	BT275	1.9	neg	neg	neg
	BT334	4.2	neg	neg	neg
	BT358	0.9	neg	neg	neg
	BT373	1.6	neg	neg	neg
	BT421	8.6	neg	neg	neg
	BT443	2.8	neg	neg	neg

a: MET/HGF mRNA measured by real time PCR and reported as 40-Ct;
b: MET protein measured by flow-cytometry. Percentage of positive cells was reported as mean ± SEM.
c: HGF protein measured by western blot on NS lysates. HGF densitometric quantification was normalized on β-actin.
a.u.: arbitrary units. n.a.: not available.

Table 2. MET/HGF expression in neurospheres

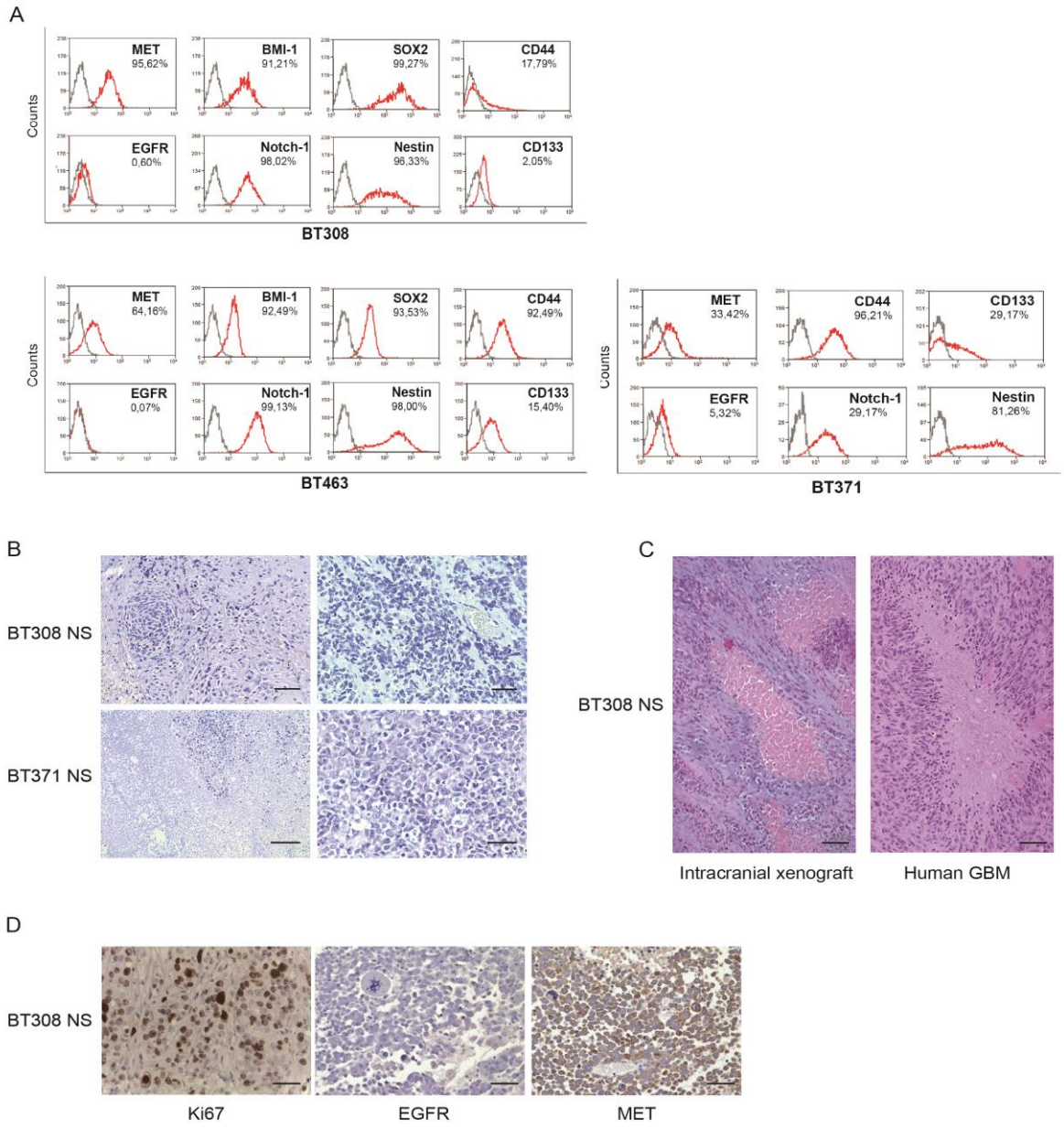

Figure 1. Phenotypic characterization of neurospheres and GBMs generated by neurosphere transplantation. A. Flow-cytometric analysis of MET, EGFR and stem markers (BMI-1, SOX2, CD44, Notch-1, Nestin, CD133, red lines) in three representative MET-pos-NS (BT308, BT463, BT371). Grey line: negative controls; **B.** Representative images of tumors generated by subcutaneous injection of 10^5 cells (BT308 and BT371NS). Scale bar, 100 µm (left, 20× magnification; right, 40× magnification). **C.** Representative images of tumors generated by orthotopic injection of 10^5 cells (BT308NS) which reproduce the intraparenchymal invasion pattern with pseudo-palisade cells surrounding necrosis area, typical of human GBM. Scale bar, 100 µm (20x magnification). **D.** Representative immunohistochemical staining of Ki67, EGFR and MET in intracranial tumors generated by injection of BT308 NS. Scale bar, 100 µm (40x magnification).

2. The neurosphere GSC subpopulation is positively selected by ionizing radiation

It has been well demonstrated that ionizing radiation (IR) destroy the tumor bulk but not GSCs, which drive tumor recurrence [19].

By definition, NS are clones deriving from expansion of single self-renewing GSCs. However, each NS entails a certain degree of phenotypic heterogeneity, which arises within the progeny of the founder GSC, and implies loss of stem properties, including radioresistance. We thus investigated whether, within the whole MET-positive heterogeneous NS, the GSC subpopulation was more radioresistant than its non-stem progeny and whether it was positively selected by IR. Indeed, we showed that irradiation positively selected cells displaying stem-like properties, as measured by limiting dilution assays (LDA) performed *in vitro* and *in vivo*. In a representative panel of MET-pos-NS, irradiation with 5 Gy significantly increased the frequency of sphere-forming cells *in vitro* (Figure 2A).

To conclusively demonstrate that IR positively selects the GSC subpopulation, we performed a serial xeno-transplantation experiment. This is inspired to the classical repopulation assay used to identify true hematopoietic stem cells [140]. As depicted in Figure 2B, NS were irradiated *in vitro* (NS-IR, p0) and, after 24 h, transplanted subcutis in the mouse (p1). In parallel, an equal number of non-irradiated NS cells (NS-ctrl) were transplanted as control. Both NS-IR and NS-ctrl generated tumors (p1) from which secondary NS were re-cultured; then an equal number of NS cells was transplanted into new recipients for a second passage (p2). Next, NS derived from tumors generated in p2 were assessed for their tumorigenic potential by performing an *in vivo* limiting dilution assay, by transplanting from 10 to 10^4 cells in p3 mice.

Of note, during serial transplantation we could observe that the median volume of tumors generated by both NS-IR and NS-ctrl progressively increased, according to the notion that stem-like subpopulations are positively selected during this procedure [22]. However, the tumors generated by NS-IR, still comparable to those generated by NS-ctrl at p1, were significantly larger than controls in the subsequent passages (Figure 2C-D). The latter observation indicates that the GSC subpopulation was further enriched from the start by irradiation. Consistently, the *in vivo* GSC frequency, estimated by performing p3 as LDA, was ~11-fold higher in tumors originated from NS-IR, as compared with tumors from NS-ctrl (Figure 2E-F). In addition, *in vitro* LDA with cells derived from p3 tumors showed that also the sphere-forming ability significantly increased in cells from tumors that originated from NS-IR, as compared with controls (Figure 2G).

Finally, an increased GSC frequency was also observed in a second GBM model treated with radiotherapy. In order to mimic the human protocol of irradiation, xenografts established by intracranic injection of MET-pos-NS, were treated with fractionated IR (2 Gy × 3 days). Secondary NS isolated from intracranial tumors were assessed by *in vitro* LDA 62 days after *in vivo* treatment, showing that the irradiated GBM displayed a significantly higher frequency of GSCs (Figure 2H-I). Collectively, these results show that the cell subpopulation endowed with the clonogenic and tumorigenic properties that qualify GSCs is positively selected by IR.

A

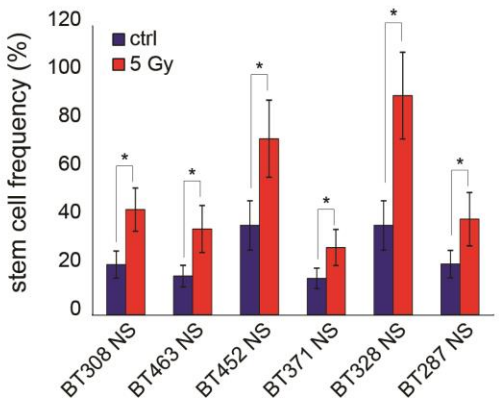

B

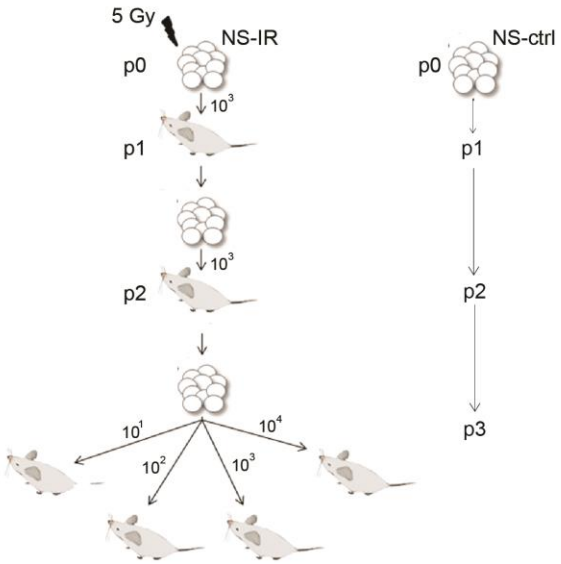

C

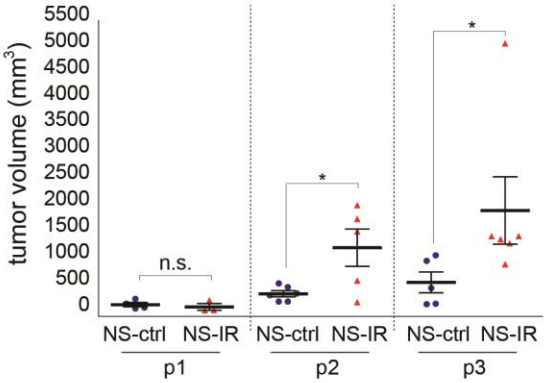

D

treatment		tumor take	tumor volume (mm^3)
p1	ctrl	4/4	122.39 ± 41.2
	p0-IR	3/4	79.41 ± 62.9
p2	ctrl	6/6	329.01 ± 57.3
	p0-IR	5/6	1200.8 ± 352.8
p3	ctrl	5/6	543.58 ± 196.5
	p0-IR	6/6	1905.2 ± 637.4

E

p3	n° cells per injection	tumor incidence (n° tumors/n° injections)
NS-ctrl	10^4 10^3 10^2 10^1	6/6 5/6 5/6 0/6
NS-IR	10^4 10^3 10^2 10^1	6/6 6/6 6/6 2/6

F

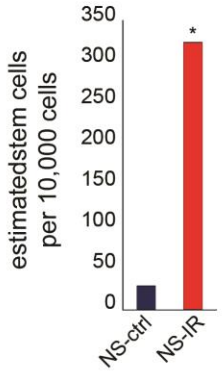

G

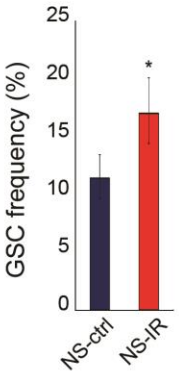

H

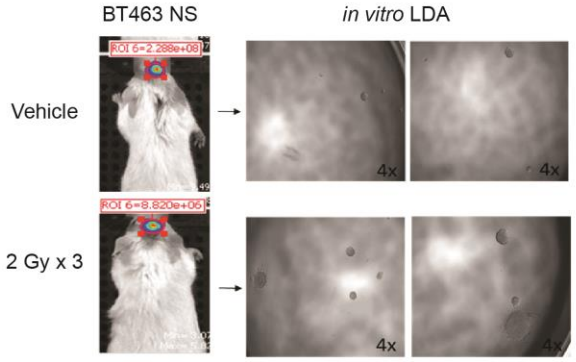

I

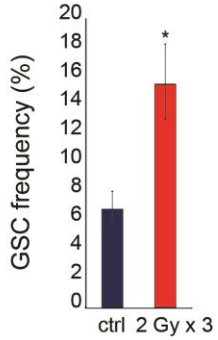

Figure 2. The neurosphere GSC subpopulation is positively selected by ionizing radiation. A. LDA (sphere-forming) measuring the enrichment of GSCs after IR (5 Gy). Ctrl: non-irradiated cells *: χ^2 test, $P < 0.05$. n = 2. **B.** Schematic representation of serial xenotransplantation. Control (NS-ctrl) and irradiated (NS-IR) BT308NS were tested for tumor-initiating ability by serial subcutaneous injection of the indicated number of cells (p1, n = 4; p2, n = 6; p3, n = 6 for each condition). **C.** Scatter plot showing take and volume (14 weeks after cell injection) of tumors generated by control (NS-ctrl) and irradiated (NS-IR) NS for each transplantation passage (10^3 cells). *: t-test, $P < 0.05$; n.s. not significant. n = 4 for p1; n = 6 for p2 and p3. **D.** Table showing data represented in (C). **E.** Tumor incidence in the LDA performed in p3 mice, as described in (B). **F.** Histogram showing the *in vivo* GSC frequency measured by LDA in p3 tumors. GSC frequency (95% CI) was as follows: NS-ctrl, 1/258.2 (97.67-683.9); NS-IR 1/22.1 (8.05-62.6). χ^2*: test, $P = 1.6 \times 10^{-4}$. n = 6. **G.** LDA (sphere-forming) measuring the *in vitro* frequency of GSCs in cells derived from p3 tumors. *: X^2 test, P = 0.0006. n = 3. **H.** Schematic representation of intracranial tumors generated by BT463 NS and irradiated *in vivo* (2 Gy × 3 days) (n = 3). Tumor growth was monitored by bioluminescence imaging. 62 days after radiotherapy brain tumors were explanted and dissociate to perform *in vitro* LDA. **I.** LDA (sphere-forming) measuring the *in vitro* frequency of GSCs in cells derived from intracranial tumors represented in (H). Ctrl: non-irradiated tumors. *: χ^2 test, $P = 2.04 \times 10^{-11}$. Data information: Data are represented as mean ± CI in (F,G,I) or ±SEM in (A,C).

3. MET expressing GSCs are selected by irradiation in experimental models

We have previously shown that MET is a marker of the GSC subpopulation (MET^{high}) [96] in a subset of MET-pos-NS (Figure 3A) and that MET promotes radioresistance of conventional cancer cell lines [95]. Based on these premises, in the subset of MET-pos-NS from our panel (table 2), we investigated the relationship between MET expression and GSC radioresistance.

Accordingly with our previous data, *in vitro* LDA showed that the MET^{high} subpopulation, sorted from representative MET-pos-NS, was enriched in GSCs (Figure 3B). As assessed by flow cytometry, in MET-pos-NS, the number of MET-expressing cells, and their mean fluorescence intensity (MFI), significantly increased 24 h after irradiation (Figure 3C) and an even higher enrichment of MET-expressing cells was observed after a chronic IR treatment (Figure 3D). Accordingly, in tumors established by subcutaneous transplantation of MET-pos-NS, the number of MET-expressing cells and the intensity of staining were significantly increased 72 h after receiving the last *in vivo* fractionated irradiation dose (2Gy x 3 days) (Figure 3E-G). Moreover, western blot performed on lysate of the whole tumor tissue confirm a significant increase of the MET protein in the irradiated group as compared to controls (Figure 3H).

Collectively, these data indicate that MET-expressing GSCs are radioresistant, likely due to cell-positive selection mechanism.

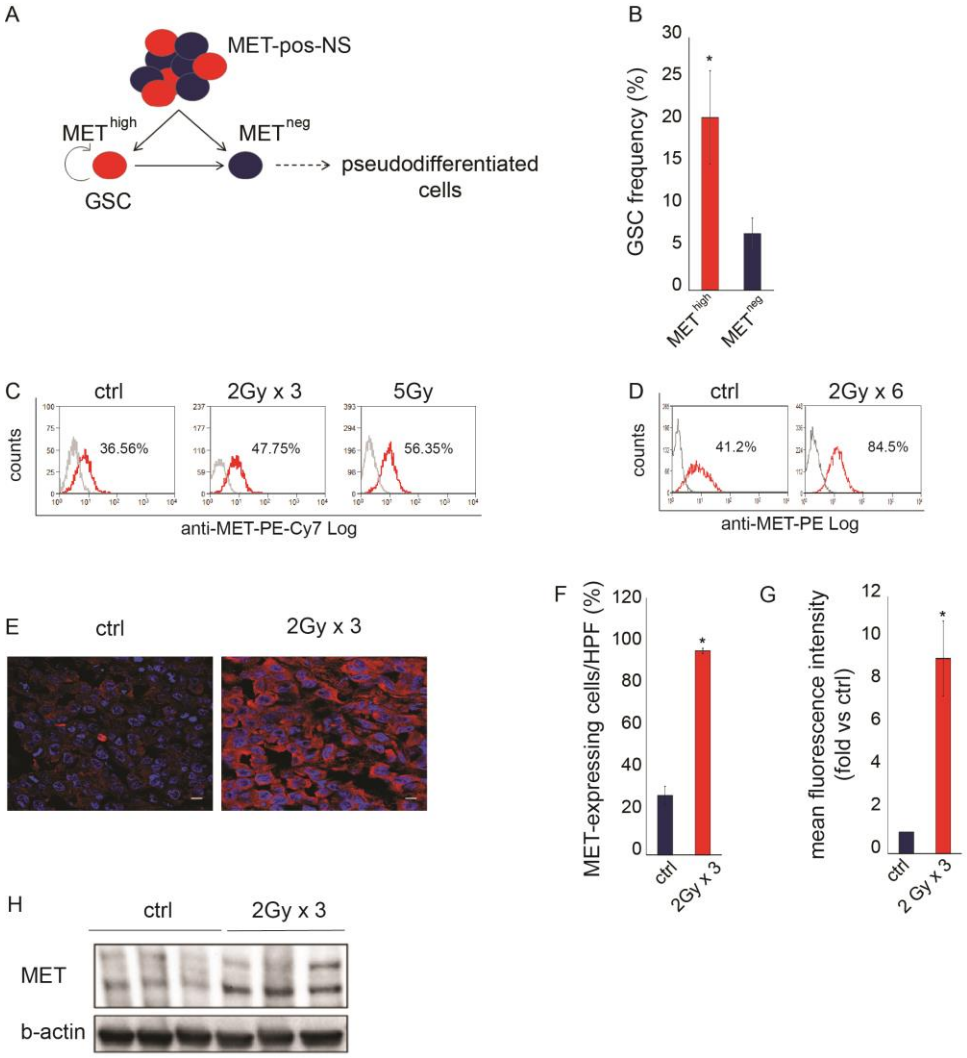

Figure 3. MET expressing GSCs are selected by irradiation. In MET-pos-NS, the MET^{high} subpopulation retains GSC properties and generates a heterogeneous progeny including also MET^{neg} pseudodifferentiated cells. **B.** LDA (sphere-forming) measuring the GSC frequency after IR (5 Gy) in MET^{high} and MET^{neg} subpopulations sorted from BT308NS. *: χ^2 test, P = 0.001. n = 2. **C.** Flow cytometric analysis of MET in irradiated BT308NS, 24 h after the last irradiation (2 Gy × 3 days or a single dose of 5 Gy). Dotted lines: threshold to define the percentage of MET-expressing cells. Ctrl: non-irradiated cells. The MFI was as follows: ctrl, 18; 2 Gy × 3, 22.77; 5 Gy, 19.49. **D.** Flow cytometric analysis of MET in BT308NS weekly treated with IR (2 Gy) for 6 weeks. Dotted lines: threshold to define the percentage of MET-expressing cells. Ctrl: non-irradiated cells. **E.** Representative immunofluorescence staining of MET (red) on tumors generated by subcutaneous injection of BT308NS irradiated (2 Gy × 3) and explanted 72 h after the last irradiation. Nuclei are counterstained with DAPI (blue). Ctrl: non-irradiated tumors. Scale bar, 10 µm (63× magnification). **F.** Quantification of the percentage of MET-expressing cells in tumor sections represented in (E) (n = 12 HPF/group). HPF: high-power field. *: t-test, P = 0.001. **G.** Quantification of MET mean fluorescence intensity in tumor sections represented in (E) (n = 12 HPF/group, fold versus non-irradiated cells, ctrl). *: t-test,P = 0.00016. **H.** Western blot showing MET expression in tumor sample represented in (C) (n= 3/group). β-actin was used as loading control. Data information: Data are represented as mean ± CI in (B, F, G).

4. MET expression is enriched in recurrent glioblastoma

We asked whether radioresistance of MET-expressing GSCs could drive tumor recurrence in patients by positive selection under therapeutic pressure. To this aim, we collected a panel of 19 pairs of GBMs, each including a primary tumor removed by surgery without prior treatment, and the matched recurrent tumor, arising after adjuvant chemo-radiotherapy (Table 3). Immunohistochemical analysis of whole patients' tissues showed that significant MET expression (MET cumulative score ≥ 2) was detectable in 36% of primary tumors (7/19), but in 84% of recurrent tumors (16/19) (Table 4). Remarkably, in the majority of cases, the percentage of MET-positive cells and/or the intensity of MET staining (summed in the cumulative score) increased in the recurrent as compared with the matched primary tumor (Figure 4A and Table 4). MET expression enrichment in the recurrent GBMs suggests that, in primary tumors, MET-positive cells, being resistant to the standard chemo-radiotherapy, can drive tumor recurrence. Although we do not provide functional proofs, we reason that the MET-positive cell subpopulation expanded in the recurrent tumor can largely correspond to stem-like cells because: (i) In MET-pos-NS, the MET-negative cell subpopulation is devoid of stem properties, as previously shown [96] and further investigated by *in vitro* LDA (Figure 3B); and (ii) GSC differentiation is characterized by loss of MET expression, as shown *in vitro* [95].

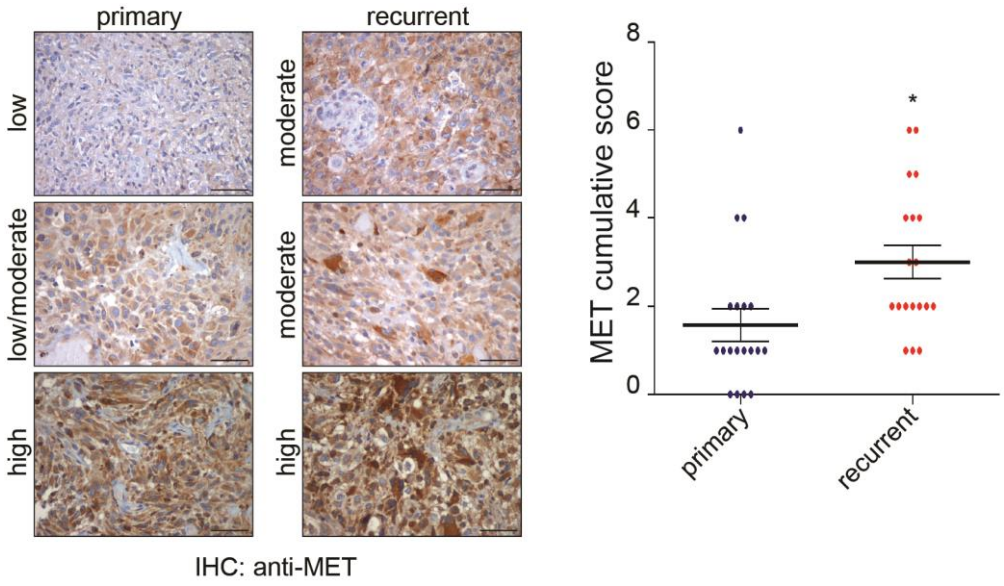

Figure 4. A. MET expression is enriched in recurrent glioblastoma. Representative MET immunohistochemical staining of matched primary and recurrent tumors. Scale bar, 50 µm (40x magnification). **B.** Dot plot representing the MET cumulative score (MET-positive cell score + MET staining intensity score) in 19 primary and recurrent tumors *: Wilcoxon test, P < 0,02. Data information: Data are represented as mean ± SEM in (B).

Patient	Gender	Age	Location	RTOG-RPA	1st surgery	MGMT	Adjuvant treatment after 1st surgery	DFS (months)	OS (months)
1	F	25	T	III	Partial	NM	RT+CT	1	10
2	M	56	N	IV	Total/subtotal	M	RT+CT	4	22
3	F	59	P	IV	Partial	NM	RT+CT	34	50
4	M	63	T	IV	Total/subtotal	NM	RT+CT	14	27
5	M	45	F	III	Partial	n.a.	RT+CT	15	26
6	M	65	P	IV	Total/subtotal	n.a.	RT+CT	6	8
7	M	65	P	V	Total/subtotal	n.a.	RT+CT	10	23
8	M	47	T	III	Total/subtotal	n.a.	RT+CT	23	32
9	M	65	T	IV	Total/subtotal	NM	RT+CT	17	25
10	M	50	T	V	Total/subtotal	NM	RT+CT	11	21
11	F	39	F	III	Partial	NM	RT+CT	4	10
12	F	62	P	IV	Total/subtotal	NM	RT+CT	7	9
13	M	52	T	IV	Total/subtotal	M	RT+CT	17	42
14	M	64	F	III	Total/subtotal	NM	RT+CT	11	15
15	M	51	T	V	Total/subtotal	NM	RT+CT	4	16
16	M	55	F	IV	Total/subtotal	NM	RT+CT	10	15
17	F	48	F	I	Total/subtotal	M	RT+CT	12	19
18	F	54	T	V	Total/subtotal	NM	RT+CT	17	22
19	M	68	T	IV	Total/subtotal	NM	RT+CT	7	18

Location: T (temporal); F (frontal); P (parietal); N (basal nuclei). RTOG-RPA: Radiation Therapy Oncology Group recursive partitioning analysis. MGMT: NM (non-methylated); M (methylated); n.a. (not available). Treatment: RT, radiotherapy; CT, chemotherapy (Temozolomide). DSF: Disease Free Survival; OS: Overall Survival.

Table 3. Clinical data of matched primary and recurrent GBMs

Patient	Primary GBM			Recurrent GBM		
	MET positive cells (score)[a]	MET staining intensity (score)[b]	MET cumulative score (a+b)	MET positive cells (score)[a]	MET staining intensity (score)[b]	MET cumulative score (a+b)
1	0	1	1	3	3	6
2	1	1	2	2	2	4
3	0	0	0	1	1	2
4	0	1	1	0	1	1
5	0	1	1	1	1	2
6	0	1	1	0	1	1
7	1	1	2	1	1	2
8	0	0	0	2	1	3
9	1	1	2	1	1	2
10	3	1	4	3	1	4
11	0	0	0	3	2	5
12	3	3	6	3	3	6
13	0	0	0	0	1	1
14	2	2	4	3	2	5
15	1	1	2	1	1	2
16	0	1	1	1	1	2
17	0	1	1	2	2	4
18	0	1	1	2	1	3
19	0	1	1	1	1	2

a: positivity scores: 0, 0-5% cells; 1, 6-29% cells; 2, 30-69% cells; 3, 70-100% cells.
b: staining intensity scores: 0, negative; 1, low; 2, moderate; 3, high.

Table 4. MET expression (immunohistochemistry: cumulative score) in matched primary and recurrent GBMs

5. MET^{high} GSCs are more radioresistant than the MET^{neg} subpopulation and efficiently activate DNA damage repair (DDR)

The biological response to IR of the MET-expressing stem-like subpopulation was assessed in MET^{high} and MET^{neg} cells sorted from MET-pos-NS. Viability, measured in dose–response experiments 24 h after IR, was significantly higher in MET^{high} than in MET^{neg} cells at all doses tested (Figure 5A). Consistently, in radiobiological clonogenic assays, the surviving fraction of MET^{high} cells remained almost unchanged even after irradiation with the highest dose (10 Gy), while that of MET^{neg} cells significantly decreased after 10 Gy (Figure 5B). Cell death of the MET-negative subpopulation was likely due to apoptosis, as shown by western blot analysis of PARP and caspase-3 activation, which was evident in sorted and irradiated MET^{neg} cells, but not in MET^{high} cells (Figure 5C).

The radioresistance of the MET^{high} subpopulation was then correlated with constitutive activation of two crucial DDR signal transducers: (i) ATM, the apical kinase unleashed by DNA damage sensors, responsible for H2AX phosphorylation[64] and (ii) the ATM substrate Chk2, whose activation correlates with GSC radioresistance [19]. Indeed, untreated MET^{high}, but not MET^{neg} cells, displayed constitutive phosphorylation of ATM and Chk2 kinases. After irradiation ATM phosphorylation was significantly increased in MET^{high} cells, but only weakly induced in MET^{neg} (Figure 5D). Accordingly, histone H2AX phosphorylation, a key step in the nucleation of DNA repair complex at double strand-breaks (DSB) [141, 142], was undetectable in MET^{high} indicating DSB repair. Conversely, in MET^{neg} cells, H2AX was still phosphorylated 24 h after irradiation (Figure 5D), suggesting DSB persistence.

Collectively, these findings indicate that the positive selection of MET^{high} GSCs by IR resides on the intrinsic radioresistance of this subpopulation, likely conferred by enhanced basal activity, and efficient hyperactivation of DDR effectors after irradiation.

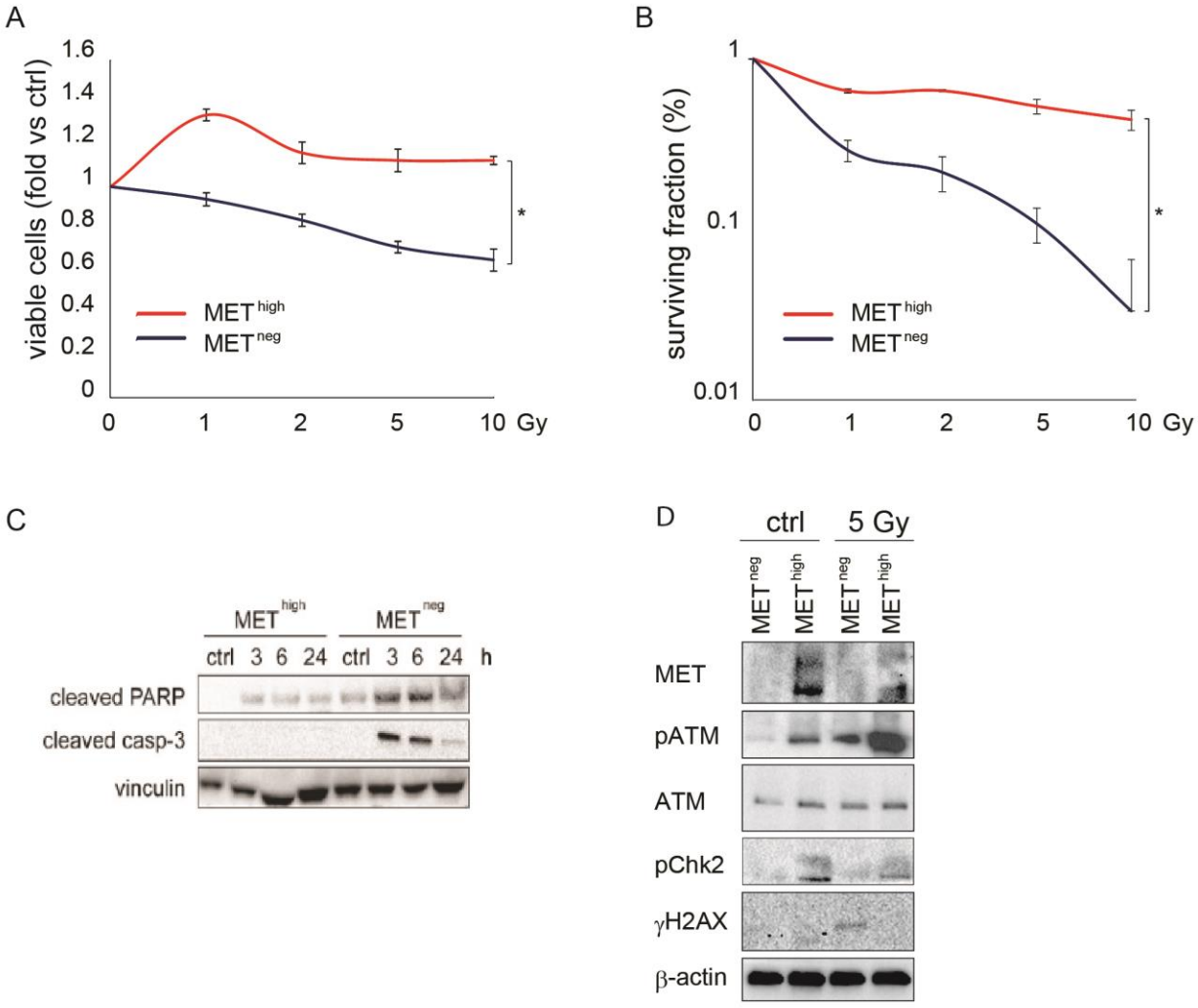

Figure 5. MET^{high} GSCs are more radioresistant than the MET^{neg} subpopulation and efficiently activate DNA damage repair (DDR). A. Cell viability of MET^{high} and MET^{neg} subpopulations sorted from BT308NS, measured 96 h after IR (1–10 Gy, fold versus non-irradiated cells, ctrl). *: t-test, P < 0.001. n = 2. **B.** Clonogenic assay with MET^{high} and MET^{neg} subpopulations sorted from BT308NS and irradiated (1–10 Gy, fold versus non-irradiated cells, ctrl). *: t-test, P < 0.05. n = 3. **C.** Western blot of MET^{neg} and MET^{high} subpopulations sorted from BT452NS, showing activation of PARP (cleaved PARP) and caspase-3 (cleaved casp-3) after IR (5 Gy). Vinculin was used as a loading control **D.** Western blot of MET^{neg} and MET^{high} subpopulations sorted from BT308NS, showing constitutive (ctrl) and/or IR-induced phosphorylation of ATM (pATM), Chk2 (pChk2), and H2AX (γH2AX) 24 h after IR (5 Gy). Total ATM protein is also shown. b-actin was used as a loading control. Data information: data are representative as mean ± SEM in (A, B).

6. MET inhibition radiosensitizes GSCs by impairing ATM and p21 activity

The above results indicate that MET is a marker of a radioresistant GSC subpopulation. We thus investigated whether MET signaling has a functional role in sustaining radioresistance, and whether its inhibition can radiosensitize GSCs. MET-pos-NS were kept in a standard EGF/bFGF medium, supplied with HGF to better mimick the brain (tumor) microenvironment [143, 144]. In this condition, after irradiation, MET gets hyperphosphorylated (Figure 6A) consistently with previous results obtained in cell lines [95, 145]. We then showed that association of the specific MET inhibitor JNJ-38877605 to IR significantly reduced cell viability as compared with treatment with IR alone (Figure 6B). Consistently, caspase-3 activation was barely detectable in cells treated with IR alone, to become well evident in those treated with IR and the MET inhibitor (Figure 6C). These outcomes, observed in whole NS, were obviously due to the activity of the inhibitors in MET-expressing GSCs and not in the MET-negative non-stem subpopulation, which, by definition, lacks the target. Finally, in LDA (*in vitro* sphere-forming assay) performed on MET^{high} and MET^{neg} sorted subpopulations, the GSC frequency of the MET^{high} subpopulation was abated by combination of IR with the MET inhibitor, while, as expected, the low GSC frequency of the MET^{neg} subpopulation was further decreased only by IR (Figure 6D). Interestingly, a significant decrease of MET^{high} GSC frequency was also observed after treatment with the MET inhibitor alone, indicating that HGF present in the culture medium plays a role in sustaining self-renewal, as previously shown [96, 121] (Figure 6D).

These findings show that MET behaves as a functional marker of radioresistance, whose inhibition efficiently radiosensitizes MET^{high} GSCs.

We thus asked whether MET inhibition directly impinges on the molecular mechanisms regulating DDR. We previously showed that, after irradiation of conventional cell lines, ATM upregulates MET expression through NF-κB transcription factor [95]. We now show that MET, in turn, triggers a signal transduction cascade that sustains ATM activity and DDR. We found that, in irradiated MET-pos-NS kept in the standard medium, addition of HGF increased ATM and Chk2 phosphorylation, and RAD51 expression (Figure 6E). In a complementary experiment, in irradiated MET-pos-NS kept in the medium supplied with HGF, addition of the MET inhibitor significantly reduced ATM and Chk2 phosphorylation, and the expression of the DNA recombinase RAD51 [146] (Fig 6F).

Although to show the detailed interplay between MET and ATM is beyond the purpose of this thesis, the mechanistic link between the two kinases that we recently reconstructed [129] is briefly summarized here. By the use of different inhibitors of MET downstream signaling we found that MET initiates a signaling cascade whose crucial players are AKT and Aurora kinase A, which ends in sustaining ATM phosphorylation. This, in turn, activates DDR effectors including Chk2 and Rad51 (Figure 6G). When the MET inhibitor is added, this signalling cascade is blocked and ATM activity is significantly compromised. The relevance of the AKT pathway was also supported by analysis of p21. When p21 it is phosphorylated by AKT on a specific site, it is retained in the cytoplasm. Indeed, in MET-pos-NS treated with IR alone, p21 was phosphorylated on Thr145 and mainly localized in the cytoplasm. When cells were irradiated in the presence of the MET inhibitor, p21 phosphorylation by AKT was prevented and, thus, p21 translocated into the nucleus where it is known to block the cell cycle and release its inhibition on apoptosis [129] (Figure 6G).

Impairment of these signaling circuits provides a mechanistic explanation for the radiosensitizing effect of MET inhibitors.

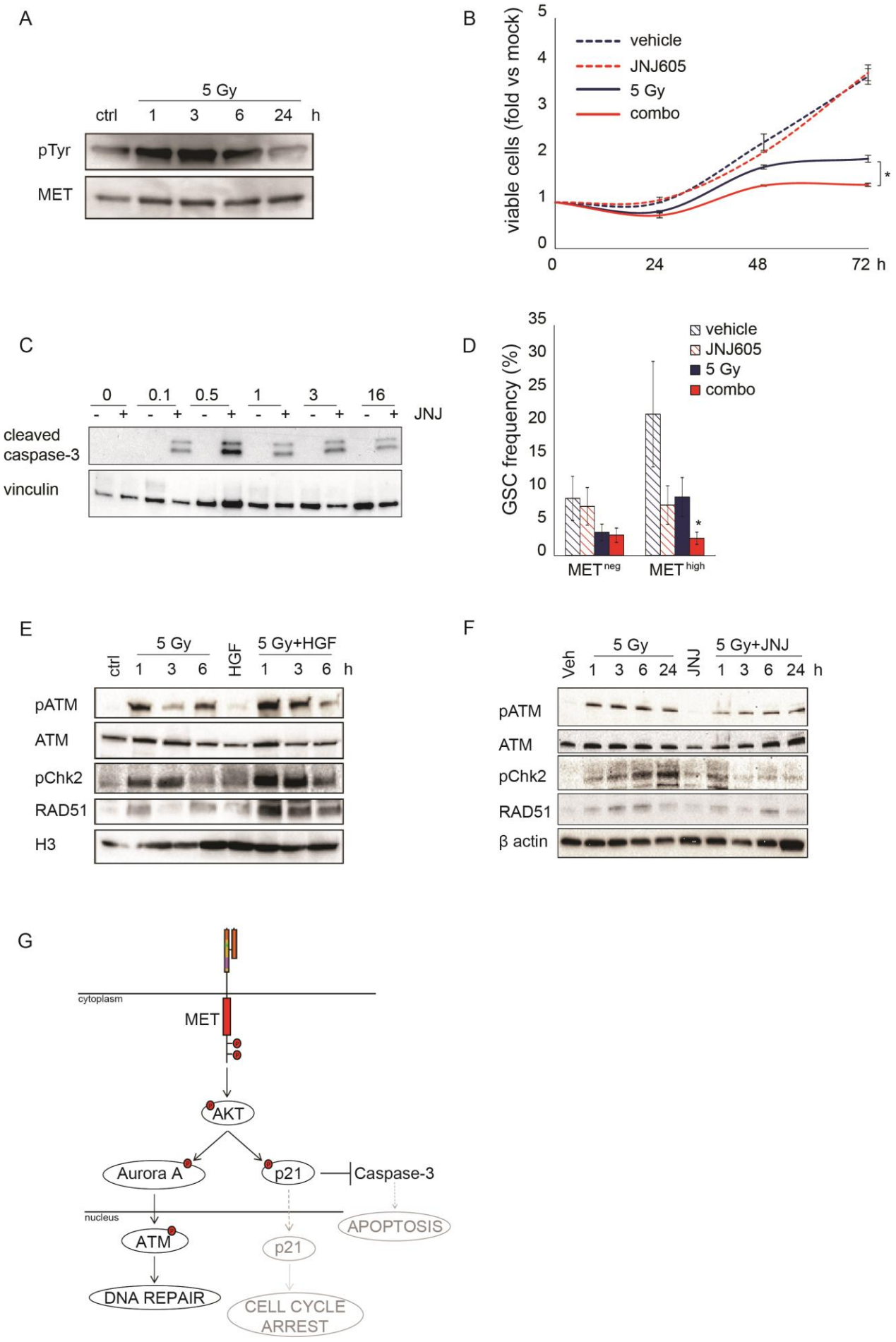
A
5 Gy
ctrl 1 3 6 24 h
pTyr
MET
B
viable cells (fold vs mock)
vehicle
JNJ605
5 Gy
combo
0 24 48 72 h
C
0 0.1 0.5 1 3 16
- + - + - + - + - + - + JNJ
cleaved caspase-3
vinculin
D
GSC frequency (%)
vehicle
JNJ605
5 Gy
combo
MET neg
MET high
E
ctrl 5 Gy HGF 5 Gy+HGF
1 3 6 1 3 6 h
pATM
ATM
pChk2
RAD51
H3
F
Veh 5 Gy JNJ 5 Gy+JNJ
1 3 6 24 1 3 6 24 h
pATM
ATM
pChk2
RAD51
β actin
G
cytoplasm
MET
AKT
Aurora A
p21
Caspase-3
nucleus
APOPTOSIS
ATM
p21
DNA REPAIR
CELL CYCLE ARREST

Figure 6. MET inhibition radiosensitizes GSCs by impairing ATM and p21 activity. A. Western blot of BT308NS showing MET tyrosine phosphorylation (pTyr) in NS kept in the presence of HGF (10 ng/ml), extracted at the indicated time points after irradiation (5 Gy). **B.** Cell viability of BT308NS, irradiated in the absence (5 Gy) or in the presence (5 Gy + JNJ) of the MET inhibitor JNJ38877605 (500 nM) and analyzed at the indicated time points. Vehicle: non-irradiated cells (fold versus vehicle-treated cells at time 0, mock). *: t-test, $P < 0.01$. n = 2. **C.** Western blot of BT308NS showing caspase-3 activation (cleaved casp-3), at the indicated time points after IR in the absence (-) or in the presence (+) of JNJ38877605. Vinculin was used as a loading control. **D.** LDA (sphere-forming assay) with MET^{neg} and MET^{high} subpopulations sorted from BT308NS, measuring GSC frequency after irradiation in the absence (5 Gy) or in the presence (5 Gy + JNJ) of JNJ38877605. Vehicle: non-irradiated vehicle-treated cells. *: χ^2 test, $P = 0.0002$. n = 2. **E.** Western blot of BT463NS showing phosphorylation of ATM (pATM) and Chk2 (pChk2), and accumulation of RAD51 at the indicated time points after IR in the absence (5 Gy) or in the presence (5 Gy + HGF) of HGF (10 ng/ml). Total ATM is also shown. H3 was used as a loading control. **F.** Western blot of BT308NS showing phosphorylation of ATM (pATM) and Chk2 (pChk2) and accumulation of RAD51 at the indicated time points after IR in the absence (5 Gy) or in the presence (5 Gy + JNJ) of the MET inhibitor JNJ38877605 (500 nM). Total ATM is also shown. β-actin was used as a loading control. Veh: non-irradiated vehicle-treated cells. **G.** Schematic representation of the MET-driven signaling pathways that sustain DNA repair and prevent apoptosis and cell cycle arrest.
Data information: data are represented as mean ± SEM in (B) and mean ± CI in (D).

7. MET inhibition sensitizes GBM xenografts to radiotherapy

In order to investigate whether combination with MET inhibitors could increase response to radiotherapy, we generated GBMs by *in vivo* transplantation of MET-pos-NS in NOD-SCID mice. As assessed, the MET inhibitor JNJ38877605 crosses the blood–brain barrier (Figure 7A). GBMs were then established by orthotopic transplantation of BT463NS transduced by GFP reporter construct. Ten days after NS injection, mice were randomized into four treatment groups: (i) vehicle, (ii) fractionated IR (2 Gy × 3 days), (iii) JNJ38877605, administered for 30 days, and (iv) combination therapy (combo, IR and JNJ38877605). Approximately 60 days after the beginning of treatment, at the onset of severe neurological symptoms in controls, mice were sacrificed and brains were analyzed by epifluorescence imaging (Figure 7B). Combination therapy dramatically reduced tumor growth, measured as GFP intensity, as compared with IR or MET inhibitor alone (Figure 7B). In a second model, tumors were established by subcutaneous transplantation of BT308NS and were treated as above (JNJ38877605 was administered for 15 days). When tumors reached the established end-point (tumor volume: 1,600 mm^3), mice were sacrificed to generate survival curves. Tumors treated with vehicle, or the MET inhibitor alone, reached the experimental endpoint within 18 or 32 days, respectively. Tumors treated with IR alone remained stable for 40 days after beginning of the treatment, leading to the experimental endpoint within 63 days. Remarkably, tumors treated with the combination therapy showed clinical regression (volume reduction > 50% as compared with day 0), which persisted until 40 days, leading to the experimental endpoint 90 days after beginning of the treatment (Figure 7C,D). A significant growth inhibition (~2-fold) by combination therapy as compared with radiotherapy alone was observed also in tumors generated by transplantation of BT371NS, although these tumors were not completely arrested by any therapy (Figure 7E). Also in this model, combination therapy significantly prolongs mice survival as compared to irradiation treatment alone (Figure 7F). Accordingly with *in vitro* data, the radiosensitizing effect of JNJ38877605 was related to the impairment of DDR pathway by significant inhibition of AKT, ATM and Chk2 phosphorylation, as shown by western blot analysis performed on whole lysate of *in vivo* treated tumors (Figure 7G). Collectively, this data demonstrate that MET-inhibitor associated with radiotherapy enhance the efficacy of radiation in blocking tumor growth and prolongs mice survival.

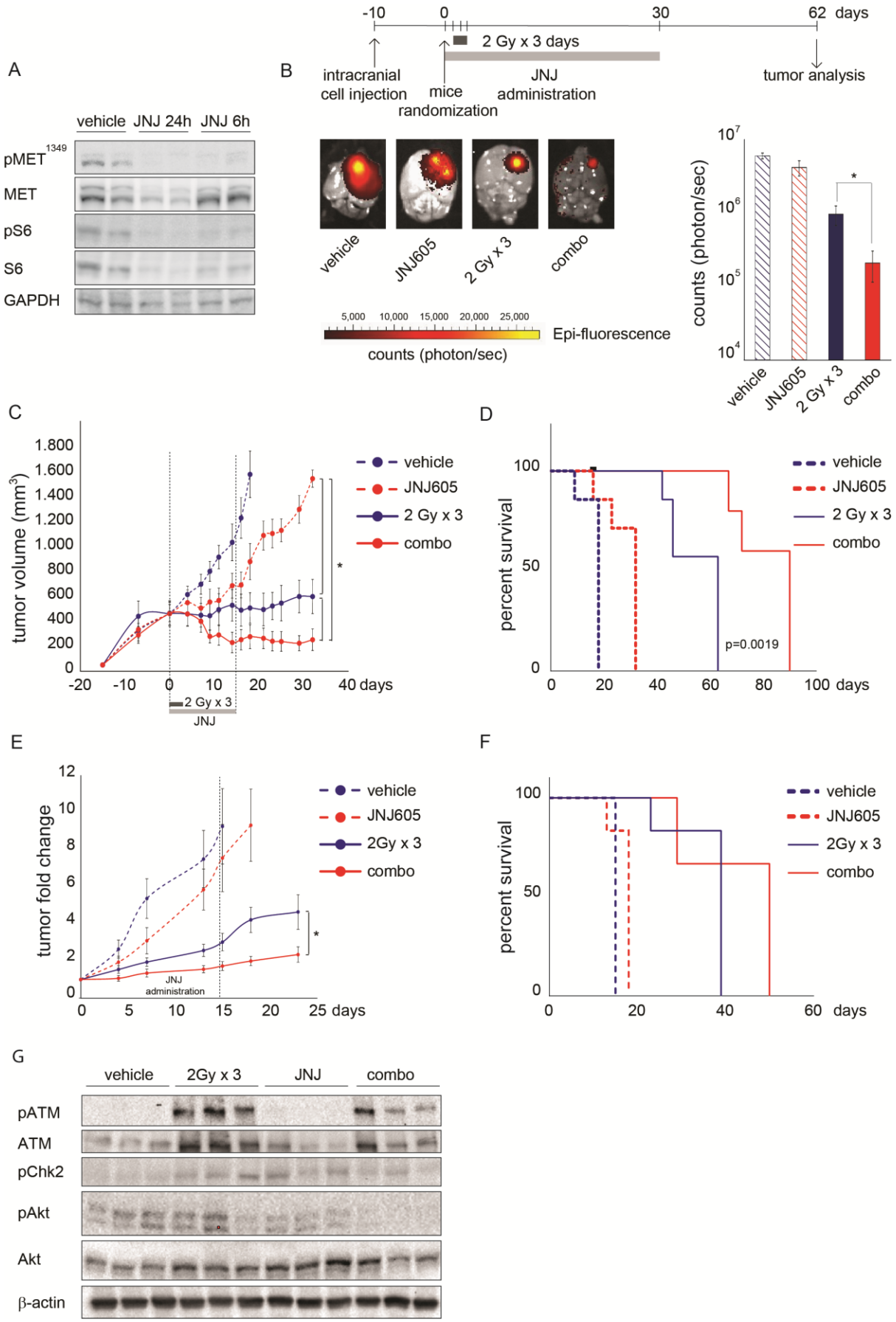
A
vehicle JNJ 24h JNJ 6h
pMET1349
MET
pS6
S6
GAPDH
B
-10
0
30
62 days
2 Gy x 3 days
intracranial cell injection
mice randomization
JNJ administration
tumor analysis
vehicle
JNJ605
2 Gy x 3
combo
5,000 10,000 15,000 20,000 25,000
Epi-fluorescence
counts (photon/sec)
counts (photon/sec)
vehicle
JNJ605
2 Gy x 3
combo
C
tumor volume (mm3)
vehicle
JNJ605
2 Gy x 3
combo
2 Gy x 3
JNJ
days
D
percent survival
vehicle
JNJ605
2 Gy x 3
combo
p=0.0019
days
E
tumor fold change
vehicle
JNJ605
2Gy x 3
combo
JNJ administration
days
F
percent survival
vehicle
JNJ605
2Gy x 3
combo
days
G
vehicle
2Gy x 3
JNJ
combo
pATM
ATM
pChk2
pAkt
Akt
β-actin

Figure 7. MET inhibition sensitizes GBM xenografts to radiotherapy. A. Western blot showing phosphorylation of MET ($pMET^{1349}$) and the phospho-S6 kinase (pS6) on tumors, generated by intracranial injection of GTL-16 cells, and treated for three consecutive days by oral administration with the MET inhibitor JNJ38877605. Tumors were collected at the indicated time points after the last administration and analyzed. GAPDH was used as loading control (n=2/condition) **B.** Timeline of therapeutic treatments undergone by mice intracranially injected with BT463NS. Left: Representative images of *ex vivo* epifluorescent GFP signal of intracranial tumors, generated by injection of BT463NS and explanted 62 days after IR in the absence (2 Gy × 3 days) or in the presence (combo) of the MET inhibitor JNJ38877605 (50 mg/kg). Right: Quantification of epifluorescent GFP signal (logarithmic scale) from tumors represented on the left (n = 4/condition). Vehicle: non-irradiated vehicle-treated tumors. *: one-way ANOVA, $P = 5.5 \times 10^{-5}$. **C.** Growth curves of tumors, generated by subcutaneous injection of BT308NS, irradiated in the absence (2 Gy × 3 days) or in the presence (combo) of JNJ38877605, which was administered for 15 days as indicated (n = 7/condition). Vehicle: non-irradiated vehicle-treated tumors. *: one-way ANOVA, P = 0.0006. **D.** Survival analysis of mice bearing tumors generated and treated as in (C). Black dot: censored mouse. Log-rank (Mantel-Cox) test, (combo) versus (2 Gy × 3 days), P = 0.0019. **E.** Growth curves of tumors, generated by subcutaneous injection of BT371 NS, irradiated in the absence (2 Gy × 3 days) or in the presence (combo) of JNJ38877605, supplied from day 0 to 15 (n = 6/condition). Vehicle: non-irradiated vehicle-treated tumors. Data are represented as fold change vs. day 0. *: one-way ANOVA test, $p<0.05$. **F.** Survival analysis of mice bearing tumors generated and treated as in (E). Log-rank (Mantel-Cox) test, $p<0.0001$. **G.** Western blot showing phosphorylation of ATM (pATM), Chk2 (pChk2) and AKT (pAKT) on tumors, generated by subcutaneous injection of BT308NS and treated as in (B). Tumors were collected 24h after the last *in vivo* radiation dose and analyzed. β-actin was used as loading control (n=3/condition).
Data information: data are represented as mean ± SEM in (B,C,E).

8. MET inhibition associated with radiotherapy depletes GSCs *in vivo*

As depicted in Figure 8A, we performed an independent experiment with tumors generated by subcutaneous transplantation of MET-pos BT308 NS and xenografts were treated as above. Ten days after beginning of the treatment, that is when tumor regression was observed (Figure 8B), we isolated NS from tumors of each condition and analyzed by LDA. Both *in vitro* clonogenic (Figure 8C) and *in vivo* tumorigenic (Figure 8D–F) LDA indicated a significant GSC frequency decrease in tumors treated with combination therapy, as compared with controls or radiotherapy or the MET inhibitor alone. Of note, *in vitro* but not *in vivo* LDA (p1) allowed to detect an increased GSC frequency after radiotherapy alone. This is expected, as *in vivo* LDA, measuring tumorigenic potential, requires at least two serial passages (p2) to highlight positive selection and enrichment of GSCs by irradiation, as shown above (Figure 2C-F). However, in this experiment, further serial passaging was prevented by the minimal volume, and poor cell viability, of tumors generated by the first passage (p1) after combination therapy (Figure 8G).

Collectively, these data indicate that radiosensitization of GBM by MET inhibitor not only impairs tumor growth, but also target and depletes the GSC subpopulation, responsible for tumor generation and recurrence.

A

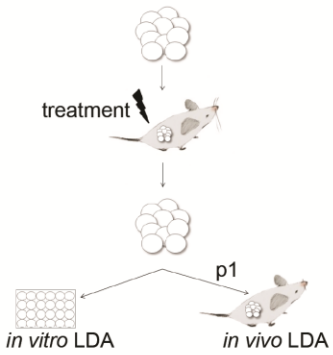

B

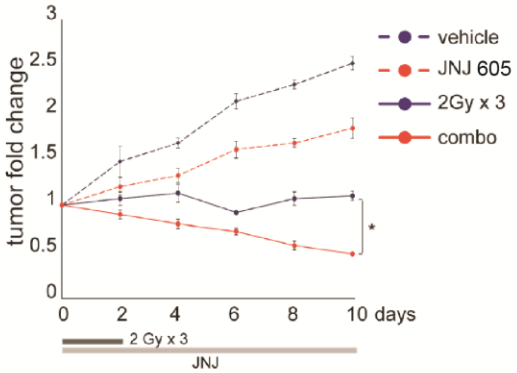

C

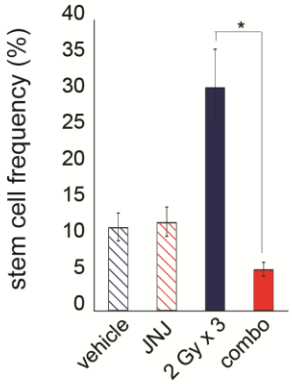

D

	n° cells per injection	tumor incidence (n° tumors/n° injections)
vehicle	10^4 10^3 10^2 10^1	6/6 6/6 6/6 4/6
JNJ	10^4 10^3 10^2 10^1	4/6 4/6 4/6 2/6
2Gyx3	10^4 10^3 10^2 10^1	4/6 4/6 4/6 2/6
combo	10^4 10^3 10^2 10^1	6/6 5/6 2/6 1/6

E

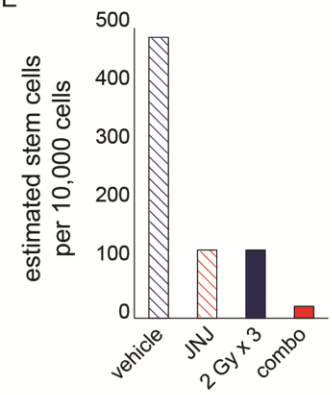

F

treatment	GSCs frequency (95% CI)	estimated GSCs per 10.000 cells	enrichment factor	*P* value (Chisq)
vehicle	1/14.7 (5.25-43.3)	474.308	1	5.47×10^{-6}
JNJ	1/67.5 (27.63-165.7)	115.02	0.242	
2 Gy x 3	1/67.5 (27.63-165.7)	115.02	0.242	
combo	1/384.4 (157-942.1)	20.22	0.042	

G

cell number	mean tumor volume ± SEM (mm^3)			
	vehicle	JNJ	2 Gy x 3	combo
10^4	1891.5±402.9	1423.98±313.5	1198.245±228.2	695.84±170.5
10^3	1753.6±402.6	1192.02±285.9	1959.36±276.9	279.774±39.7
10^2	1132.41±271.9	309.15±101.8	327.07± 180.1	52.305±4.2
10^1	171.87± 47.3	63.85±8.14	98.91± 10	32.7

Figure 8. MET inhibition associated with radiotherapy depletes GSCs *in vivo.* A. Experimental design to measure GSC frequency in tumors treated as in (B) (JNJ was administered for 10 days). Explanted tumors were dissociated and viable cells were tested by *in vitro* sphere-forming LDA or *in vivo* single-passage (p1) LDA. **B.** Growth curves of tumors, generated by subcutaneous injection of BT308 NS, irradiated in the absence (2 Gy × 3 days) or in the presence (combo) of JNJ38877605, supplied from day 0 to 10 (n = 3/condition). Vehicle: non-irradiated vehicle-treated tumors. Data are represented as fold change vs. day 0 *: one-way ANOVA test, p<0.05. **C.** *In vitro* LDA (sphere-forming) measuring GSC frequencies as described in (A) (n= 3/condition). * χ^2 test, P < 10^{-5}. **D.** Tumor incidence in the *in vivo* LDA performed on tumors generated and treated as described in (A). **E.** Histogram showing GSC frequencies measured by *in vivo* LDA, as described in (A). *, χ^2 test, P = 5.47 x 10^{-6}. **F.** Table showing GSC frequencies measured by *in vivo* LDA, represented in (E). **G.** *In vivo* LDA: table showing the volume of tumors obtained by injection of the indicated number of cells, derived from tumors treated as indicated in (B).
Data information: Data are represented as mean ± SEM in (B) or mean ± CI in (C, E).

9. MET is extensively expressed in locally advanced rectal adenocarcinoma

Recently, Senetta R. et al., have shown that, in an ample cohort of rectal adenocarcinoma biopsies, MET is expressed in 50% of patients and that MET is a predictive factor of poor response to neoadjuvant chemo/radiotherapy, usually administered before surgical resection [118]. Based on these findings, we set out to further investigate whether MET-expressing rectal cancer could be radiosensitized by MET-inhibition, and whether radiosensitization results from depletion of cancer stem-like cells.

From the patient-derived xenograft (PDX) platform already established in our institute by the group of Trusolino and Bertotti [128], we identified a panel of 28 locally advanced rectal cancers (according to TNM classification) including both neoadjuvant irradiated and naïve (non-neoadjuvant treated) tumors (Table 5). In collaboration with pathologists, we screened the corresponding paraffin-embedded tumor samples from the original patients for MET expression, in order to identify representative MET-expressing and control cancers to proceed with derivation of stem-like cells (rectospheres, RS).

In patients' tissue samples MET expression was evaluated by immunohistochemistry and scored semi-quantitatively by evaluating the percentage of positive cells and the staining intensity. Samples with a strong staining intensity (at least 2+) and a high number of positive cells (>75%) were classified as MET high-positive rectal tumors (4/28), while the others, showing a lower intensity and/or a focal positivity, were classified as mid- (15/28) or low-MET positive tumors (6/28). Only the tumors with an almost complete absence of expression in the membrane or cytoplasm were considered as MET-negative cases (2/28) (Figure 9A,B and Table 6). To our surprise, in our panel we found that MET is actually expressed in the majority of rectal cancers (26/28). The apparent discordance with the previous study [118] is probably due to the different sampling methodology used to assess MET expression: in this study an extensive analysis (at least three sections/patient) of the whole tumor was performed, which could spot even focal positivity, while, in the previous study, only single small biopsies were analyzed from each tumor, which could have resulted in MET expression underestimation.

In the MET-positive group, 6/26 patients received neoadjuvant radiotherapy while the others (20/26) did not. The two MET-negative rectal cancers were both naïve (Figure 9B). Interestingly the subset of neoadjuvant irradiated tumors is enriched (although without reaching statistical significance) with cases expressing mid to high levels of MET (MID: 4/6;

HIGH: 2/6); vice-versa, naïve tumors tend to express lower MET levels (HIGH: 2/20; MID:12/20; LOW: 6/20; NEG: 2/20) (Table 6).

The MET-positive tumors derived from naive patients are a suitable model in order to study the primary response to the association of radiotherapy with MET-inhibitors, while those removed from patients that received neoadjuvant irradiation could be exploited to study a possible enrichment in radioresistant cells. Moreover, it would be intriguing to study the response of the rare MET-negative tumors, either naïve or not, which we are trying to collect in adequate number by currently screening additional patients.

Patient	Gender	Code	TNM	Neo-adj CRT	pTNM post-treatment	Mandard TRG
1	F	R1190	T3N0M0	naive		
2	F	R1170	T4N0M0	naive		
3	F	R1142	T3N1M0	naive		
4	M	R1363	T3N1M0	naive		
5	M	R1356	T3N1M0	naive		
6	F	R1382	T3N0M0	naive		
7	M	R1357	T2N0M0	naive		
8	M	R1304	T4N1M0	naive		
9	M	R1381	T4N0M0	naive		
10	M	R1435	T3N1M0	naive		
11	M	R1197	T3N0M0	naive		
12	M	R1436	T3N2M1	naive		
13	F	R1354	T4N1M0	naive		
14	M	R0288	T3N0M0	SCRT	T2N0	4
15	M	R0368	T3N2M1	FU+Bevacizumab	T3N2b	4
16	M	R0373	T3N2M0	naive		
17	F	R0374	T2N1M0	SCRT	T2N1b	4
18	M	R0567	T3N1M0	naive		
19	M	R0679	T2N0M0	naive		
20	M	R0622	T2N0M0	naive		
21	M	R0750	T2N0M0	naive		
22	M	R0462	T3N0M0	naive		
23	F	R0476	T3N1M0	naive		
24	F	R0468	T3N1M1	SCRT	T3N1a	4/5
25	F	R0481	T3N1M1	naive		
26	M	R0446	T3N2M0	naive		
27	M	R0506	T3N0M0	LCRT	T3N0	3
28	M	R0514	T3N1M0	LCRT+Capecitabine	T3N1b	4

TNM staging (American Joint Committee for Cancer); Neo-adj CRT: Neo-adjuvant chemo/radiotherapy; SCRT : Short course radiotherapy (5Gy x 5 days); LCRT: long course radiotherapy (2 Gy x 4-5 weeks: 45-50 Gy); FU: fluorouracil; Mandard TRG (Tumor Regression Grade): response to neoadjuvant RT/CRT according to Mandard criteria [147], which are classified into five grades from TRG1 (complete regression) to TRG5 (no regression), based on the presence of residual cancer cells and on the degree of fibrotic changes.

Table 5. Clinical data of locally advanced rectal cancer

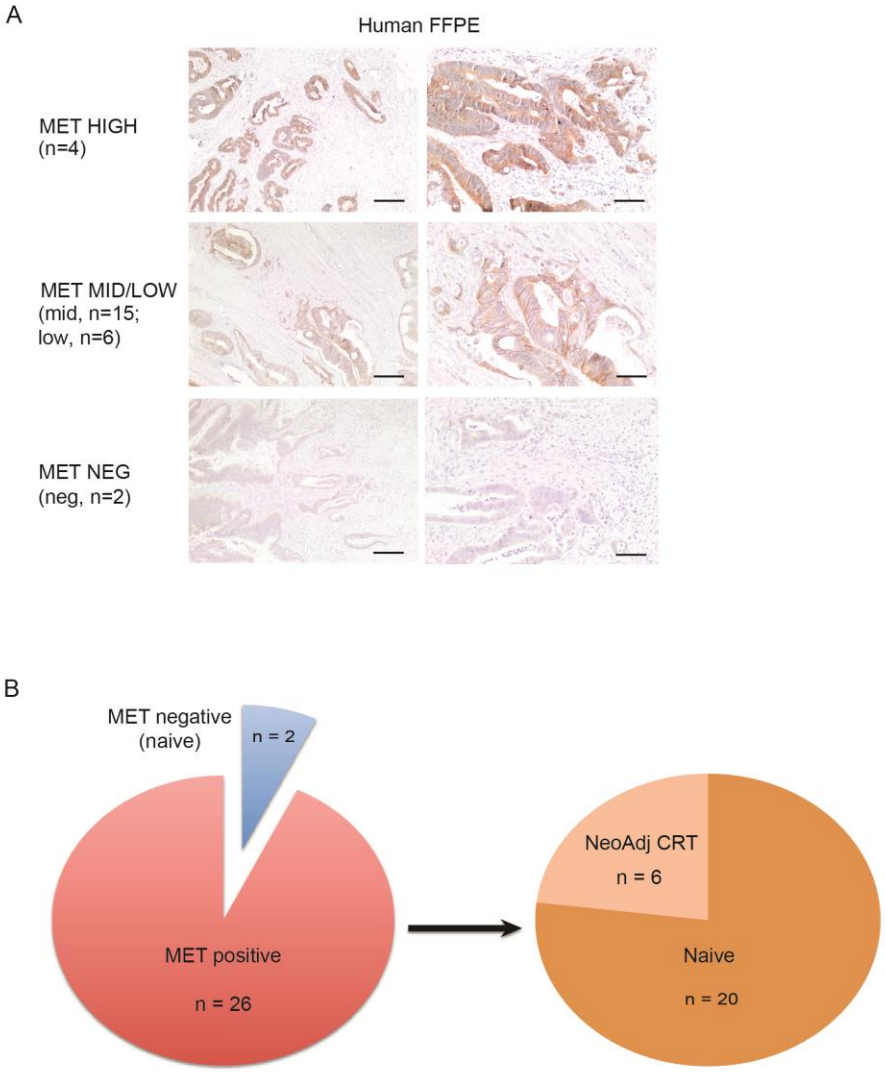

Figure 9. MET expression in locally advanced rectal adenocarcinoma. A. Representative MET immunohistochemical staining of locally advanced rectal cancer. Left: Scale bar, 500 µm (4x magnification); Right: Scale bar, 200 µm (10x magnification). **B.** Pie chart representing distribution of MET expression and the proportion of naïve and neodjuvant, chemo-radio treated rectal cancer (NeoAdj CRT).

Patient	Code	Neo-adj CRT	Mandard TRG	MET positive cells (%)	MET staining intensity (Cytoplasm)	MET staining intensity (Membrane)	MET expression
1	R1190	naive		> 35% ≤75%	2+	2+	MID
2	R1170	naive		>75%	2+	3+	HIGH
3	R1142	naive		≥ 5% ≤35%	1+	3+	LOW
4	R1363	naive		≥ 5% ≤35%	1+	1+	LOW
5	R1356	naive		> 35% ≤75%	2+	2+	MID
6	R1382	naive		>75%	2+	2+	HIGH
7	R1357	naive		<5%	1+	neg.	NEG
8	R1304	naive		> 35% ≤75%	2+	3+	MID
9	R1381	naive		> 35% ≤75%	2+	2+	MID
10	R1435	naive		<5%	1+	neg.	NEG
11	R1197	naive		> 35% ≤75%	2+	2+	MID
12	R1436	naive		≥ 5% ≤35%	1+	2+	LOW
13	R1354	naive		> 35% ≤75%	2+	3+	MID
14	R0288	SCRT	4	> 35% ≤75%	1+	2+	MID
15	R0368	FU+Bevacizumab	4	> 35% ≤75%	2+	2+	MID
16	R0373	naive		> 35% ≤75%	2+	2+	MID
17	R0374	SCRT	4	> 35% ≤75%	2+	3+	MID
18	R0567	naive		≥ 5% ≤35%	1+	2+	LOW
19	R0679	naive		≥ 5% ≤35%	1+	neg.	LOW
20	R0622	naive		n.a.	n.a.	n.a.	n.a.
21	R0750	naive		> 35% ≤75%	2+	neg.	MID
22	R0462	naive		> 35% ≤75%	1+	2+	MID
23	R0476	naive		> 35% ≤75%	2+	2+	MID
24	R0468	SCRT	4/5	>75%	2+	3+	HIGH
25	R0481	naive		> 35% ≤75%	2+	1+	MID
26	R0446	naive		≥ 5% ≤35%	1+	neg.	LOW
27	R0506	LCRT	3	>75%	2+	2+	HIGH
28	R0514	LCRT+Capecitabine	4	> 35% ≤75%	2+	neg.	MID

Mandard TRG (Tumor Regression Grade): response to neoadjuvant RT/CRT (radiotherapy/chemoradiotherapy) according to Mandard criteria[147], which are classified into five grades from TRG1 (complete regression) to TRG5 (no regression) based on the presence of residual cancer cells and on the degree of fibrotic changes. Staining intensity score: neg., negative; 1+ low; 2+ moderate; 3+ high. n.a. =not assessed. MET expression score: NEG: negative < 5% cells; LOW: 5-35 % cells; MID: 36-75% cells; HIGH: > 75%.

Table 6. MET expression (immunohistochemistry: cumulative score) in naïve and neoadjuvant treated locally advanced rectal cancer

10. Genetic, phenotypic and functional characterization of patient-derived rectal stem-like cells (RCSCs)

PDX models of colorectal cancer were validated as faithful representative of the original tumors, able to retain the genetic and phenotypic features across multiple serial passages [128]. Moreover, as demonstrated in previous works from our laboratory [130, 148], colospheres derived from metastatic colorectal PDX ("xenospheres") display the operational properties of cancer stem-like cells and are a reliable *in vitro* model to investigate the therapeutic response at stem cell level. To unveil the mechanisms underlying the putative radioresistance of rectal cancer-stem like cells (RCSCs), taking advantage of the xenopatient-xenospheres platform (Figure 10A), we derived from PDX (xenopatients) a panel of RCSCs that were long-term propagated in culture as "xeno-rectospheres"(x-RS), and we used them to generate secondary tumors in recipient mice ("spheropatients"). In parallel, despite technical difficulties, we tried to isolate RS directly from human samples, in order to generate the so-called "patient-rectospheres", p-RS (Figure 10A). PDX models are also amenable to directly undergo radiotherapy and combination treatments and, most importantly, from treated xenografts, x-RS can be derived *in vitro* to evaluate stem-like cell frequency in response to therapy.

We could observe that the levels of MET expression of the human tumors were maintained after transplantation and propagation as PDX (Figure 10B). From 10 xenopatients displaying different levels of MET, five distinct x-RS lineages were established that displayed the ability to long-term self-propagate *in vitro* (efficiency of x-RS derivation: 50%). Two x-RS were derived from naïve tumors, while three x-RS were obtained from neoadjuvant irradiated samples (Figure 10C). Based on the standard protocol for CSC derivation, rectal spheroids were selected in serum-free medium supplemented with EGF and bFGF. This procedure revealed to be significantly longer than in cases of more aggressive tumors such as metastatic colorectal cancer or glioblastomas, thus the isolation of additional x-RS and p-RS is still ongoing.

The established PDX and the corresponding matched x-RS underwent analysis of genetic alterations frequently occurring in colorectal cancer: mutations of APC, TP53, KRAS, NRAS, BRAF and PIK3CA and copy number alteration of APC, EGFR, MET, PIK3CA, IGF2 . So far, from our panel we genetically characterized two naïve x-RS and one naïve PDX (Table 7).

x-RS 1436 and 1190 (derived from naïve patients) were then analyzed for expression of MET and markers previously used to isolate and characterize CSCs, such as BMI-1, SOX2, CD133, CD44 and CD24 [37] (Figure 10D). Flow-cytometric analysis showed that MET was highly and homogeneously expressed, thus both R1436 and R1190 were classified as MET-positive-x-RS. Both x-RS expressed high levels of BMI-1 and SOX2 in >90% of cells, and of CD44 and CD24 in at least 50% of cells; CD133, previously used to prospectively isolate CSCs from colorectal cancer [7], was expressed in 50% of cells in R1190 and in 20 % of cells in R1436.

To assess the tumorigenic potential of R1190 and R1436, 10^5 cells were injected subcutaneously into NOD/SCID mice to generate "spheropatients". Spheropatients reproduced the same morphology and showed a highly similar immunostaining pattern as the corresponding original human tumors (Figure 10E,F). Both spheropatients and patients expressed cytokeratin 20 (CK20) and CDX2, but not cytokeratin 7 (CK7) (Figure 10F), which is a typical pattern of rectal cancer tumors [36, 149], thus confirming the tumorigenic and pseudo-differentiating ability of RSCs [7, 22, 37, 150]. Like in GBM and metastatic colorectal cancer, secondary x-RS could be rederived from spheropatients, which retained the same *in vitro* properties and tumorigenicity of the primary x-RS, namely the ability to sustain serial transplantation (data not shown).

A

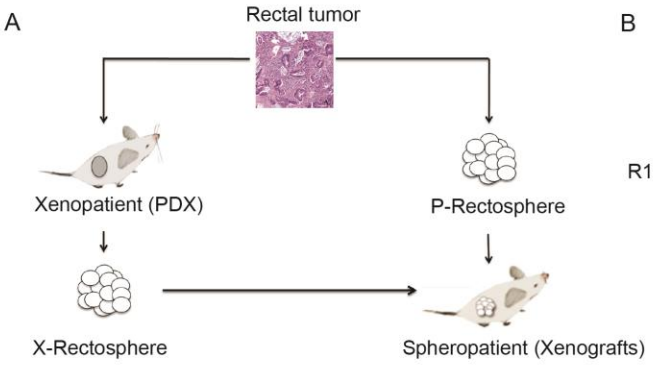

B

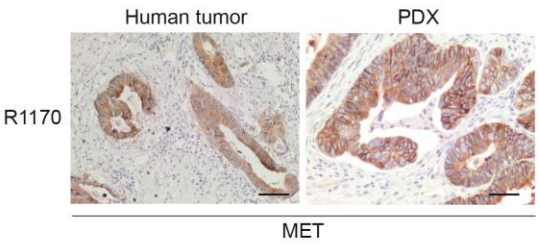

C

	X-Rectospheres	MET expression (IHC)	Derivation
Naive	R1190	mid	YES
	R1436	low	YES
	R1170	high	Ongoing
	R1142	low	NO
Neoadj RT	R0374	mid	YES
	R0288	mid	YES
	R0368	mid	NO
	R0468	high	NO
	R0506	high	NO
	R0514	mid	YES

D

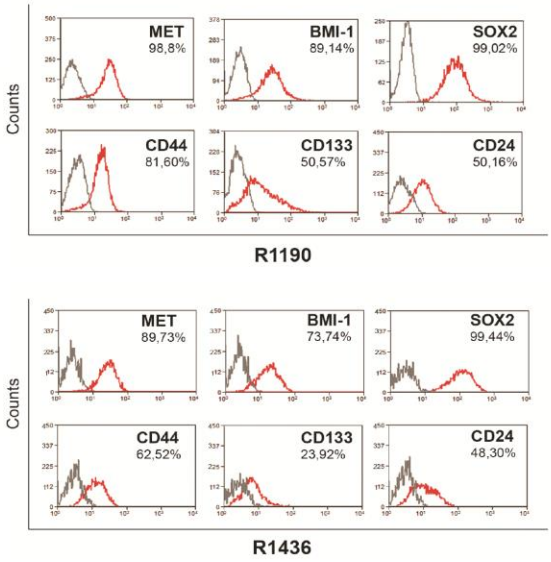

E

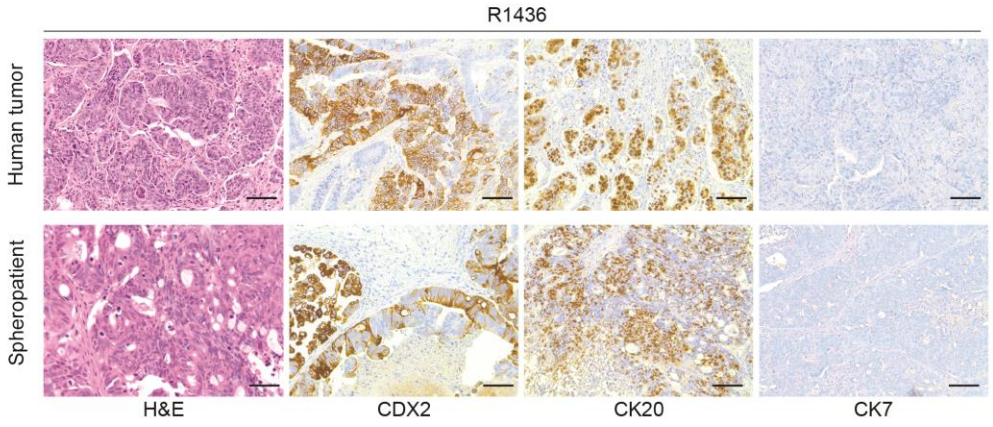

Figure 10. Characterization of patient-derived rectal stem-like cells (RCSCs). A. The xenopatient–xenosphere–spheropatient platform. The patient's surgical sample is xenografted in NOD/SCID mice and propagated (xenopatient, PDX). From these xenografts, cancer stem-like cells are selected and expanded in stem cell medium (X-rectospheres). RS could be also directly derived from patients' samples (P-Rectospheres). After transplantation in mice (spheropatient), these cells generate tumors that faithfully retain the genotypic and phenotypic features of the original tissues. **B.** Representative MET immunohistochemical staining on patient sample and the corresponding PDX. Scale bar, 50 µm (40x magnification). **C.** Table showing derivation of RS from 10 MET-expressing rectal cancer PDX. % of established RS: 50% **D.** Flow-cytometric analysis of MET and stem markers (BMI-1, SOX2, CD44, CD133, CD24, red lines) in two representative RS (R1190, R1436); Grey line: negative control; **E.** Representative hematoxylin and eosin (H&E) staining and immunohistochemical analysis of relative differentiation markers (CK20, CDX2, CK7) in original human tumor and the corresponding spheropatient (R1436). H&E Scale bar, 50 µm (40x magnification). Immunohistochemistry, Scale bar 100 µm (20x).

X-Rectosphere code						APC (full coding region Ex15)		TP53 (full coding region - Ex3)		KRAS (hot spot)		BRAF (hot spot)		NRAS (hot spot)		PIK3CA (hot spot)	
	$EGFR^{CNA}$	HGF^{CNA}	MET^{CNA}	$PIK3CA^{CNA}$	$IGF2^{CNA}$	Mutation	Consequence	Mutation	Consequence	Mutation	Consequence	Mutation	Consequence	Mutation	Consequence	Mutation	Consequence
R1436	wt	wt	+	wt	wt	c.3883G>T	p.E1295*	c.731G>A	p.G244D	c.35G>C	p.G12A	-	-	-	-	-	-
R1190	wt	-	wt	wt	++	c. 3949G>C c.4012C>T	p. E1317Q p. Q1338*	c.844C>T	p.R282W	-	-	-	-	-	-	-	-

PDX - code						APC (full coding region Ex15)		TP53 (full coding region - Ex3)		KRAS (hot spot)		BRAF (hot spot)		NRAS (hot spot)		PIK3CA (hot spot)	
	$EGFR^{CNA}$	HGF^{CNA}	MET^{CNA}	$PIK3CA^{CNA}$	$IGF2^{CNA}$	Mutation	Consequence	Mutation	Consequence	Mutation	Consequence	Mutation	Consequence	Mutation	Consequence	Mutation	Consequence
R1170	-	-	wt	wt	wt	c.3927_3931delAAAGA	p.E1309fs*4	-	-	-	-	-	-	-	-	-	-

Table 7. Genetic alterations in rectospheres and rectal cancer PDX. Copy number alterations are expressed as follows: -: heterozygous loss (copy number <1.5); wt: copy number between 1.5 and 3; ++: amplification (IGF2 copy number >9; copy number difference between EGFR and HGF or MET and HGF greater than 5) +: copy number gain (copy number >3 in absence of amplification). APC, TP53, KRAS, BRAF, NRAS, PIK3CA are indicated on both coding and protein sequences.

11. MET inhibition radiosensitize RCSCs *in vitro*

Having shown that MET is a therapeutic target for radioresensitization of the GSC subpopulation, next we investigated whether it could be exploited to radiosensitize MET-pos-RS as well.

First, in cell viability assays, we observed that the representative MET-positive $KRAS^{wt}$ x-RS (R1190) proliferated only in the presence of standard exogenous growth factors(EGF-bFGF), whereas representative $KRAS^{mut}$ x-RS (R1436) displayed the same proliferation rate irrespective of exogenous growth factors, and its proliferation was not further increased by either EGF and/or bFGF supplied to the medium (Figure 11A). These data confirmed that proliferation of RAS^{wt} but not RAS^{mut} xenospheres requires exogenous growth factors, as previously shown by Luraghi et al. in an ample panel of xenospheres derived from metastatic colorectal cancer [130]. To assess radiosensitization of xeno-rectospheres, R1190 x-RS were kept in a standard EGF/bFGF medium, supplied with HGF to better mimick the tumor-microenviroment and warrant MET activation. HGF supply did not further increase proliferation (not shown). R1436 x-RS was kept in basal medium devoid of any exogenous growth factors, as this x-RS not only displayed proliferative autonomy, but also a HGF/MET autocrine loop (data not shown). In both x-RS, the association of the specific MET inhibitor JNJ-38877605 to irradiation significantly and similarly reduced cells viability as compared with irradiation alone (Figure 11B,C).

Accordingly with our findings in neurospheres, also in MET-positive x-RS, in time-point experiments, we found that MET phosphorylation was markedly increased by irradiation, peaking at 30' after treatment and lasting, although progressively decreasing, at least for 48 hours. MET phosphorylation was accompanied by sustained AKT and ATM phosphorylation. IR-induced MET phosphorylation was fully prevented by the MET inhibitor, while AKT and ATM phosphorylation was significantly inhibited only at late time-points. Interestingly, distinctive markers of apoptosis activation, such as PARP and caspase 3 cleaved forms, significantly increased in cells irradiated in the presence of the MET inhibitor, concomitantly with ATM and AKT inhibition (Figure 11D). Together, these findings indicate that also in MET-positive xeno-rectospheres, MET inhibition efficiently radiosensitizes cancer stem-like cells.

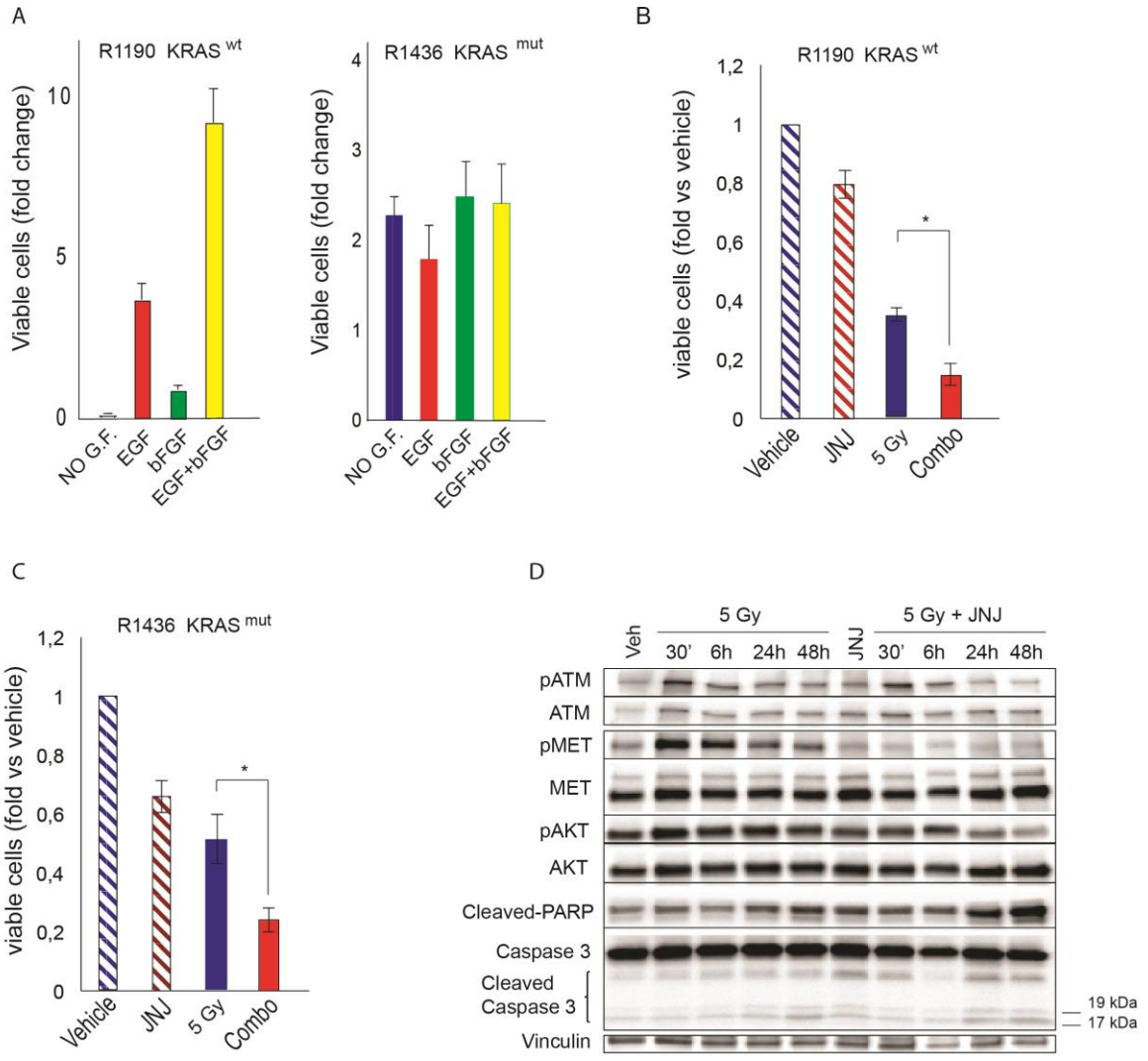

Figure 11. MET inhibition radiosensitize RCSCs *in vitro.* A. Cell viability of x-RS kept in basal stem-cell medium either alone (no growth factors) or with the indicated growth factors for 7 days. Columns, relative cell viability versus cell viability at time 0. Left: R1190 x-RS ($KRAS^{wt}$); Right: R1436 x-RS ($KRAS^{mut}$); n=3. **B.** Cell viability of R1190 x-RS ($KRAS^{wt}$) cultured in standard stem-cell medium (EGF-bFGF) supplied with HGF (10ng/ul), irradiated in the absence (5 Gy) or in the presence (5 Gy + JNJ) of the MET inhibitor JNJ38877605 (500 nM). Cell viability was assessed at day 7. Vehicle: non-irradiated cells (fold versus vehicle-treated cells at time 0, mock). *: t-test, P <0.001 . n=2. **C.** Cell viability of R1436 x-RS ($KRAS^{mut}$) cultured in basal stem-cell medium (no growth factors, GF), irradiated in the absence (5 Gy) or in the presence (5 Gy + JNJ) of the MET inhibitor JNJ38877605 (500 nM). Cell viability was assessed at day 7. Vehicle: non-irradiated cells (fold versus vehicle-treated cells at time 0, mock). *: t-test, P <0.05. n=2. **D.** Western blot of R1436 x-RS showing phosphorylation of ATM (pATM), MET (pMET), AKT (pAKT) and activation of PARP (cleaved-PARP) and caspase 3 (cleaved-caspase 3) at the indicated time points after IR in the absence (5 Gy) or in the presence (5 Gy + JNJ) of the MET inhibitor JNJ38877605 (500 nM). Total ATM, MET and AKT are also shown. Vinculin was used as a loading control. Veh: non-irradiated vehicle-treated cells.
Data information: data are represented as mean ± SEM in (A,B,C).

12. MET inhibition sensitizes rectal cancer PDX to radiotherapy and targets RCSCs *in vivo*

While isolating and characterizing rectal stem-like cells from PDX, we started to assess whether MET inhibitors can radiosensitize rectal xenopatients and decrease their CSC content.

As performed in GBM xenografts, MET-expressing rectal cancer PDX underwent a tomotherapy treatment established in collaboration with the Radiotherapy Unit in our institute, which mimicks the human neoadjuvant irradiation protocol, it is targeted to the tumor area and it is well tolerated by NOD-SCID mice [151]. PDX were also treated in combination or in alternative with the MET inhibitor JNJ38877605.

First, we tried to radiosensitize R1436 PDX (as mentioned above derived from a naive rectal cancer harboring KRAS mutation and a HGF/MET autocrine loop). Once established, PDX were randomized into four treatment groups: (i) vehicle, (ii) fractionated IR (1,8 Gy x 3 days), (iii) JNJ38877605, administred for 20 days starting from the day before the first irradiation, and (iv) combination therapy (combo, IR and JNJ38877605). As showed in Figure 12A, this tumor was highly radioresistant, as radiotherapy alone negligibly impaired tumor growth. Remarkably, xenopatients responded to combination therapy with tumor stabilization, which lasted for 30 days. Of note, the survival analysis showed that the experimental endpoint of 1600 mm^3 in tumor volume was reached significantly later in the combo group as compared with the radiotherapy alone group (Figure 12B).

Next, the radiosensitizing effect of MET-inhibition was assessed on R1170 PDX (another naïve rectal cancer lacking mutations in KRAS, BRAF, NRAS and PIK3CA- referred to as quadruple wild type). Once established, rectal PDX were randomized in four groups and treated as described above. Also R1170 xenopatients displayed a remarkable radioresistance as radiotherapy alone slowed down tumor growth for a few days, but then the tumor size doubled within 18 days from the beginning of treatments. Interestingly, association of MET-inhibition with radiotherapy induced desease stabilization for 20 days (Figure 12C). Then, tumors in the combo group restarted to grow slowly, reaching the establish tumor volume endpoint after 40 days. Consistently, survival analysis showed that, also in this model, combination therapy significantly enhanced mouse survival as compared with other treatments alone (Figure 12D).

In an independent experiment, performed again with R1436 PDX, the effect of MET targeting associated with radiotherapy was also assessed by the use of the clinically

approved, promiscuous small-molecule inhibitor crizotinib (targeting MET and ALK kinases). Xenopatients were treated as described above and MET-inhibitors were supplied for 10 days. As showed in Figure 13A, crizotinib blocked tumor growth, displaying a radiosensitizing effect comparable with JNJ38877605. Ten days after the beginning of the therapy, in tumors treated with the association of MET-inhibitors (crizotinib or JNJ38877605) and radiotherapy, Ki67 index showed to be significantly reduced as compared with tumors in the other treatment arms (Figure 13B). Notably, together with a reduced tumor volume and Ki67 index, in combo-treated PDX we could observe larger necrotic areas as compared with PDX that received each other treatment alone (Figure 13B and data not shown). As compared with the other treatment arms, tumors of combo groups showed also a significant reduction in phosphorylated S6 kinase, a surrogate biomarker of MET inhibition, as observed by immunohistochemistry (Figure 13 C).

To further assess whether MET inhibition associated with radiotherapy results in targeting rectal-stem like cells *in vivo*, we isolated RCSCs from explanted tumors of each treatment arm, and evaluated their frequency by *in vitro* (sphere-forming) LDA. Although the RCSC frequency measured by this assay is relatively low even in untreated tumors, a significant RCSC depletion was observed in tumors treated with combination therapy with either inhibitor, as compared with the other treatment arms.

Collectively, these data indicate that MET inhibitors radiosensitize MET-expressing rectal PDX. Radiosensitization likely occurs at the level of the whole tumor cell population, which extensively express MET, and affects also the cancer stem cell subpopulation.

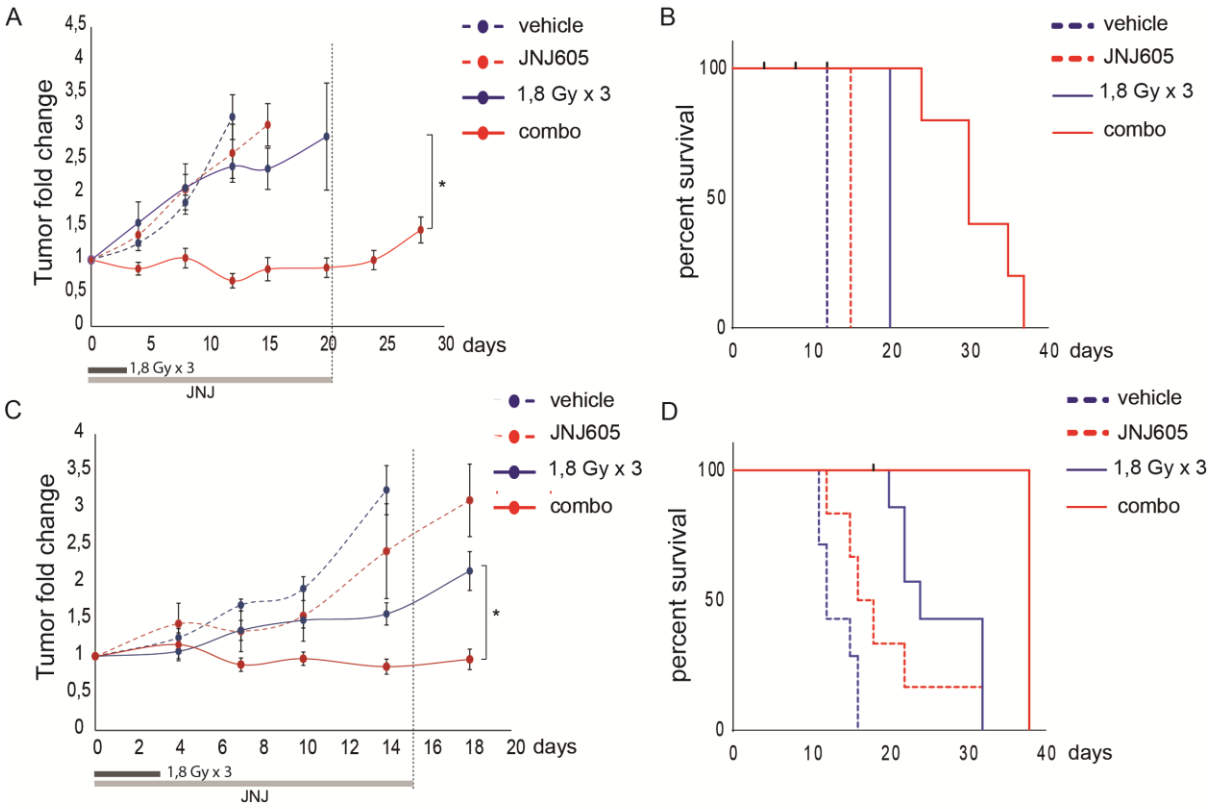

Figure 12. MET inhibition sensitizes rectal cancer PDX. A. Growth curves of rectal R1436 PDX ($KRAS^{mut}$), irradiated in the absence (1,8 Gy × 3 days) or in the presence (combo) of JNJ38877605, which was administered for 20 days as indicated (n = 7/condition). Vehicle: non-irradiated vehicle-treated PDX. Data are represented as fold change vs. day 0. One-way ANOVA, P = 0,0247; *: t test, (combo) vs (1,8Gy x 3 days), P < 0,05. **B.** Survival analysis of R1436 PDX treated as in (A). Black dot: censored mice. Log-rank (Mantel-Cox) test, p = 0,0019; Log-Rank (Mantel Cox) test, (combo) versus (1,8 Gy × 3 days), P = 0,0027. **C.** Growth curves of rectal R1170 PDX (quadruple wt), irradiated in the absence (1,8 Gy × 3 days) or in the presence (combo) of JNJ38877605, supplied from day 0 to 15 (n = 7/condition). Vehicle: non- irradiated vehicle-treated PDX. Data are represented as fold change vs. day 0. One-way ANOVA test, P=0,014; *: t test, (combo) vs (1,8Gy x 3 days), P < 0.05 **D.** Survival analysis of R1170 PDX treated as in (C). Black dot: censored mouse. Log-rank (Mantel-Cox) test, p=0.0003; (combo) vs (1,8Gy x 3 days), Log-Rank (Mantel Cox) test, p = 0.01.
Data information: data are represented as mean ± SEM in (A,C).

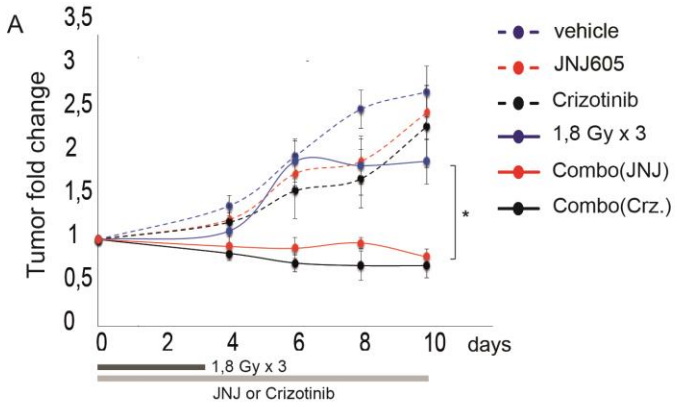
A
Tumor fold change
3,5
3
2,5
2
1,5
1
0,5
0
0
2
4
6
8
10
days
1,8 Gy x 3
JNJ or Crizotinib
vehicle
JNJ605
Crizotinib
1,8 Gy x 3
Combo(JNJ)
Combo(Crz.)
*

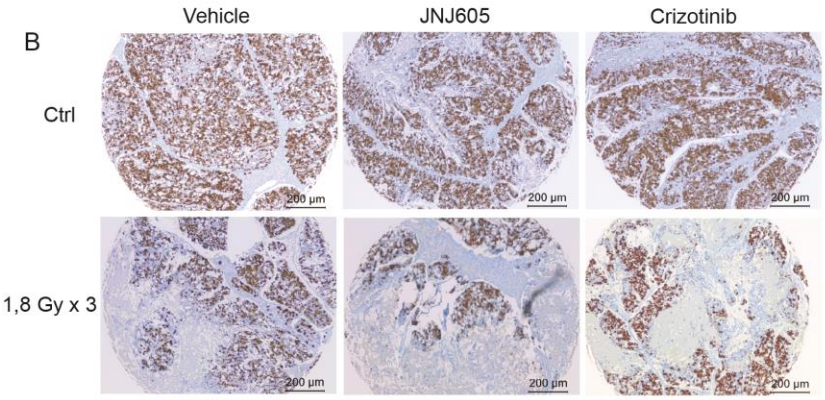
B
Vehicle
JNJ605
Crizotinib
Ctrl
1,8 Gy x 3
200 µm

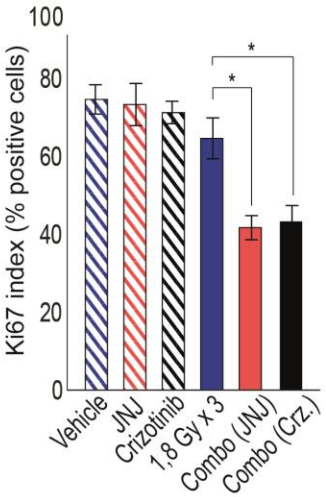
Ki67 index (% positive cells)
100
80
60
40
20
0
*
*
Vehicle
JNJ
Crizotinib
1,8 Gy x 3
Combo (JNJ)
Combo (Crz.)

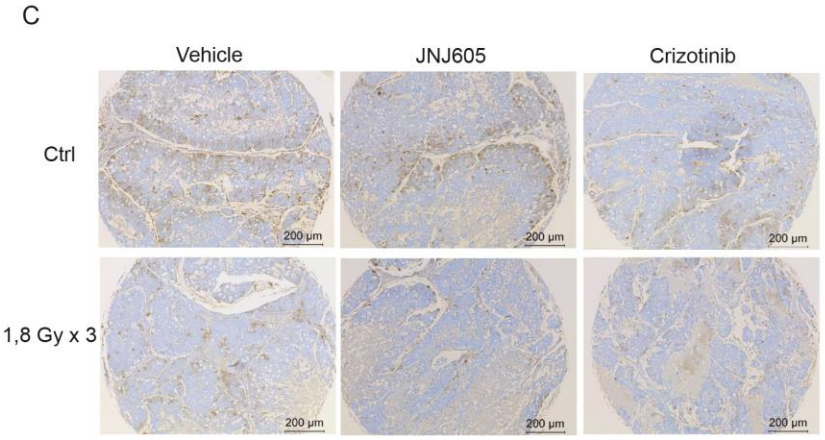
C
Vehicle
JNJ605
Crizotinib
Ctrl
1,8 Gy x 3
200 µm

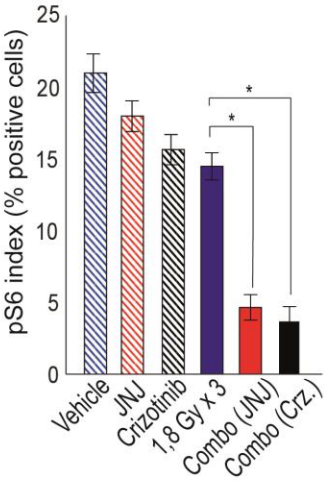
pS6 index (% positive cells)
25
20
15
10
5
0
*
*
Vehicle
JNJ
Crizotinib
1,8 Gy x 3
Combo (JNJ)
Combo (Crz.)

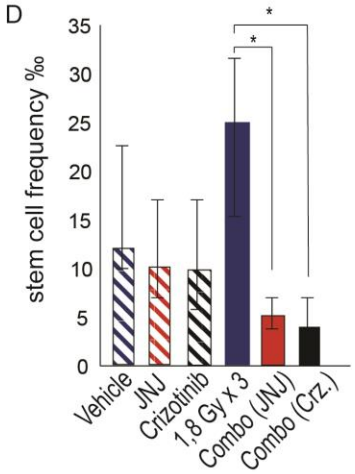
D
stem cell frequency ‰
35
30
25
20
15
10
5
0
*
*
Vehicle
JNJ
Crizotinib
1,8 Gy x 3
Combo (JNJ)
Combo (Crz.)

Figure 13. Analysis of tissues and stem-cell frequency in PDX radiosensitized with MET inhibitors. **A.** Growth curves of rectal R1436 PDX ($KRAS^{mut}$), irradiated in the absence (1,8 Gy × 3 days) or in the presence (combo) of JNJ38877605 or Crizotinib (Crz.) respectively. Small molecule inhibitors were administered for 10 days (n = 3/condition). Vehicle: non-irradiated vehicle-treated PDX. Data are represented as fold change vs. day 0. One-way ANOVA, P = 0,006; **B.** Left: Ki67 immunohistochemical staining of R1436 PDX tumor TMA (tissue microarray) sections treated as indicated in (A). Scale bar, 200 µm (10x magnification). Right: Quantification of Ki67 positive cells (n = 9 HPF/group). HPF: high-power field. One-way ANOVA, p < 0.0001; *: t-test, (comboJNJ) vs (1,8Gy x 3 days), p= 0,002; (comboCrz.) vs (1,8Gy x 3 days), p= 0,0065 **C.** Left: pS6 immunohistochemical staining of R1436 PDX tumor TMA sections treated as indicated in (A). Scale bar, 200 µm (10x magnification). Right: Quantification of pS6 positive cells (n=9 HPF/group). One-way ANOVA, p < 0,0001; *: t-test, (comboJNJ) vs (1,8Gy x 3 days), p <0.0001; (comboCrz.) vs (1,8Gy x 3 days), p < 0.0001. **D.** LDA (Sphere-forming) measuring the *in vitro* frequency of RCSCs in tumors treated as indicated in (A) (n= 3/condition) * χ^2 test, p = 0,0017; (comboJNJ) vs (1,8Gy x 3 days), p= 0,0002.
Data information: data are represented as mean ± SEM in (A,B,C) or mean ± CI in (D).

Discussion

Radiation therapy is a double-edge sword in cancer treatment [76, 152]. On the one hand, thanks to continuous technological progress, ionizing radiation (IR) can be very precisely targeted to the tumor bulk, effectively killing tumor cells while sparing the surrounding normal tissues; on the other hand, it often promotes positive selection of a subpopulation of radioresistant cells that drive recurrence of intractable tumors. The genetic and molecular basis of tumor radioresistance are still poorly understood and deserve accurate elucidation in order to identify therapeutic targets to circumvent radiotherapy pitfalls. In GBM the inevitable failure of current standard treatments and targeted monotherapies has been associated with the existence of GBM cancer stem-like cells (GSCs), which may drive tumor recurrence [153]. Pioneering works have been shown that these resilient GSCs are endowed with the intrinsic ability to efficiently activate DDR in response to IR and/or chemotherapy [19, 52, 70, 138, 154-156], a property conceivably inherited from the cell of origin, a neural stem/progenitor cell [157]. The intrinsic radioresistance of GSCs has been significantly associated also with the ability to efficiently activate pro-survival pathways, either through the direct modulation of anti-apoptotic mechanisms, or by regulation of the DNA repair machinery itself [76, 83, 88, 158]. These pathways are largely controlled by receptor tyrosine kinases (RTKs), such as the epidermal growth factor receptor (EGFR), which is known for sustaining the stem and tumorigenic phenotype of GSCs, propagated *in vitro* as neurospheres [92]. As suggested by previous studies, the typical EGFR amplification, usually harbored by neurospheres displaying the so-called 'classical' GBM signature [96, 123], could play a key role in conferring radioresistance to GSCs [76]. More recently, GSC radioresistance has been distinctively associated with the GBM 'mesenchymal' transcriptional profile [159]. These findings imply a causal role for the subtype-specific genetic lesions and/or signaling circuits, in particular of the NF-κB pathway [159]. Interestingly, previous work in our laboratory, showed that MET is a transcriptional target of NF-κB, upregulated by ionizing radiation and inflammatory signals, such as TNF-α, often released by irradiated tumor cells and microenvironment [95, 160]. Thus, in mesenchymal and proneural neurospheres, usually lacking EGFR amplification [96], we investigated whether a relevant role in radioresistance could be played by the wild-type MET oncogene, which was previously associated with the mesenchymal profile in both GBM tissues [123, 138] and neurospheres [96], and is usually expressed in a mutually exclusive fashion with EGFR [96, 123].

Building on previous studies by our laboratory and others, showing that MET is a marker of a GSC subtype, which identifies and sustains the stem phenotype [96, 121, 125], we showed that MET is a functional marker of GSC radioresistance.

We previously reported that about 40% of neurosphere lineages derived from primary GBM express MET [96]. In each lineage, every neurosphere is a heterogeneous mix of cells that either highly express MET (MET^{high}) or that do not express MET at all (MET^{neg}). The MET^{high} subpopulation, in each neurosphere, displays the distinctive characteristics of stem-like cells [96]. In the current study, we found that the MET^{high} subpopulation is selectively enriched upon irradiation of MET-positive neurospheres *in vitro,* and of xenografts derived by neurosphere transplantation in immunocompromised mice. We hypothesized that the observed enrichment is due to the intrinsic radioresistance of the MET^{high} stem-like cells, and indeed we found that the MET^{high} subpopulation was significantly more radioresistant than its MET^{neg} counterpart. Moreover, in the MET^{high} cells, the DDR kinase ATM and its downstream kinase Chk2 [63] were constitutively active, and their activities were further increased by IR. Such a heightened DDR response conceivably allowed these cells to efficiently repair radiation-induced DNA damage and successfully survive IR.

The protective role of MET likely operates in human GBMs treated with the standard combination of radio- and chemotherapy [161]. Indeed, in the analyzed panel of patients' recurrent GBM, MET expression was significantly enriched as compared with the matched primary tumor. This evidence suggests the expansion of MET-expressing (stem-like) cells, likely benefitting of a selective advantage under therapeutic pressure, and thus possibly mediating the peculiar radioresistance of the recurrent tumor. Not surprisingly, analysis of the TCGA dataset indicates that a high MET expression in primary GBM is associated with primary therapeutic resistance and poorer prognosis [129]. On these premises it would be expected that MET amplification would confer distinctive radioresistance to primary GBM. Unfortunately, this genetic alteration being found only in 3% of all GBM [162], we had no representative neurosphere to assess. However, the hypothesis is supported by an independent experimental model of murine high grade gliomas, where irradiation leads to development of tumors with frequent MET amplification [112]. In summary, considering that (i) IR transcriptionally upregulates MET; (ii) MET-expressing GSCs are positively selected by IR; and (iii) MET amplification can be induced and positively selected by IR, it is expected that radiotherapy could both generate and select MET-overexpressing GSCs that would

drive tumor recurrence and therapy resistance.

This evidence compelled us to investigate the possibility to overcome GSC radioresistance by MET inhibition. Indeed, we show that MET small molecule kinase inhibitors combined with IR decrease the radioresistance of GSCs (MET^{high}) to levels comparable with non-stem (MET^{neg}) cells. Importantly, we could also observe that the addition of HGF increased radiation-induced ATM and Chk2 activation, while the MET inhibitor impairs ATM phosphorylation and the downstream DDR pathway.

Till now, the relationship between receptor tyrosine kinase signaling and DDR has been poorly characterized. To mechanistically elucidate the link between MET signaling and ATM activation, we examined two pathways downstream MET, the PI3K-AKT and MAP kinase (MAPK) signaling cascades [103]. We found that both AKT and MAP kinases are hyperphosphorylated in irradiated cells. This hyperactivation depends on MET, as it is prevented by combining IR with the MET inhibitor. Moreover, IR combination with either MAPK or AKT inhibitors showed that AKT, but not MAPK, is the likely connection between MET and ATM phosphorylation. Interestingly, AKT activation has been previously correlated with poor prognosis in GBM [138], and with radioresistance in other brain tumors [93]. However, it was currently unknown whether AKT can directly affect ATM phosphorylation. We showed that a plausible intermediary is Aurora A, known to be both an AKT substrate and a kinase active on ATM [64], but not yet implied in DDR modulation by growth factor signaling. AKT appears to play also an additional role in MET-mediated radioresistance: AKT-dependent phosphorylation of p21 has been shown to result in cytoplasmic retention of p21, where it exerts anti-apoptotic functions [163]. We showed that MET activation in MET-positive neurospheres results in p21 phosphorylation and its cytoplasmic retention, and that this can be reversed by MET inhibition. Thus, MET appears to promote GSC survival both by stimulating DSB repair as well as by inhibiting apoptosis.

Translationally, these results clearly indicate that MET inhibition may be a possible strategy for sensitizing GSCs to IR in the clinical setting. To provide proof of concept, we established tumors by intracranial or subcutaneous xenotransplantation of MET-positive neurospheres in NOD-SCID mice, which faithfully recapitulate the histology of the original tumors. Xenografts were treated with a combination of fractionated radiotherapy and JNJ38877605, a MET inhibitor that crosses the blood-brain barrier, as shown by us [129]. Indeed, we found that the combination treatment significantly delayed tumor growth and, in some cases, lead

to tumor regression, increasing mice survival as compared to radiotherapy alone. Importantly, combination treatment not only caused tumor shrinkage, but also reduced the GSC content. We think that the evaluation of the therapeutic outcome on cancer stem cells is essential to establish whether a treatment has the potential to be long-term effective, and, ideally, curative. Disappointedly, this kind of evaluation is mostly disregarded in conventional settings testing either radio-chemotherapy and/or targeted agents, which remain based on assessment of tumor shrinkage [50, 156, 164].

These findings open new perspectives for combination therapy in GBM patients expressing the MET receptor and/or its downstream effectors. Inhibitors for MET, AKT, and Aurora-A are already in clinical trials, and, most recently, crizotinib—a small-molecule MET inhibitor, has been shown to drive tumor regression in adult and pediatric glioma patients [165, 166]. Although the effect of crizotinib (or other inhibitors given as monotherapy), is likely negligible in the absence of a genetic alteration of the target, our pre-clinical data provide a strong rationale for the concomitant administration of IR and MET inhibitors in all patient that express wild-type MET. It must be also considered that MET expression can be heterogeneous within a single GBM (our unpublished data). In these cases, the tumor is likely to contain, together with MET-positive 'mesenchymal'/'proneural' areas, also MET-negative 'classical' areas that usually harbor EGFR amplification (our unpublished data and [167]). Therefore, it would be appropriate to model heterogeneous tumor in the mouse and assess strategies to concomitantly radiosensitize MET-positive and MET-negative areas. In the latter, EGFR inhibition could be effective.

Results obtained in GBM prompted us to further investigate whether this combinatorial approach could be extended to other tumors whose radioresistance depends on MET, possibly to achieve depletion of the stem cell subpopulation. Senetta and colleagues, recently found that in locally advanced rectal adenocarcinoma, MET expression reliably predicts a lack of response to neoadjuvant chemo-radiotherapy (CRT) [118], thus suggesting a protecting role of MET.

The role of MET in the development of intestinal epithelium [168] and in the pathogenesis of colorectal cancer has been extensively described [169, 170]. More recently it was shown that MET amplification is a mechanism of both primary and secondary resistance to anti-EGFR therapies [101] and that HGF can sustain the WNT self-renewal pathway [122, 171], a well-known regulator of normal and cancer stem cell self-renewal. Accumulating evidence

indicates that also in colorectal cancer the CSC subpopulation is responsible for cancer initiation, relapse, and metastasis [6, 7, 36, 37, 130, 172]. In a previous study from our laboratory, Luraghi and colleagues demonstrate that MET was expressed in xenospheres of metastatic colorectal cancer and that HGF sustains their long-term proliferation [130]. Moreover, in xenospheres MET was downregulated upon differentiation *in vitro*, suggesting a specific association of MET expression with the stem/progenitor compartment. Although colon CSCs have been widely described, limited information is available on those derived from rectal cancer. In addition, the gradual changes in colorectal cancer molecular features within the bowel [173, 174] can cause significant biological differences between colon and rectal CSCs (RCSCs). Recently, in rectospheres derived from primary rectal cancer, Fan and coworkers identified a CD44+/CD54+ RCSC subpopulation that retained the peculiar CSC features, and efficiently resisted to a conventional chemotherapeutic regimen and/or to cetuximab *in vitro* and *in vivo* [175]. Interestingly, the CD44+/CD54+ cell subpopulation displayed a mesenchymal phenotype [175] previously associated with poor prognosis in colorectal cancer patients [176]. Although the colorectal mesenchymal signature has been recently associated to extensive contamination by cancer-associated stroma [177] much evidence shows that epithelial-mesenchymal transition is associated with the cancer stem cell phenotype [18], and it is reminiscent of the invasive growth phenotype induced by MET [97].

Based on this evidence, we set out to study the role of MET in RCSCs. To this end we collected a panel of 28 locally advanced cancer both naïve or treated with neoadjuvant radiotherapy, finding that MET is widely expressed in most samples. We then isolated RCSCs as xeno-rectospheres (x-RS), i.e. from xenopatients (PDX) established by transplantation of MET expressing tumors inspiring to previous work that showed the validity of this model to evaluate the therapeutic response at stem cell level [130, 148, 178]. x-RS displayed MET expression and the operational properties of CSCs. Indeed, they showed long-term self-renewal ability *in vitro*, and, when implanted in immunocompromised mice, formed tumors almost indistinguishable from the originals, with a pattern of markers expression highly similar to the corresponding original human tumors. So far, we have fully characterized two x-RS harboring distinct genetic lesions and growth factor requirements for proliferation and self-renew, confirming the relevance of the KRAS gene status for proliferation and survival.

Indeed, KRAS mutation self-sustains x-RS growth which cannot be further stimulated by exogenous growth factors [130].

Although we did not provide functional evidence of the role of MET in supporting the stem phenotype in RCSCs, we could observe that, like in MET- positive neurospheres, MET inhibition significantly radiosensitizes both x-RS, irrespectively of their genetic makeup. Moreover, we found that in RCSCs, upon irradiation, MET was hyperphosphorylated and efficiently activated the pro-survival PI-3 kinase-AKT pathway. Consistently, MET inhibition not only prevented IR-induced MET phosphorylation but also inhibited AKT and ATM activation, thereby quenching the DDR pathway and inducing cell apoptosis. This study, provided also preclinical evidence that MET inhibition associated with radiotherapy can radiosensitize highly radioresistant rectal PDX and significantly prolong mouse survival. Importantly, in a case harboring a RAS mutation and expressing an autocrine HGF/MET loop, both the specific MET inhibitor JNJ38877605 or the clinically approved- MET/ALK inhibitor – crizotinib, combined with radiotherapy, efficiently impaired tumor growth by depletion of the RCSC subpopulation.

Even though in both GBM and rectal cancer models we could target and decrease the CSC frequency within tumors radiosensitized by MET inhibition, in some mice we could not achieve a complete depletion of the CSC subpopulation, which resulted in tumor regrowth. A possible explanation could reside in the limited bioavailability of the small molecules agents and/or not appropriate irradiation protocol. In this respect, it is known that MET-expressing CSCs may be located in hypoxic niches, adjacent to necrotic areas, with little or no blood perfusion [106, 125]. This relative CSC inaccessibility could be critical especially if the plasma half-life of the drug is short. Taking into account this important issue, we are currently trying to assess different protocols by changing doses, administration schedules and drug delivery systems to optimize the outcome of the combinatorial treatments. Another explanation for the incomplete elimination of CSCs in the tumor relates with the issue of intratumor heterogeneity, well evident in GBM as mentioned above, but also possible in colorectal cancer. It is becoming clear that genetic heterogeneity reflects at the cancer stem cell level [57, 179]. As result, distinct and coexistent stem-like cell subclones might be differentially selected under the therapeutic pressure targeting a single CSC subpopulation [55-58, 180]. In addition, as reported by recent findings, targeted elimination of CSCs could be hindered by the plasticity of the CSC status, which implies the possibility of

CSC regeneration from the differentiated non-CSCs through extracellular signals and reprogramming mechanisms [17, 59, 181]. Notwithstanding these reservations, targeting tyrosine kinases and the DDR pathway in CSCs is a promising strategy to improve the efficacy of radiotherapy by depletion of CSCs subpopulation.

In targeting MET in GBM and rectal cancer patients, like in the case of any other targeted therapy, the success of MET inhibitors or antibodies will ultimately depend on the accurate identification of patients expressing the functional target. According to the analysis presented in this and previous studies [96, 118, 182] it is expected that a relevant fraction of GBM patients (~40%) and the majority of rectal cancer will be MET-positive. In the clinical setting, to identify these patients it should be recommended to integrate protein expression and genetic data, ideally obtained by analysis of multiple tumor tissue specimens or more accessible biological samples containing traces of tumor proteins and DNA (liquid biopsy).

References

1. Bonnet, D., and Dick, J.E. (1997). Human acute myeloid leukemia is organized as a hierarchy that originates from a primitive hematopoietic cell. Nat Med *3*, 730-737.
2. Reya, T., Morrison, S.J., Clarke, M.F., and Weissman, I.L. (2001). Stem cells, cancer, and cancer stem cells. Nature *414*, 105-111.
3. Clarke, M.F., Dick, J.E., Dirks, P.B., Eaves, C.J., Jamieson, C.H., Jones, D.L., Visvader, J., Weissman, I.L., and Wahl, G.M. (2006). Cancer stem cells--perspectives on current status and future directions: AACR Workshop on cancer stem cells. Cancer Res *66*, 9339-9344.
4. Singh, S.K., Clarke, I.D., Terasaki, M., Bonn, V.E., Hawkins, C., Squire, J., and Dirks, P.B. (2003). Identification of a cancer stem cell in human brain tumors. Cancer Res *63*, 5821-5828.
5. Galli, R., Binda, E., Orfanelli, U., Cipelletti, B., Gritti, A., De Vitis, S., Fiocco, R., Foroni, C., Dimeco, F., and Vescovi, A. (2004). Isolation and characterization of tumorigenic, stem-like neural precursors from human glioblastoma. Cancer Res *64*, 7011-7021.
6. O'Brien, C.A., Pollett, A., Gallinger, S., and Dick, J.E. (2007). A human colon cancer cell capable of initiating tumour growth in immunodeficient mice. Nature *445*, 106-110.
7. Ricci-Vitiani, L., Lombardi, D.G., Pilozzi, E., Biffoni, M., Todaro, M., Peschle, C., and De Maria, R. (2007). Identification and expansion of human colon-cancer-initiating cells. Nature *445*, 111-115.
8. Al-Hajj, M., Wicha, M.S., Benito-Hernandez, A., Morrison, S.J., and Clarke, M.F. (2003). Prospective identification of tumorigenic breast cancer cells. Proc Natl Acad Sci U S A *100*, 3983-3988.
9. Valent, P., Bonnet, D., De Maria, R., Lapidot, T., Copland, M., Melo, J.V., Chomienne, C., Ishikawa, F., Schuringa, J.J., Stassi, G., et al. (2012). Cancer stem cell definitions and terminology: the devil is in the details. Nat Rev Cancer *12*, 767-775.
10. Batlle, E., and Clevers, H. (2017). Cancer stem cells revisited. Nat Med *23*, 1124-1134.
11. Schepers, A.G., Snippert, H.J., Stange, D.E., van den Born, M., van Es, J.H., van de Wetering, M., and Clevers, H. (2012). Lineage tracing reveals Lgr5+ stem cell activity in mouse intestinal adenomas. Science *337*, 730-735.
12. Chen, J., Li, Y., Yu, T.S., McKay, R.M., Burns, D.K., Kernie, S.G., and Parada, L.F. (2012). A restricted cell population propagates glioblastoma growth after chemotherapy. Nature *488*, 522-526.
13. Driessens, G., Beck, B., Caauwe, A., Simons, B.D., and Blanpain, C. (2012). Defining the mode of tumour growth by clonal analysis. Nature *488*, 527-530.
14. Magee, J.A., Piskounova, E., and Morrison, S.J. (2012). Cancer stem cells: impact, heterogeneity, and uncertainty. Cancer Cell *21*, 283-296.
15. Pece, S., Tosoni, D., Confalonieri, S., Mazzarol, G., Vecchi, M., Ronzoni, S., Bernard, L., Viale, G., Pelicci, P.G., and Di Fiore, P.P. (2010). Biological and molecular heterogeneity of breast cancers correlates with their cancer stem cell content. Cell *140*, 62-73.
16. Gupta, P.B., Chaffer, C.L., and Weinberg, R.A. (2009). Cancer stem cells: mirage or reality? Nat Med *15*, 1010-1012.
17. Scheel, C., and Weinberg, R.A. (2012). Cancer stem cells and epithelial-mesenchymal transition: concepts and molecular links. Semin Cancer Biol *22*, 396-403.
18. Shibue, T., and Weinberg, R.A. (2017). EMT, CSCs, and drug resistance: the mechanistic link and clinical implications. Nat Rev Clin Oncol *14*, 611-629.
19. Bao, S., Wu, Q., McLendon, R.E., Hao, Y., Shi, Q., Hjelmeland, A.B., Dewhirst, M.W., Bigner, D.D., and Rich, J.N. (2006). Glioma stem cells promote radioresistance by preferential activation of the DNA damage response. Nature *444*, 756-760.
20. Phillips, T.M., McBride, W.H., and Pajonk, F. (2006). The response of CD24(-/low)/CD44+ breast cancer-initiating cells to radiation. J Natl Cancer Inst *98*, 1777-1785.
21. Medema, J.P. (2013). Cancer stem cells: the challenges ahead. Nat Cell Biol *15*, 338-344.

22. Kreso, A., and Dick, J.E. (2014). Evolution of the cancer stem cell model. Cell Stem Cell *14*, 275-291.
23. Dirks, P.B. (2008). Brain tumor stem cells: bringing order to the chaos of brain cancer. J Clin Oncol *26*, 2916-2924.
24. Vescovi, A.L., Galli, R., and Reynolds, B.A. (2006). Brain tumour stem cells. Nat Rev Cancer *6*, 425-436.
25. Venere, M., Fine, H.A., Dirks, P.B., and Rich, J.N. (2011). Cancer stem cells in gliomas: identifying and understanding the apex cell in cancer's hierarchy. Glia *59*, 1148-1154.
26. Pastrana, E., Silva-Vargas, V., and Doetsch, F. (2011). Eyes wide open: a critical review of sphere-formation as an assay for stem cells. Cell Stem Cell *8*, 486-498.
27. Ishiguro, T., Ohata, H., Sato, A., Yamawaki, K., Enomoto, T., and Okamoto, K. (2017). Tumor-derived spheroids: Relevance to cancer stem cells and clinical applications. Cancer Sci *108*, 283-289.
28. Reynolds, B.A., and Rietze, R.L. (2005). Neural stem cells and neurospheres--re-evaluating the relationship. Nat Methods *2*, 333-336.
29. Reynolds, B.A., and Weiss, S. (1992). Generation of neurons and astrocytes from isolated cells of the adult mammalian central nervous system. Science *255*, 1707-1710.
30. Johansson, C.B., Svensson, M., Wallstedt, L., Janson, A.M., and Frisén, J. (1999). Neural stem cells in the adult human brain. Exp Cell Res *253*, 733-736.
31. Uchida, N., Buck, D.W., He, D., Reitsma, M.J., Masek, M., Phan, T.V., Tsukamoto, A.S., Gage, F.H., and Weissman, I.L. (2000). Direct isolation of human central nervous system stem cells. Proc Natl Acad Sci U S A *97*, 14720-14725.
32. Hemmati, H.D., Nakano, I., Lazareff, J.A., Masterman-Smith, M., Geschwind, D.H., Bronner-Fraser, M., and Kornblum, H.I. (2003). Cancerous stem cells can arise from pediatric brain tumors. Proc Natl Acad Sci U S A *100*, 15178-15183.
33. Ignatova, T.N., Kukekov, V.G., Laywell, E.D., Suslov, O.N., Vrionis, F.D., and Steindler, D.A. (2002). Human cortical glial tumors contain neural stem-like cells expressing astroglial and neuronal markers in vitro. Glia *39*, 193-206.
34. Lee, J., Kotliarova, S., Kotliarov, Y., Li, A., Su, Q., Donin, N.M., Pastorino, S., Purow, B.W., Christopher, N., Zhang, W., et al. (2006). Tumor stem cells derived from glioblastomas cultured in bFGF and EGF more closely mirror the phenotype and genotype of primary tumors than do serum-cultured cell lines. Cancer Cell *9*, 391-403.
35. Singh, S.K., Hawkins, C., Clarke, I.D., Squire, J.A., Bayani, J., Hide, T., Henkelman, R.M., Cusimano, M.D., and Dirks, P.B. (2004). Identification of human brain tumour initiating cells. Nature *432*, 396-401.
36. Todaro, M., Alea, M.P., Di Stefano, A.B., Cammareri, P., Vermeulen, L., Iovino, F., Tripodo, C., Russo, A., Gulotta, G., Medema, J.P., et al. (2007). Colon cancer stem cells dictate tumor growth and resist cell death by production of interleukin-4. Cell Stem Cell *1*, 389-402.
37. Vermeulen, L., Todaro, M., de Sousa Mello, F., Sprick, M.R., Kemper, K., Perez Alea, M., Richel, D.J., Stassi, G., and Medema, J.P. (2008). Single-cell cloning of colon cancer stem cells reveals a multi-lineage differentiation capacity. Proc Natl Acad Sci U S A *105*, 13427-13432.
38. Beier, D., Hau, P., Proescholdt, M., Lohmeier, A., Wischhusen, J., Oefner, P.J., Aigner, L., Brawanski, A., Bogdahn, U., and Beier, C.P. (2007). CD133(+) and CD133(-) glioblastoma-derived cancer stem cells show differential growth characteristics and molecular profiles. Cancer Res *67*, 4010-4015.
39. Taylor, M.D., Poppleton, H., Fuller, C., Su, X., Liu, Y., Jensen, P., Magdaleno, S., Dalton, J., Calabrese, C., Board, J., et al. (2005). Radial glia cells are candidate stem cells of ependymoma. Cancer Cell *8*, 323-335.
40. Hermann, P.C., Huber, S.L., Herrler, T., Aicher, A., Ellwart, J.W., Guba, M., Bruns, C.J., and Heeschen, C. (2007). Distinct populations of cancer stem cells determine tumor growth and metastatic activity in human pancreatic cancer. Cell Stem Cell *1*, 313-323.

41. Lee, A., Kessler, J.D., Read, T.A., Kaiser, C., Corbeil, D., Huttner, W.B., Johnson, J.E., and Wechsler-Reya, R.J. (2005). Isolation of neural stem cells from the postnatal cerebellum. Nat Neurosci *8*, 723-729.
42. Clevers, H. (2011). The cancer stem cell: premises, promises and challenges. Nat Med *17*, 313-319.
43. Son, M.J., Woolard, K., Nam, D.H., Lee, J., and Fine, H.A. (2009). SSEA-1 is an enrichment marker for tumor-initiating cells in human glioblastoma. Cell Stem Cell *4*, 440-452.
44. Chen, R., Nishimura, M.C., Bumbaca, S.M., Kharbanda, S., Forrest, W.F., Kasman, I.M., Greve, J.M., Soriano, R.H., Gilmour, L.L., Rivers, C.S., et al. (2010). A hierarchy of self-renewing tumor-initiating cell types in glioblastoma. Cancer Cell *17*, 362-375.
45. Shmelkov, S.V., Butler, J.M., Hooper, A.T., Hormigo, A., Kushner, J., Milde, T., St Clair, R., Baljevic, M., White, I., Jin, D.K., et al. (2008). CD133 expression is not restricted to stem cells, and both CD133+ and CD133- metastatic colon cancer cells initiate tumors. J Clin Invest *118*, 2111-2120.
46. Dalerba, P., Dylla, S.J., Park, I.K., Liu, R., Wang, X., Cho, R.W., Hoey, T., Gurney, A., Huang, E.H., Simeone, D.M., et al. (2007). Phenotypic characterization of human colorectal cancer stem cells. Proc Natl Acad Sci U S A *104*, 10158-10163.
47. Doetsch, F., Petreanu, L., Caille, I., Garcia-Verdugo, J.M., and Alvarez-Buylla, A. (2002). EGF converts transit-amplifying neurogenic precursors in the adult brain into multipotent stem cells. Neuron *36*, 1021-1034.
48. Ahmed, K.M., and Li, J.J. (2007). ATM-NF-kappaB connection as a target for tumor radiosensitization. Curr Cancer Drug Targets *7*, 335-342.
49. Jordan, C.T., Guzman, M.L., and Noble, M. (2006). Cancer stem cells. N Engl J Med *355*, 1253-1261.
50. Baumann, M., Krause, M., and Hill, R. (2008). Exploring the role of cancer stem cells in radioresistance. Nat Rev Cancer *8*, 545-554.
51. Diehn, M., Cho, R.W., Lobo, N.A., Kalisky, T., Dorie, M.J., Kulp, A.N., Qian, D., Lam, J.S., Ailles, L.E., Wong, M., et al. (2009). Association of reactive oxygen species levels and radioresistance in cancer stem cells. Nature *458*, 780-783.
52. Diehn, M., Cho, R.W., and Clarke, M.F. (2009). Therapeutic implications of the cancer stem cell hypothesis. Semin Radiat Oncol *19*, 78-86.
53. Rycaj, K., and Tang, D.G. (2014). Cancer stem cells and radioresistance. Int J Radiat Biol *90*, 615-621.
54. Barcellos-Hoff, M.H., Park, C., and Wright, E.G. (2005). Radiation and the microenvironment - tumorigenesis and therapy. Nat Rev Cancer *5*, 867-875.
55. Anderson, K., Lutz, C., van Delft, F.W., Bateman, C.M., Guo, Y., Colman, S.M., Kempski, H., Moorman, A.V., Titley, I., Swansbury, J., et al. (2011). Genetic variegation of clonal architecture and propagating cells in leukaemia. Nature *469*, 356-361.
56. Greaves, M., and Maley, C.C. (2012). Clonal evolution in cancer. Nature *481*, 306-313.
57. Piccirillo, S.G., Colman, S., Potter, N.E., van Delft, F.W., Lillis, S., Carnicer, M.J., Kearney, L., Watts, C., and Greaves, M. (2015). Genetic and functional diversity of propagating cells in glioblastoma. Stem Cell Reports *4*, 7-15.
58. Orzan, F., De Bacco, F., Crisafulli, G., Pellegatta, S., Mussolin, B., Siravegna, G., D'ambrosio, A., Comoglio, P.M., Finocchiaro, G., and Boccaccio, C. (2017). Genetic Evolution of Glioblastoma Stem-like Cells from Primary to Recurrent Tumor. Stem Cells.
59. Lagadec, C., Vlashi, E., Della Donna, L., Dekmezian, C., and Pajonk, F. (2012). Radiation-induced reprogramming of breast cancer cells. Stem Cells *30*, 833-844.
60. Dolecek, T.A., Propp, J.M., Stroup, N.E., and Kruchko, C. (2012). CBTRUS statistical report: primary brain and central nervous system tumors diagnosed in the United States in 2005-2009. Neuro Oncol *14 Suppl 5*, v1-49.

61. Osuka, S., and Van Meir, E.G. (2017). Overcoming therapeutic resistance in glioblastoma: the way forward. J Clin Invest *127*, 415-426.
62. Hegi, M.E., Diserens, A.C., Gorlia, T., Hamou, M.F., de Tribolet, N., Weller, M., Kros, J.M., Hainfellner, J.A., Mason, W., Mariani, L., et al. (2005). MGMT gene silencing and benefit from temozolomide in glioblastoma. N Engl J Med *352*, 997-1003.
63. Smith, J., Tho, L.M., Xu, N., and Gillespie, D.A. (2010). The ATM-Chk2 and ATR-Chk1 pathways in DNA damage signaling and cancer. Adv Cancer Res *108*, 73-112.
64. Shiloh, Y., and Ziv, Y. (2013). The ATM protein kinase: regulating the cellular response to genotoxic stress, and more. Nat Rev Mol Cell Biol *14*, 197-210.
65. Jazayeri, A., Falck, J., Lukas, C., Bartek, J., Smith, G.C., Lukas, J., and Jackson, S.P. (2006). ATM- and cell cycle-dependent regulation of ATR in response to DNA double-strand breaks. Nat Cell Biol *8*, 37-45.
66. Myers, J.S., and Cortez, D. (2006). Rapid activation of ATR by ionizing radiation requires ATM and Mre11. J Biol Chem *281*, 9346-9350.
67. MacDougall, C.A., Byun, T.S., Van, C., Yee, M.C., and Cimprich, K.A. (2007). The structural determinants of checkpoint activation. Genes Dev *21*, 898-903.
68. Duursma, A.M., Driscoll, R., Elias, J.E., and Cimprich, K.A. (2013). A role for the MRN complex in ATR activation via TOPBP1 recruitment. Mol Cell *50*, 116-122.
69. Boutros, R., Lobjois, V., and Ducommun, B. (2007). CDC25 phosphatases in cancer cells: key players? Good targets? Nat Rev Cancer *7*, 495-507.
70. Cheng, L., Wu, Q., Huang, Z., Guryanova, O.A., Huang, Q., Shou, W., Rich, J.N., and Bao, S. (2011). L1CAM regulates DNA damage checkpoint response of glioblastoma stem cells through NBS1. EMBO J *30*, 800-813.
71. Squatrito, M., Brennan, C.W., Helmy, K., Huse, J.T., Petrini, J.H., and Holland, E.C. (2010). Loss of ATM/Chk2/p53 pathway components accelerates tumor development and contributes to radiation resistance in gliomas. Cancer Cell *18*, 619-629.
72. Facchino, S., Abdouh, M., Chatoo, W., and Bernier, G. (2010). BMI1 confers radioresistance to normal and cancerous neural stem cells through recruitment of the DNA damage response machinery. J Neurosci *30*, 10096-10111.
73. Carruthers, R., Ahmed, S.U., Strathdee, K., Gomez-Roman, N., Amoah-Buahin, E., Watts, C., and Chalmers, A.J. (2015). Abrogation of radioresistance in glioblastoma stem-like cells by inhibition of ATM kinase. Mol Oncol *9*, 192-203.
74. Venere, M., Hamerlik, P., Wu, Q., Rasmussen, R.D., Song, L.A., Vasanji, A., Tenley, N., Flavahan, W.A., Hjelmeland, A.B., Bartek, J., et al. (2014). Therapeutic targeting of constitutive PARP activation compromises stem cell phenotype and survival of glioblastoma-initiating cells. Cell Death Differ *21*, 258-269.
75. Moncharmont, C., Levy, A., Gilormini, M., Bertrand, G., Chargari, C., Alphonse, G., Ardail, D., Rodriguez-Lafrasse, C., and Magné, N. (2012). Targeting a cornerstone of radiation resistance: cancer stem cell. Cancer Lett *322*, 139-147.
76. Squatrito, M., and Holland, E.C. (2011). DNA damage response and growth factor signaling pathways in gliomagenesis and therapeutic resistance. Cancer Res *71*, 5945-5949.
77. Huse, J.T., and Holland, E.C. (2010). Targeting brain cancer: advances in the molecular pathology of malignant glioma and medulloblastoma. Nat Rev Cancer *10*, 319-331.
78. Bandyopadhyay, D., Mandal, M., Adam, L., Mendelsohn, J., and Kumar, R. (1998). Physical interaction between epidermal growth factor receptor and DNA-dependent protein kinase in mammalian cells. J Biol Chem *273*, 1568-1573.
79. Dittmann, K., Mayer, C., Fehrenbacher, B., Schaller, M., Raju, U., Milas, L., Chen, D.J., Kehlbach, R., and Rodemann, H.P. (2005). Radiation-induced epidermal growth factor receptor nuclear import is linked to activation of DNA-dependent protein kinase. J Biol Chem *280*, 31182-31189.

80. Dittmann, K., Mayer, C., and Rodemann, H.P. (2005). Inhibition of radiation-induced EGFR nuclear import by C225 (Cetuximab) suppresses DNA-PK activity. Radiother Oncol *76*, 157-161.
81. Huang, S.M., Bock, J.M., and Harari, P.M. (1999). Epidermal growth factor receptor blockade with C225 modulates proliferation, apoptosis, and radiosensitivity in squamous cell carcinomas of the head and neck. Cancer Res *59*, 1935-1940.
82. Huang, S.M., and Harari, P.M. (2000). Modulation of radiation response after epidermal growth factor receptor blockade in squamous cell carcinomas: inhibition of damage repair, cell cycle kinetics, and tumor angiogenesis. Clin Cancer Res *6*, 2166-2174.
83. Golding, S.E., Morgan, R.N., Adams, B.R., Hawkins, A.J., Povirk, L.F., and Valerie, K. (2009). Pro-survival AKT and ERK signaling from EGFR and mutant EGFRvIII enhances DNA double-strand break repair in human glioma cells. Cancer Biol Ther *8*, 730-738.
84. Learn, C.A., Hartzell, T.L., Wikstrand, C.J., Archer, G.E., Rich, J.N., Friedman, A.H., Friedman, H.S., Bigner, D.D., and Sampson, J.H. (2004). Resistance to tyrosine kinase inhibition by mutant epidermal growth factor receptor variant III contributes to the neoplastic phenotype of glioblastoma multiforme. Clin Cancer Res *10*, 3216-3224.
85. Li, B., Yuan, M., Kim, I.A., Chang, C.M., Bernhard, E.J., and Shu, H.K. (2004). Mutant epidermal growth factor receptor displays increased signaling through the phosphatidylinositol-3 kinase/AKT pathway and promotes radioresistance in cells of astrocytic origin. Oncogene *23*, 4594-4602.
86. Lammering, G., Hewit, T.H., Valerie, K., Contessa, J.N., Amorino, G.P., Dent, P., and Schmidt-Ullrich, R.K. (2003). EGFRvIII-mediated radioresistance through a strong cytoprotective response. Oncogene *22*, 5545-5553.
87. Kao, G.D., Jiang, Z., Fernandes, A.M., Gupta, A.K., and Maity, A. (2007). Inhibition of phosphatidylinositol-3-OH kinase/Akt signaling impairs DNA repair in glioblastoma cells following ionizing radiation. J Biol Chem *282*, 21206-21212.
88. Mukherjee, B., McEllin, B., Camacho, C.V., Tomimatsu, N., Sirasanagandala, S., Nannepaga, S., Hatanpaa, K.J., Mickey, B., Madden, C., Maher, E., et al. (2009). EGFRvIII and DNA double-strand break repair: a molecular mechanism for radioresistance in glioblastoma. Cancer Res *69*, 4252-4259.
89. Johns, T.G., McKay, M.J., Cvrljevic, A.N., Gan, H.K., Taylor, C., Xu, H., Smyth, F.E., and Scott, A.M. (2010). MAb 806 enhances the efficacy of ionizing radiation in glioma xenografts expressing the de2-7 epidermal growth factor receptor. Int J Radiat Oncol Biol Phys *78*, 572-578.
90. Ozawa, T., Brennan, C.W., Wang, L., Squatrito, M., Sasayama, T., Nakada, M., Huse, J.T., Pedraza, A., Utsuki, S., Yasui, Y., et al. (2010). PDGFRA gene rearrangements are frequent genetic events in PDGFRA-amplified glioblastomas. Genes Dev *24*, 2205-2218.
91. Geng, L., Shinohara, E.T., Kim, D., Tan, J., Osusky, K., Shyr, Y., and Hallahan, D.E. (2006). STI571 (Gleevec) improves tumor growth delay and survival in irradiated mouse models of glioblastoma. Int J Radiat Oncol Biol Phys *64*, 263-271.
92. Mazzoleni, S., Politi, L.S., Pala, M., Cominelli, M., Franzin, A., Sergi Sergi, L., Falini, A., De Palma, M., Bulfone, A., Poliani, P.L., et al. (2010). Epidermal growth factor receptor expression identifies functionally and molecularly distinct tumor-initiating cells in human glioblastoma multiforme and is required for gliomagenesis. Cancer Res *70*, 7500-7513.
93. Hambardzumyan, D., Becher, O.J., Rosenblum, M.K., Pandolfi, P.P., Manova-Todorova, K., and Holland, E.C. (2008). PI3K pathway regulates survival of cancer stem cells residing in the perivascular niche following radiation in medulloblastoma in vivo. Genes Dev *22*, 436-448.
94. Medová, M., Aebersold, D.M., and Zimmer, Y. (2013). The Molecular Crosstalk between the MET Receptor Tyrosine Kinase and the DNA Damage Response-Biological and Clinical Aspects. Cancers (Basel) *6*, 1-27.

95. De Bacco, F., Luraghi, P., Medico, E., Reato, G., Girolami, F., Perera, T., Gabriele, P., Comoglio, P.M., and Boccaccio, C. (2011). Induction of MET by ionizing radiation and its role in radioresistance and invasive growth of cancer. J Natl Cancer Inst *103*, 645-661.
96. De Bacco, F., Casanova, E., Medico, E., Pellegatta, S., Orzan, F., Albano, R., Luraghi, P., Reato, G., D'Ambrosio, A., Porrati, P., et al. (2012). The MET oncogene is a functional marker of a glioblastoma stem cell subtype. Cancer Res *72*, 4537-4550.
97. Boccaccio, C., and Comoglio, P.M. (2014). MET, a driver of invasive growth and cancer clonal evolution under therapeutic pressure. Curr Opin Cell Biol *31*, 98-105.
98. Mani, S.A., Guo, W., Liao, M.J., Eaton, E.N., Ayyanan, A., Zhou, A.Y., Brooks, M., Reinhard, F., Zhang, C.C., Shipitsin, M., et al. (2008). The epithelial-mesenchymal transition generates cells with properties of stem cells. Cell *133*, 704-715.
99. Comoglio, P.M., Giordano, S., and Trusolino, L. (2008). Drug development of MET inhibitors: targeting oncogene addiction and expedience. Nat Rev Drug Discov *7*, 504-516.
100. Turke, A.B., Zejnullahu, K., Wu, Y.L., Song, Y., Dias-Santagata, D., Lifshits, E., Toschi, L., Rogers, A., Mok, T., Sequist, L., et al. (2010). Preexistence and clonal selection of MET amplification in EGFR mutant NSCLC. Cancer Cell *17*, 77-88.
101. Bardelli, A., Corso, S., Bertotti, A., Hobor, S., Valtorta, E., Siravegna, G., Sartore-Bianchi, A., Scala, E., Cassingena, A., Zecchin, D., et al. (2013). Amplification of the MET receptor drives resistance to anti-EGFR therapies in colorectal cancer. Cancer Discov *3*, 658-673.
102. Trusolino, L., Bertotti, A., and Comoglio, P.M. (2010). MET signalling: principles and functions in development, organ regeneration and cancer. Nat Rev Mol Cell Biol *11*, 834-848.
103. Gherardi, E., Birchmeier, W., Birchmeier, C., and Vande Woude, G. (2012). Targeting MET in cancer: rationale and progress. Nat Rev Cancer *12*, 89-103.
104. Yang, H., Lee, H.W., Kim, Y., Lee, Y., Choi, Y.S., Kim, K.H., Jin, J., Lee, J., Joo, K.M., and Nam, D.H. (2013). Radiosensitization of brain metastasis by targeting c-MET. Lab Invest *93*, 344-353.
105. Bhardwaj, V., Cascone, T., Cortez, M.A., Amini, A., Evans, J., Komaki, R.U., Heymach, J.V., and Welsh, J.W. (2013). Modulation of c-Met signaling and cellular sensitivity to radiation: potential implications for therapy. Cancer *119*, 1768-1775.
106. Pennacchietti, S., Michieli, P., Galluzzo, M., Mazzone, M., Giordano, S., and Comoglio, P.M. (2003). Hypoxia promotes invasive growth by transcriptional activation of the met protooncogene. Cancer Cell *3*, 347-361.
107. Deorukhkar, A., and Krishnan, S. (2010). Targeting inflammatory pathways for tumor radiosensitization. Biochem Pharmacol *80*, 1904-1914.
108. Naugler, W.E., and Karin, M. (2008). NF-kappaB and cancer-identifying targets and mechanisms. Curr Opin Genet Dev *18*, 19-26.
109. Medová, M., Aebersold, D.M., and Zimmer, Y. (2012). MET inhibition in tumor cells by PHA665752 impairs homologous recombination repair of DNA double strand breaks. Int J Cancer *130*, 728-734.
110. Hwang, C.I., Matoso, A., Corney, D.C., Flesken-Nikitin, A., Körner, S., Wang, W., Boccaccio, C., Thorgeirsson, S.S., Comoglio, P.M., Hermeking, H., et al. (2011). Wild-type p53 controls cell motility and invasion by dual regulation of MET expression. Proc Natl Acad Sci U S A *108*, 14240-14245.
111. Muller, P.A., Trinidad, A.G., Timpson, P., Morton, J.P., Zanivan, S., van den Berghe, P.V., Nixon, C., Karim, S.A., Caswell, P.T., Noll, J.E., et al. (2013). Mutant p53 enhances MET trafficking and signalling to drive cell scattering and invasion. Oncogene *32*, 1252-1265.
112. Camacho, C.V., Todorova, P.K., Hardebeck, M.C., Tomimatsu, N., Gil del Alcazar, C.R., Ilcheva, M., Mukherjee, B., McEllin, B., Vemireddy, V., Hatanpaa, K., et al. (2015). DNA double-strand breaks cooperate with loss of Ink4 and Arf tumor suppressors to generate glioblastomas with frequent Met amplification. Oncogene *34*, 1064-1072.

113. Bosset, J.F., Collette, L., Calais, G., Mineur, L., Maingon, P., Radosevic-Jelic, L., Daban, A., Bardet, E., Beny, A., Ollier, J.C., et al. (2006). Chemotherapy with preoperative radiotherapy in rectal cancer. N Engl J Med *355*, 1114-1123.
114. Medich, D., McGinty, J., Parda, D., Karlovits, S., Davis, C., Caushaj, P., and Lembersky, B. (2001). Preoperative chemoradiotherapy and radical surgery for locally advanced distal rectal adenocarcinoma: pathologic findings and clinical implications. Dis Colon Rectum *44*, 1123-1128.
115. Wheeler, J.M., Dodds, E., Warren, B.F., Cunningham, C., George, B.D., Jones, A.C., and Mortensen, N.J. (2004). Preoperative chemoradiotherapy and total mesorectal excision surgery for locally advanced rectal cancer: correlation with rectal cancer regression grade. Dis Colon Rectum *47*, 2025-2031.
116. Duldulao, M.P., Lee, W., Streja, L., Chu, P., Li, W., Chen, Z., Kim, J., and Garcia-Aguilar, J. (2013). Distribution of residual cancer cells in the bowel wall after neoadjuvant chemoradiation in patients with rectal cancer. Dis Colon Rectum *56*, 142-149.
117. Grade, M., Wolff, H.A., Gaedcke, J., and Ghadimi, B.M. (2012). The molecular basis of chemoradiosensitivity in rectal cancer: implications for personalized therapies. Langenbecks Arch Surg *397*, 543-555.
118. Senetta, R., Duregon, E., Sonetto, C., Spadi, R., Mistrangelo, M., Racca, P., Chiusa, L., Munoz, F.H., Ricardi, U., Arezzo, A., et al. (2015). YKL-40/c-Met expression in rectal cancer biopsies predicts tumor regression following neoadjuvant chemoradiotherapy: a multi-institutional study. PLoS One *10*, e0123759.
119. Boccaccio, C., and Comoglio, P.M. (2006). Invasive growth: a MET-driven genetic programme for cancer and stem cells. Nat Rev Cancer *6*, 637-645.
120. Nicoleau, C., Benzakour, O., Agasse, F., Thiriet, N., Petit, J., Prestoz, L., Roger, M., Jaber, M., and Coronas, V. (2009). Endogenous hepatocyte growth factor is a niche signal for subventricular zone neural stem cell amplification and self-renewal. Stem Cells *27*, 408-419.
121. Li, Y., Li, A., Glas, M., Lal, B., Ying, M., Sang, Y., Xia, S., Trageser, D., Guerrero-Cázares, H., Eberhart, C.G., et al. (2011). c-Met signaling induces a reprogramming network and supports the glioblastoma stem-like phenotype. Proc Natl Acad Sci U S A *108*, 9951-9956.
122. Vermeulen, L., De Sousa E Melo, F., van der Heijden, M., Cameron, K., de Jong, J.H., Borovski, T., Tuynman, J.B., Todaro, M., Merz, C., Rodermond, H., et al. (2010). Wnt activity defines colon cancer stem cells and is regulated by the microenvironment. Nat Cell Biol *12*, 468-476.
123. Verhaak, R.G., Hoadley, K.A., Purdom, E., Wang, V., Qi, Y., Wilkerson, M.D., Miller, C.R., Ding, L., Golub, T., Mesirov, J.P., et al. (2010). Integrated genomic analysis identifies clinically relevant subtypes of glioblastoma characterized by abnormalities in PDGFRA, IDH1, EGFR, and NF1. Cancer Cell *17*, 98-110.
124. Sun, Y., Goderie, S.K., and Temple, S. (2005). Asymmetric distribution of EGFR receptor during mitosis generates diverse CNS progenitor cells. Neuron *45*, 873-886.
125. Joo, K.M., Jin, J., Kim, E., Ho Kim, K., Kim, Y., Gu Kang, B., Kang, Y.J., Lathia, J.D., Cheong, K.H., Song, P.H., et al. (2012). MET signaling regulates glioblastoma stem cells. Cancer Res *72*, 3828-3838.
126. Calabrese, C., Poppleton, H., Kocak, M., Hogg, T.L., Fuller, C., Hamner, B., Oh, E.Y., Gaber, M.W., Finklestein, D., Allen, M., et al. (2007). A perivascular niche for brain tumor stem cells. Cancer Cell *11*, 69-82.
127. Boccaccio, C., and Comoglio, P.M. (2013). The MET oncogene in glioblastoma stem cells: implications as a diagnostic marker and a therapeutic target. Cancer Res *73*, 3193-3199.
128. Bertotti, A., Migliardi, G., Galimi, F., Sassi, F., Torti, D., Isella, C., Corà, D., Di Nicolantonio, F., Buscarino, M., Petti, C., et al. (2011). A molecularly annotated platform of patient-derived xenografts ("xenopatients") identifies HER2 as an effective therapeutic target in cetuximab-resistant colorectal cancer. Cancer Discov *1*, 508-523.

129. De Bacco, F., D'Ambrosio, A., Casanova, E., Orzan, F., Neggia, R., Albano, R., Verginelli, F., Cominelli, M., Poliani, P.L., Luraghi, P., et al. (2016). MET inhibition overcomes radiation resistance of glioblastoma stem-like cells. EMBO Mol Med *8*, 550-568.
130. Luraghi, P., Reato, G., Cipriano, E., Sassi, F., Orzan, F., Bigatto, V., De Bacco, F., Menietti, E., Han, M., Rideout, W.M., et al. (2014). MET signaling in colon cancer stem-like cells blunts the therapeutic response to EGFR inhibitors. Cancer Res *74*, 1857-1869.
131. Vigna, E., Cavalieri, S., Ailles, L., Geuna, M., Loew, R., Bujard, H., and Naldini, L. (2002). Robust and efficient regulation of transgene expression in vivo by improved tetracycline-dependent lentiviral vectors. Mol Ther *5*, 252-261.
132. Hu, Y., and Smyth, G.K. (2009). ELDA: extreme limiting dilution analysis for comparing depleted and enriched populations in stem cell and other assays. J Immunol Methods *347*, 70-78.
133. Prat, M., Crepaldi, T., Pennacchietti, S., Bussolino, F., and Comoglio, P.M. (1998). Agonistic monoclonal antibodies against the Met receptor dissect the biological responses to HGF. J Cell Sci *111 (Pt 2)*, 237-247.
134. Franken, N.A., Rodermond, H.M., Stap, J., Haveman, J., and van Bree, C. (2006). Clonogenic assay of cells in vitro. Nat Protoc *1*, 2315-2319.
135. Baralis, E., Bertotti, A., Fiori, A., and Grand, A. (2012). LAS: a software platform to support oncological data management. J Med Syst *36 Suppl 1*, S81-90.
136. Abdouh, M., Facchino, S., Chatoo, W., Balasingam, V., Ferreira, J., and Bernier, G. (2009). BMI1 sustains human glioblastoma multiforme stem cell renewal. J Neurosci *29*, 8884-8896.
137. Doetsch, F. (2003). The glial identity of neural stem cells. Nat Neurosci *6*, 1127-1134.
138. Phillips, H.S., Kharbanda, S., Chen, R., Forrest, W.F., Soriano, R.H., Wu, T.D., Misra, A., Nigro, J.M., Colman, H., Soroceanu, L., et al. (2006). Molecular subclasses of high-grade glioma predict prognosis, delineate a pattern of disease progression, and resemble stages in neurogenesis. Cancer Cell *9*, 157-173.
139. Bolós, V., Blanco, M., Medina, V., Aparicio, G., Díaz-Prado, S., and Grande, E. (2009). Notch signalling in cancer stem cells. Clin Transl Oncol *11*, 11-19.
140. Bock, T.A., Ziegler, B.L., Bühring, H.J., Scheding, S., Brugger, W., and Kanz, L. (1999). Characterization of purified and ex vivo manipulated human hematopoietic progenitor and stem cells in xenograft recipients. Ann N Y Acad Sci *872*, 200-207; discussion 207-210.
141. Olive, P.L., and Banáth, J.P. (2004). Phosphorylation of histone H2AX as a measure of radiosensitivity. Int J Radiat Oncol Biol Phys *58*, 331-335.
142. Olive, P.L. (2004). Detection of DNA damage in individual cells by analysis of histone H2AX phosphorylation. Methods Cell Biol *75*, 355-373.
143. Kunkel, P., Müller, S., Schirmacher, P., Stavrou, D., Fillbrandt, R., Westphal, M., and Lamszus, K. (2001). Expression and localization of scatter factor/hepatocyte growth factor in human astrocytomas. Neuro Oncol *3*, 82-88.
144. Xie, Q., Bradley, R., Kang, L., Koeman, J., Ascierto, M.L., Worschech, A., De Giorgi, V., Wang, E., Kefene, L., Su, Y., et al. (2012). Hepatocyte growth factor (HGF) autocrine activation predicts sensitivity to MET inhibition in glioblastoma. Proc Natl Acad Sci U S A *109*, 570-575.
145. Lal, B., Xia, S., Abounader, R., and Laterra, J. (2005). Targeting the c-Met pathway potentiates glioblastoma responses to gamma-radiation. Clin Cancer Res *11*, 4479-4486.
146. van Gent, D.C., Hoeijmakers, J.H., and Kanaar, R. (2001). Chromosomal stability and the DNA double-stranded break connection. Nat Rev Genet *2*, 196-206.
147. Mandard, A.M., Dalibard, F., Mandard, J.C., Marnay, J., Henry-Amar, M., Petiot, J.F., Roussel, A., Jacob, J.H., Segol, P., and Samama, G. (1994). Pathologic assessment of tumor regression after preoperative chemoradiotherapy of esophageal carcinoma. Clinicopathologic correlations. Cancer *73*, 2680-2686.
148. Luraghi, P., Bigatto, V., Cipriano, E., Reato, G., Orzan, F., Sassi, F., De Bacco, F., Isella, C., Bellomo, S.E., Medico, E., et al. (2017). A molecularly annotated model of patient-derived

colon cancer stem-like cells to assess genetic and non-genetic mechanisms of resistance to anti-EGFR therapy. Clin Cancer Res.
149. O'Brien, C.A., Kreso, A., Ryan, P., Hermans, K.G., Gibson, L., Wang, Y., Tsatsanis, A., Gallinger, S., and Dick, J.E. (2012). ID1 and ID3 regulate the self-renewal capacity of human colon cancer-initiating cells through p21. Cancer Cell *21*, 777-792.
150. Bu, P., Chen, K.Y., Chen, J.H., Wang, L., Walters, J., Shin, Y.J., Goerger, J.P., Sun, J., Witherspoon, M., Rakhilin, N., et al. (2013). A microRNA miR-34a-regulated bimodal switch targets Notch in colon cancer stem cells. Cell Stem Cell *12*, 602-615.
151. Miranti, A., D'Ambrosio, A., Cattari, G., Garibaldi, E., Bresciani, S., Gabriele, P., and Stasi, M. (2016). NOD-SCID mice irradiation with medical accelerators: Dosimetric and radiobiological results. Phys Med *32*, 1453-1460.
152. Koch, U., Krause, M., and Baumann, M. (2010). Cancer stem cells at the crossroads of current cancer therapy failures--radiation oncology perspective. Semin Cancer Biol *20*, 116-124.
153. Lathia, J.D., Mack, S.C., Mulkearns-Hubert, E.E., Valentim, C.L., and Rich, J.N. (2015). Cancer stem cells in glioblastoma. Genes Dev *29*, 1203-1217.
154. Ahmed, S.U., Carruthers, R., Gilmour, L., Yildirim, S., Watts, C., and Chalmers, A.J. (2015). Selective Inhibition of Parallel DNA Damage Response Pathways Optimizes Radiosensitization of Glioblastoma Stem-like Cells. Cancer Res *75*, 4416-4428.
155. Pajonk, F., Vlashi, E., and McBride, W.H. (2010). Radiation resistance of cancer stem cells: the 4 R's of radiobiology revisited. Stem Cells *28*, 639-648.
156. Vlashi, E., and Pajonk, F. (2015). Cancer stem cells, cancer cell plasticity and radiation therapy. Semin Cancer Biol *31*, 28-35.
157. Blanpain, C., Mohrin, M., Sotiropoulou, P.A., and Passegué, E. (2011). DNA-damage response in tissue-specific and cancer stem cells. Cell Stem Cell *8*, 16-29.
158. Friedmann, B., Caplin, M., Hartley, J.A., and Hochhauser, D. (2004). Modulation of DNA repair in vitro after treatment with chemotherapeutic agents by the epidermal growth factor receptor inhibitor gefitinib (ZD1839). Clin Cancer Res *10*, 6476-6486.
159. Bhat, K.P.L., Balasubramaniyan, V., Vaillant, B., Ezhilarasan, R., Hummelink, K., Hollingsworth, F., Wani, K., Heathcock, L., James, J.D., Goodman, L.D., et al. (2013). Mesenchymal differentiation mediated by NF-κB promotes radiation resistance in glioblastoma. Cancer Cell *24*, 331-346.
160. Bigatto, V., De Bacco, F., Casanova, E., Reato, G., Lanzetti, L., Isella, C., Sarotto, I., Comoglio, P.M., and Boccaccio, C. (2015). TNF-α promotes invasive growth through the MET signaling pathway. Mol Oncol *9*, 377-388.
161. Stupp, R., Hegi, M.E., Mason, W.P., van den Bent, M.J., Taphoorn, M.J., Janzer, R.C., Ludwin, S.K., Allgeier, A., Fisher, B., Belanger, K., et al. (2009). Effects of radiotherapy with concomitant and adjuvant temozolomide versus radiotherapy alone on survival in glioblastoma in a randomised phase III study: 5-year analysis of the EORTC-NCIC trial. Lancet Oncol *10*, 459-466.
162. Brennan, C.W., Verhaak, R.G., McKenna, A., Campos, B., Noushmehr, H., Salama, S.R., Zheng, S., Chakravarty, D., Sanborn, J.Z., Berman, S.H., et al. (2013). The somatic genomic landscape of glioblastoma. Cell *155*, 462-477.
163. Abbas, T., and Dutta, A. (2009). p21 in cancer: intricate networks and multiple activities. Nat Rev Cancer *9*, 400-414.
164. Krause, M., Yaromina, A., Eicheler, W., Koch, U., and Baumann, M. (2011). Cancer stem cells: targets and potential biomarkers for radiotherapy. Clin Cancer Res *17*, 7224-7229.
165. Chi, A.S., Batchelor, T.T., Kwak, E.L., Clark, J.W., Wang, D.L., Wilner, K.D., Louis, D.N., and Iafrate, A.J. (2012). Rapid radiographic and clinical improvement after treatment of a MET-amplified recurrent glioblastoma with a mesenchymal-epithelial transition inhibitor. J Clin Oncol *30*, e30-33.

166. Project, I.C.G.C.P.T. (2016). Recurrent MET fusion genes represent a drug target in pediatric glioblastoma. Nat Med *22*, 1314-1320.
167. Sottoriva, A., Spiteri, I., Piccirillo, S.G., Touloumis, A., Collins, V.P., Marioni, J.C., Curtis, C., Watts, C., and Tavaré, S. (2013). Intratumor heterogeneity in human glioblastoma reflects cancer evolutionary dynamics. Proc Natl Acad Sci U S A *110*, 4009-4014.
168. Joosten, S.P.J., Zeilstra, J., van Andel, H., Mijnals, R.C., Zaunbrecher, J., Duivenvoorden, A.A.M., van de Wetering, M., Clevers, H., Spaargaren, M., and Pals, S.T. (2017). MET Signaling Mediates Intestinal Crypt-Villus Development, Regeneration, and Adenoma Formation and Is Promoted by Stem Cell CD44 Isoforms. Gastroenterology *153*, 1040-1053.e1044.
169. Samamé Pérez-Vargas, J.C., Biondani, P., Maggi, C., Gariboldi, M., Gloghini, A., Inno, A., Volpi, C.C., Gualeni, A.V., di Bartolomeo, M., de Braud, F., et al. (2013). Role of cMET in the development and progression of colorectal cancer. Int J Mol Sci *14*, 18056-18077.
170. Birchmeier, C., Birchmeier, W., Gherardi, E., and Vande Woude, G.F. (2003). Met, metastasis, motility and more. Nat Rev Mol Cell Biol *4*, 915-925.
171. Rasola, A., Fassetta, M., De Bacco, F., D'Alessandro, L., Gramaglia, D., Di Renzo, M.F., and Comoglio, P.M. (2007). A positive feedback loop between hepatocyte growth factor receptor and beta-catenin sustains colorectal cancer cell invasive growth. Oncogene *26*, 1078-1087.
172. Todaro, M., Gaggianesi, M., Catalano, V., Benfante, A., Iovino, F., Biffoni, M., Apuzzo, T., Sperduti, I., Volpe, S., Cocorullo, G., et al. (2014). CD44v6 is a marker of constitutive and reprogrammed cancer stem cells driving colon cancer metastasis. Cell Stem Cell *14*, 342-356.
173. Tamas, K., Walenkamp, A.M., de Vries, E.G., van Vugt, M.A., Beets-Tan, R.G., van Etten, B., de Groot, D.J., and Hospers, G.A. (2015). Rectal and colon cancer: Not just a different anatomic site. Cancer Treat Rev *41*, 671-679.
174. Missiaglia, E., Jacobs, B., D'Ario, G., Di Narzo, A.F., Soneson, C., Budinska, E., Popovici, V., Vecchione, L., Gerster, S., Yan, P., et al. (2014). Distal and proximal colon cancers differ in terms of molecular, pathological, and clinical features. Ann Oncol *25*, 1995-2001.
175. Fan, C.W., Chen, T., Shang, Y.N., Gu, Y.Z., Zhang, S.L., Lu, R., OuYang, S.R., Zhou, X., Li, Y., Meng, W.T., et al. (2013). Cancer-initiating cells derived from human rectal adenocarcinoma tissues carry mesenchymal phenotypes and resist drug therapies. Cell Death Dis *4*, e828.
176. De Sousa E Melo, F., Wang, X., Jansen, M., Fessler, E., Trinh, A., de Rooij, L.P., de Jong, J.H., de Boer, O.J., van Leersum, R., Bijlsma, M.F., et al. (2013). Poor-prognosis colon cancer is defined by a molecularly distinct subtype and develops from serrated precursor lesions. Nat Med *19*, 614-618.
177. Isella, C., Terrasi, A., Bellomo, S.E., Petti, C., Galatola, G., Muratore, A., Mellano, A., Senetta, R., Cassenti, A., Sonetto, C., et al. (2016). Corrigendum: Stromal contribution to the colorectal cancer transcriptome. Nat Genet *48*, 1296.
178. Boccaccio, C., Luraghi, P., and Comoglio, P.M. (2014). MET-mediated resistance to EGFR inhibitors: an old liaison rooted in colorectal cancer stem cells. Cancer Res *74*, 3647-3651.
179. Piccirillo, S.G., Combi, R., Cajola, L., Patrizi, A., Redaelli, S., Bentivegna, A., Baronchelli, S., Maira, G., Pollo, B., Mangiola, A., et al. (2009). Distinct pools of cancer stem-like cells coexist within human glioblastomas and display different tumorigenicity and independent genomic evolution. Oncogene *28*, 1807-1811.
180. Greaves, M. (2013). Cancer stem cells as 'units of selection'. Evol Appl *6*, 102-108.
181. Doherty, M.R., Smigiel, J.M., Junk, D.J., and Jackson, M.W. (2016). Cancer Stem Cell Plasticity Drives Therapeutic Resistance. Cancers (Basel) *8*.
182. Koochekpour, S., Jeffers, M., Rulong, S., Taylor, G., Klineberg, E., Hudson, E.A., Resau, J.H., and Vande Woude, G.F. (1997). Met and hepatocyte growth factor/scatter factor expression in human gliomas. Cancer Res *57*, 5391-5398.